IN SITU STRESS AND GEOLOGY FROM THE MH-2 BOREHOLE, MOUNTAIN HOME, IDAHO: IMPLICATIONS FOR GEOTHERMAL EXPLORATION FROM FRACTURES, ROCK PROPERTIES, AND GEOMECHANICS

by

James Andrew Kessler

A dissertation submitted in partial fulfillment
of the requirements for the degree

of

DOCTOR OF PHILOSOPHY

in

Geology

Approved:

Dr. James P. Evans Major Professor	Dr. John W. Shervais Committee Member
Dr. Douglas R. Schmitt Committee Member	Dr. Anthony R. Lowry Committee Member
Dr. Thomas E. Lachmar Committee Member	Dr. Mark R. McLellan Vice President for Research and Dean of the School of Graduate Studies

UTAH STATE UNIVERSITY
Logan, Utah

2014

ABSTRACT

In situ Stress and Geology from the MH-2 Borehole, Mountain Home, Idaho: Implications for Geothermal Exploration from Fractures, Rock Properties, and Geomechanics

by

James A. Kessler, Doctor of Philosophy

Utah State University, 2014

Major Professor: Dr. James P. Evans
Department: Geology

The Snake River Plain in southern Idaho is a region of high crustal heat flow and has the potential for economic geothermal energy development. The MH-2 borehole was drilled into a high-temperature artesian reservoir in the western part of the Snake River Plain as part of the Snake River Scientific Drilling Project (Project Hotspot). This research characterizes the rock properties, fractures, and in situ stress state for Miocene basalts in the 1,821 m (5,974 ft) deep borehole near Mountain Home, Idaho. The methods and analyses demonstrate a workflow to conserve resources and utilize a variety of data sources in combination to fill data gaps when necessary.

Unconfined uniaxial compressive stress experiments on core samples provide direct measurement of rock properties that are used to calibrate petrophysical models that utilize wellbore wireline log data and laboratory shear and compressional sonic velocity

data. These data show a large variation in elastic rock properties and rock strength which define three classes of rock that are used to describe the mechanical stratigraphy.

The distribution of rock properties controls the distribution of fractures that are found mostly in strong, elastic rocks that exhibit brittle failure. The fractures form connected pathways that are the primary porosity and permeability in the reservoir. Weak, plastic rocks act as a cap rock seal that prevents the loss of heat and fluids from the reservoir. The research demonstrates that dynamic petrophysical models of the rock properties can be used in this region in lieu of static measurements from core and in combination of borehole and laboratory data.

Analyses of borehole breakout fractures are used to interpret the orientation and magnitudes of the local stress field around the MH-2 borehole. The state of stress is used to describe the structure around the Mountain Home region. The borehole was possibly drilled near a northeast-oriented stepover fault on a ramp between the tips of two larger northwest-oriented oblique-slip normal faults that define the boundary of a gravity high that is interpreted to be an intrabasinal uplifted block. The stepover fault likely dips to the southeast and experiences both dip-slip and strike-slip motion during failure.

(174 pages)

PUBLIC ABSTRACT

In situ Stress and Geology from the MH-2 Borehole, Mountain Home, Idaho: Implications for Geothermal Exploration from Fractures, Rock Properties, and Geomechanics

James A. Kessler

Geothermal energy is being explored as a supplement to traditional fossil fuel resources to meet growing energy demand and reduce carbon emissions. Geothermal energy plants harvest heat stored in the Earth's subsurface by bringing high temperature fluids to the surface and generating steam to produce electricity. Development of geothermal resources is often inhibited by large upfront risk and expense. Successful mitigation of those costs and risks begins with efficient characterization of the resource before development. A typically successful geothermal reservoir consists of a fractured reservoir that conducts hydrothermal fluids and a cap rock seal to limit convective heat loss through fluid leakage. The controls on the system include the density and orientation of fractures, mechanical rock properties, and the local stress field acting on those rocks.

The research presented in this dissertation utilizes diverse data sets to characterize core, wireline borehole logs, and laboratory data to describe the distribution of fractures, rock properties, and the orientation and magnitude of stresses acting on the borehole. The research demonstrates there is a potential resource in the region and describes the controls on the vertical extent of the hydrothermal fluids. The distribution of fractures is controlled by the distribution of elastic rock properties and rock strength. A cap rock seal is present that limits hydrothermal fluid loss from a fractured artesian reservoir at 1,745

m (5,726 ft). In addition to characterization of the resource, this research demonstrates that an equivalent characterization can be used in future exploration wells without the expense and risk of collecting core. It also demonstrates that multiple methods of analysis can be utilized simultaneously when some data are not available. Data collection from deep wellbores involves risk and data loss or tool failure is a possibility. In these cases, our methods show that successful characterization is still possible, saving time and money, and minimizing the financial risk of exploration.

ACKNOWLEDGMENTS

I would first like to thank Dr. James P. Evans for the opportunity to work on such a challenging and interesting project. His commitment to his students is unwavering, not to mention his compassion, generosity, and understanding when it comes to dealing with life's challenges off-campus and on. There are not words to describe the appreciation and admiration I have for him. He is an inspiration as a teacher, a scientist, and a person; truly one of a kind.

Many thanks also go to Dr. John W. Shervais who led the multidisciplinary Hotspot project and entrusted me with the responsibility to lead and manage many aspects of the project that are not presented overtly in this project. It was a once-in-a-lifetime opportunity and is greatly appreciated.

Particular thanks go to Dr. Douglas R Schmitt, who gave me the opportunity to see a new aspect of my project that changed the direction of the research in a big way. His kindness and generosity are greatly appreciated. He stepped up for me at a very difficult time; sharing his lab, his students, and his home so that I could get the data I needed for this project. He also has been extremely generous helping me get to meetings to present our research. Finally, he's just a great guy with a great sense of humor that makes you want to spend time with him. Thank you.

Many thanks to the rest of my committee: Dr. Thomas E. Lachmar and Anthony R. Lowry; other professors: Dr Jeff Walker and Dr. Lee Liberty; and outside professionals: Dr. Bill Dershowitz and Dr. Paul L. LaPointe for the insight, perspective, and opportunity to learn from your experience that wasn't required of you.

Without the help of the many students who worked at the drill sites, the USU core lab, and the University of Alberta rock physics lab, none of this work could have been accomplished. The list is too long to name everybody but a few must be mentioned. Michael Strange and Kelly Bradbury stepped in and contributed much time and effort collecting core data. Not enough can be said about their contribution. Xiwei Chen and Randy Koffman provided critical support in Edmonton doing core tests. Without them, this dissertation could not have been completed. And a collective mention of all the folks who worked so hard at the drill sites and in the core lab. You taught me much about teamwork and leadership.

This project was funded primarily through DOE grant #DE-EE0002848, funded to Dr. John W. Shervais and Dr. James P. Evans. Additional support came from the Geological Society of America Graduate Student Research Grant, the Society of Petrophysicists and Well Log Analysts Foundation Grant, and the ExxonMobil Geoscience Research Grant. Internships offered from Golder Associates, Inc., Occidental Petroleum Corporation, and Encana Oil and Gas Inc. kept me afloat while I finished and provided critical experience.

Finally, the support of friends and family, particularly those in North Carolina, was invaluable and greatly appreciated. I couldn’t have kept it up without you. I love you all.

Thank you,

James Andrew Kessler

CONTENTS

LIST OF TABLES

LIST OF FIGURES

Figures Page

CHAPTER 1

INTRODUCTION

Geothermal energy has the potential to significantly supplement conventional energy sources in some geologic settings. However, the high risk and expense of geothermal exploration often makes economic development infeasible (Tester et al., 2006). Part of the risk can be reduced through improved understanding of the distribution and nature of brittle structures that form fluid pathways for high temperature fluids in a reservoir.

The Snake River Scientific Drilling Program (Project Hotspot) was conducted to develop novel methods to enhance geothermal resources in southern Idaho (Shervais et al., 2013). To accomplish the goals of improving methods to exploit geothermal resources in Project Hotspot, I developed techniques to calculate rock properties and stress conditions that are used to describe the mechanical stratigraphy of the Snake River Plain (SRP) basalts and how this stratigraphy controls fracture distribution and orientation. Discrete fracture data, wireline log data, and unconfined compressive tests are used to model fracture development and identify probable fracture connectivity and permeability in the geothermal fields.

For economic development, the connected pathways of discontinuities must be effective fluid conductors on a scale of sub-meter to hundreds of meters away from the well (Gupta and Roy, 2007). Geothermal projects in natural fracture zones utilize existing discontinuities for fluid flow. Engineered geothermal projects, termed Enhanced Geothermal Systems (EGS), can be developed through hydrofracturing rocks in an elevated thermal zone and harvesting heat through injection and extraction of fluids

(Tester et al., 2006). The design of Enhanced Geothermal systems requires a complete geomechanical model developed from a thorough knowledge of rock mechanical properties along with stress orientations and magnitudes to predict the direction and extent of fracture propagation during stimulation. Regardless of the system, secondary permeability from faults, fractures, and discontinuities is vital for delivery of high-temperature fluids to the production wells in geothermal energy systems.

This dissertation focuses on the characterization of the mechanical properties of the rocks, stress conditions, and brittle structures that create fluid flow pathways in a moderately deep borehole (MH-2) drilled on the Mountain Home Air Force Base, Idaho, in the western Snake River Plain. The borehole was one of three drilled for the Project Hotspot (Shervais et al., 2013). Preliminary interpretation of geothermal gradients and the presence of artesian thermal water at the drill hole from the MH-2 borehole indicate that a potential commercial geothermal energy source may be present in the Mountain Home area. Exploitation of that resource requires an improved understanding of how faults and fractures form fluid pathways in the high-temperature geothermal fields. Particularly when the primary porosity and matrix permeability of rock are very low, secondary permeability features (faults, fractures, and other types of discontinuities) play an important role in delivering high-temperature fluids to geothermal production wells (Gupta and Roy, 2007; Nelson, 2001).

Project Hotspot drilled three deep slimholes to depths of ~2,000 m (6,000 ft) at three sites in the SRP (Figure 1-1). Rocks at these depths do not outcrop so the available data are confined to the one-dimensional vertical profile. Whole rock core was greater than 90% recovered and full suites of wireline borehole log data are available for analysis

from the boreholes. The first borehole, Kimama, was expected to encounter a basalt/rhyolite boundary that represents a fundamental change in the igneous processes through time (Shervais, 2010).

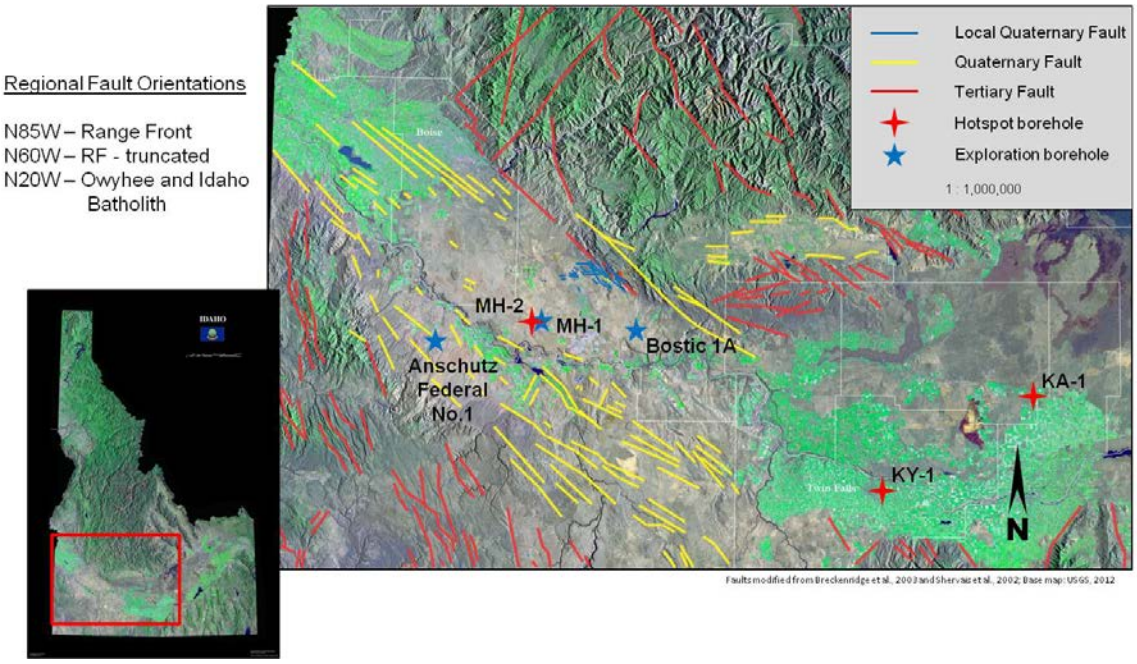

Figure 1-1. Project Hotspot boreholes and the locations of regional faults.

However, the borehole was drilled through basalt and intermittent sediment layers and never crossed the expected basalt/rhyolite boundary (Potter, 2011). The Kimberly drillhole encountered thin units of intermittent basalt layers but is predominantly rhyolite. The Mountain Home borehole passed through ~600 m (2,000 ft) of Pleistocene lake bed sediments before entering a series alternating layers of basalt, altered basalt, and hyaloclastites at ~ 950 m (3,100 ft) depth. For this project, I analyze core and wireline data from the MH-2 borehole drilled near Mountain Home to examine the mechanical stratigraphy, fracture stratigraphy, and stress state to build a geomechanical model and I

develop a geological interpretation of conditions near a potential geothermal reservoir and provide the foundation for analysis of critically stressed fractures that have the potential for high enough permeability to conduct geothermal fluids.

Exploitation of geothermal energy in volcanic regimes like the SRP requires a fundamental understanding of the distribution of fracture permeability in the high-temperature geothermal intervals. Igneous rocks typically have low matrix porosity and possess Type I fractures. Type I fractures provide the majority of storage and permeability while matrix storage and permeability is minimal to negligible (National Resource Council, 1996). Fracture characterization in SRP basalts is complicated by the large number of emplacement-related fractures that are common in low-volume basalt flows. Fractures developed through effective tectonic and overburden stresses interact with and are influenced by the presence of cooling and inflationary fractures that are a result of emplacement of the lava after eruption (Schaefer and Kattenhorn, 2004). An improved method to characterize fractures in volcanic provinces like the SRP is required to reduce risk of geothermal energy exploration. In addition to the complicated of nature of fracture characterization, few fracture or in situ stress data are available for rocks in the deep subsurface of the SRP. Project Hotspot is one of the first projects to collect core and wireline data in thermal regions at depths > 1,800 m (6,000 ft).

Location

The SRP is a volcanic province with thick sections of mantle-derived basalts that erupted in the axial portions of the plain over the past ~ 6 million years (Shervais, 2010; Champion, personal communication) that are similar in composition to oceanic island

basalts like those forming the Hawaiian island chain. Thick sequences of felsic rhyolite caldera complexes are present along the margin of the plain as a result of melting of continental crust from intrusion of the basalts from the hotspot melting source (McCurry, 1996; Pierce and Morgan, 1992). The volcanic sequences record a complete record of volcanism from ~17 Ma to 200 ka in the west and 2 ka in the east (Shervais, 2010).

The borehole at Kimama penetrates interbedded fine-grained sediment from a few meters thick to several hundred meters thick that represent discrete hiatuses between volcanism and are interpreted as relatively short-lived lake beds (Potter, 2011). In the Mountain Home borehole, a thick sequence of fine-grained sediments around 300 – 400 m (1,000 – 1,300 ft) thick below a thin section of Pleistocene basalts were deposited in the lake bed of the ancient Lake Idaho (Ruez, 2009).

The central SRP is at the intersection of several geological and structural features (Figure 1-2). The eastern SRP is a northeast-southwest oriented downwarped plain formed from lithospheric thinning as a result of passage over the hotspot that currently underlies the Yellowstone Plateau (Blackwell, 1989). The horst and graben complex of the Great Basin extends from the south to the west-northwest into eastern Oregon. The oblique-extension, fault-bounded basin of the western SRP is a result of a complex interaction with the hotspot ~17 Ma and western extension of the Basin and Range beginning ~11 Ma (Wood and Clemens, 2002; Shervais et al., 2002). The western SRP is bound by northwest-oriented, high-angle normal faults that are almost orthogonal to the hotspot track and the eastern SRP (Wood and Clemens, 2002). The Idaho batholith, a composite of emplaced plutons, is a source of igneous and metamorphic rocks and structures to the north of the central SRP (Bickford et al., 1981). The SRP is a region of

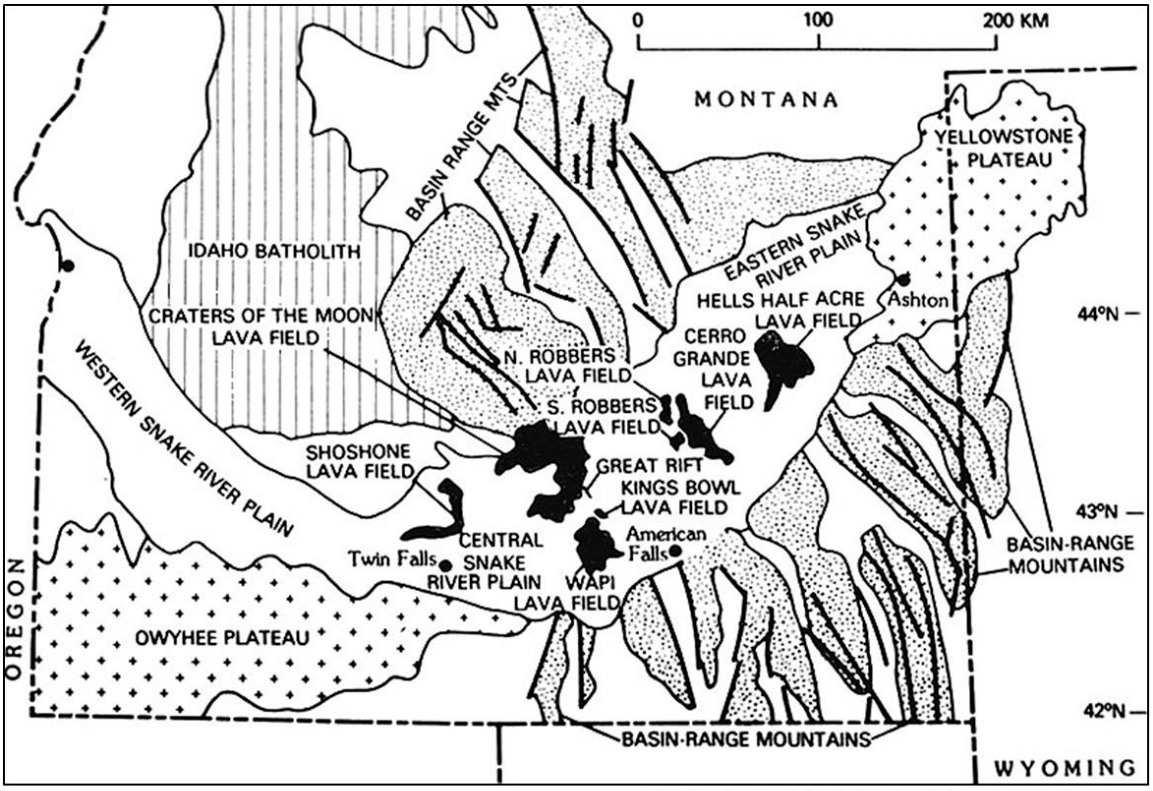

Figure 1-2. Major geological features of southern Idaho: Idaho batholith, WSRP graben, Basin and Range, ESRP downwarp, and the Great Rift.

very high heat flow (Blackwell, 2012) sourced from emplacement of a large amount of basaltic magma in the deep to intermediate-depth crust (Shervais, 2010). The style of volcanism on the SRP creates a thick sequence of high aspect ratio (width-to-height) individual lava flows (Kattenhorn and Schaefer, 2007) for up to 2,000 m (6,500 ft) or more. High-aspect-ratio flows are relatively thin compared to the lateral extent. High permeability zones occur in fracture zones and at rubble zones at the boundaries of the lava flows allow for rapid transport of groundwater in the Snake River Plain Aquifer (Smith, 2002) and geothermal fluids at greater depths.

Research Objectives

Project Hotspot was funded under DOE grant DE-EE0002848 and a grant to Dr. John Shervais from the International Continental Scientific Drilling Program (ICDP) to assess the potential for commercial geothermal energy development in the Snake River Plain, Idaho. With the highest potential for commercial development in the western SRP, this project focused on the MH-2 borehole and the characterization of the controls on the potential geothermal reservoir. With little geological data available previous to drilling MH-2, the approach here is to describe the mechanical and fracture stratigraphy in MH-2 through core analysis, test the potential to duplicate that interpretation through calculation of mechanical properties from wireline logs, describe the current state of stress, and to make a preliminary structural interpretation based on the geomechanical model and failure criteria.

The project required organizing a work flow at the drill sites and designing a core lab at Utah State University. A large number of researchers and technicians were required to handle the acquisition, shipping, storage, and analysis of the core. As part of this project, I helped design and manage the development of the work flow and manpower needed to efficiently manage the large amount of core acquired from the three boreholes. I also designed and managed the small team at the University of Alberta to conduct the unconfined uniaxial compressive experiments that provided the data for the static mechanical properties. This study is a unique approach to describing the mechanical stratigraphy and demonstrates novel methods to handle data gaps and utilize a

variety of data types to describe and compare the fracture and mechanical properties of the basalts.

Dissertation Organization

This dissertation is organized into three core chapters (chapters 2-4) that document the course of research that took place for this project. The work began with detailed logging of fractures in core from the MH-2 borehole and those data are used throughout the project. Chapter 2 describes the unconfined uniaxial compressive tests on rock core samples and the mechanical stratigraphy interpreted from the subsequent calculation of static mechanical rock properties. In Chapter 3, we test the interpretation developed in Chapter 2 with dynamic data calculated from dipole sonic to assess our ability to duplicate the interpretation from an independent set of mechanical rock properties. In Chapter 4, we provide a structural geological interpretation of the rock property distribution, fracture distribution, and stress data to describe a structural scenario that can explain our observations. The end-member conditions represent the bounding potential structural geological conditions based on geomechanics and failure theory.

References

Bickford, M.E., Chase, R.B., Nelson, B.K., Shuster, R.D., Arruda, E.C., 1981. U-Pb studies of zircon cores and overgrowths, and monazite: implications for age and petrogenesis of the northeastern Idaho batholith. J. of Geol. 89 (4), 433-457.

Blackwell, D.D., 2012. Geothermal heat flow map of the U.S. (http://www.smu.edu/~/media/Site/Dedman/Academics/Programs/Geothermal%20Lab/Graphics/SMU2011USHeatFlowMap.ashx?la=en)

Blackwell, D.D., 1989. Regional implications of heat flow of the Snake River Plain, Northwestern United States. Tectonophysics 164, 323-343.

Gupta, H., Roy, S. 2007. Geothermal Energy: An alternate resource for the 21st century. Elsevier, Amsterdam, The Netherlands, 292.

Kattenhorn, S.A., Schaefer, C.J., 2007. Thermal-Mechanical Modeling of Cooling History and Fracture Development in Inflationary Basalt Lava Flows. J. of Volc. and Geotherm. Res. 170, 181 – 197.

McCurry, M., Watkins, A. M., Parker, J. L., Wright, K., and Hughes, S. S., 1996. Preliminary volcanological constraints for sources of high-grade rheomorphic ignimbrites of the Cassia Mountains, Idaho: Implications for the evolution of the Twins Falls volcanic center. Northwest Geol. 26, 81–91.

National Research Council, 1996. Rock Fractures and Fluid Flow: Contemporary Understanding and Applications, National Academy Press, Washington D.C., 551.

Nelson, R., 2001. Geologic Analysis of Naturally Fractured Reservoirs, Gulf Publishing Co., Houston, TX, 352.

Pierce, K.L., L.A. Morgan, 1992. The track of the Yellowstone hotspot: Volcanism, faulting, and uplift. In: P.K. Link, M.A. Kuntz, L.B. Platt, (eds.), Regional Geology of Eastern Idaho and Western Wyoming: Geological Society of America Memoir 179, 1-53.

Potter, K.E., Shervais, J.W., Sant, C.J., 2011. Project Hotspot: Insight into the subsurface stratigraphy and geothermal potential of the Snake River Plain. Geotherm. Res. Counc. Trans. 35, 967-971.

Ruez Jr., D.R., 2009. Framework for stratigraphic analysis of Pliocene fossiliferous deposits at Hagerman Fossil Beds National Monument, Idaho. Rocky Mtn. Geol. 44 (1), 33-70.

Schaefer, C.J., Kattenhorn, S.A., 2004. Characterization and Evolution of Fractures in Low-Volume Pahoehoe Lava Flows, Eastern Snake River Plain, Idaho. Geol. Soc. of Am. Bul. 116, (3/4), 322 – 336.

Shervais, J.W., Schmitt, D.R., Nielson, D., Evans, J.P., Christiansen, E.H., Morgan, L, Pat Shanks, W.C., Prokopenko, A.A., Lachmar, T., Liberty, L.M., Blackwell, D.D., Glen, J.M., Champion. D., Potter, K.E., Kessler, J.A., 2013. First results from HOTSPOT: The Snake River Plain Scientific Drilling Project, Idaho. U.S.A. Sci. Dril. 15, 36 – 45.

Shervais, J.W., Evans, J.P., Christiansen, E.J., Schmitt, D.R., Liberty, L.M., Blackwell, D.D., Glen, J.M., Kessler, J.A,, Potter, K.E., Jean, M.M., Sant, C. J., Freeman, T.G., 2011. Hotspot: The Snake River Geothermal Drilling Project – An Overview. Geothermal Res. Counc. Trans. 35, 995 – 1003.

Shervais, J.W., 2010. Phase 1 Report: The Snake River Geothermal Drilling Project – Innovative Approaches to Geothermal Exploration. Report to the the Dept. of Energy DE-EE0002848. 61.

Shervais J.W., Shroff, G., Vetter, S.K., Matthews, S., Hanan, B.B., McGee, J.J., 2002. Origin and evolution of the western Snake River Plain: Implications from stratigraphy, faulting, and the geochemistry of basalts near Mountain Home, Idaho. In: Bonnichsen, B., White, C.M., McCurry, M., (Eds.), Tectonic and Magmatic Evolution of the Snake River Plain Volcanic Province. Idaho Geol. Surv. Bull. 30, 343-361.

Smith, R., 2002. Geologic Setting of the Snake River Plain Aquifer and Vadose Zone. Vadose Zone J. 3, 47 – 58.

Tester, J.W., Blackwell, D., Petty, S., Richards, M., Moore, M.C., Anderson, B., Livesay, B., Augustine, C., DiPippo, R., Nichols, K., Veatch, R., Drake, E., Toksoz, N., Baria, R., Batchelor, A.S., Garnish, J., 2006. The future of geothermal energy: An assessment of the energy supply potential of engineered geothermal systems (EGS) for the United States. Massachusetts Institute of Technology and Department of Energy Report, for the US DOE Idaho National Laboratory, INL/EXT-06-11746 (2006) presented at the 32nd Workshop on Geothermal Reservoir Engineering, Stanford University, January 22–24, 2007. Available at http://geothermal.inel.gov/publications/future_of_geothermal_energy.pdf.

Wood, S.H., Clemens, D.M., 2002. Geologic and tectonic history of the western Snake River Plain, Idaho and Oregon. In: Bonnichsen, B., White, C.M., McCurry, M., (Eds.), Tectonic and Magmatic Evolution of the Snake River Plain Volcanic Province: Idaho Geol. Surv. Bull. 30, Ê69-103.

CHAPTER 2

UNCONFINED COMPRESSIVE STRESS EXPERIMENTS ON CORE FROM THE SNAKE RIVER PLAIN, IDAHO, USA: BRITTLE FAILURE IN A BASALTIC SEQUENCE AND POTENTIAL GEOTHERMAL RESERVOIR[1]

Abstract

The western Snake River Plain exhibits high crustal heat flow with the potential for commercial geothermal energy development. A ~140°C artesian flow zone was encountered in basalt at a depth of 1,745 m (5,726 ft) in the MH-2 borehole on the Mountain Home Air Force Base, during drilling for the Snake River Scientific Drilling Project (Project Hotspot). Elastic and mechanical properties of rocks are paramount to understanding fracture permeability in crystalline reservoirs and in developing geomechanical models of potential geothermal production sites. We performed 110 unconfined uniaxial compressive stress experiments on core samples over a 530 m (1,739 ft) interval of the borehole to describe the variability in physical properties, elastic properties, and compressive strength of the rocks surrounding the geothermal reservoir. Based on these analyses we define 9 mechanical stratigraphic units. Three sections of rocks consist of relatively weak, plastic, low-permeability, highly altered, reworked basalt, hyaloclastite, and basalt-rich sediments. Those units are interbedded with three moderately strong units and three extremely strong units of unaltered fractured basalt.

---

[1] Paper with coauthors as listed:

J. A. Kessler[a], X. Chen[b], D. R Schmitt[b], M. A. Strange[a], J. P. Evans[a]

[a] Dept of Geology, Utah State University, 4505 Old Main Hill, Logan, Utah 84322 USA

[b] Dept of Physics, University of Alberta, 4-181 CCIS, Edmonton, AB T6G 2E1 Canada

Fracture characterization studies of core and image logs show that fracture density is dependent on rock properties and fracture orientation is independent of rock properties. We interpret the mechanical and fracture stratigraphy to be a control in the presence of high temperature artesian geothermal fluids and a result of inferred regional structure so that fracture orientations are dictated by the regional fault systems. Strong Unit 1 is the fractured potential geothermal reservoir and is the source of the high-temperature fluids discovered during drilling. Overlying Unit 1 is a relatively weak Unit 2 that we interpret as being a cap rock that acts as a hydrothermal seal to the underlying reservoir. The implication for this interpretation is that the cap rock/reservoir pair can be a target in future exploration wells that could be drilled to delineate the extent of the possible resource and the boundaries of the connected fracture network.

Introduction

Discontinuities in the form of fractures, rubble zones, and voids act as primary conduits for fluid flow and are the major component of connectivity, permeability, and fluid storage in low-permeability, crystalline geothermal reservoirs (Nelson, 2001). Type I fractures are those fractures that provide both the primary storage and permeability in a reservoir (Nelson, 2001). The prediction of the location, depth, orientation, and aperture of connected fracture networks in natural fracture systems depends on the understanding of the mechanical and elastic properties of the reservoir rocks. In the cases of Enhanced Geothermal Systems (EGS) or hydrofracturing of reservoir rocks, an understanding of contemporary stress conditions is paramount to understanding how the rocks will fracture during stimulation to enhance fracture permeability.

In the low-volume, stacked basalt flows of the Snake River Plain (SRP), fracture networks are assumed to be the most likely discontinuity to be connected extensively enough to produce high-temperature fluids for commercial geothermal energy development (Gudmundsson et al., 2002; Gupta and Roy, 2007; Kattenhorn and Schaefer, 2007). Vugs, voids, and rubble zones that are connected extensively enough to be viable sources of permeability may be difficult to identify and predict but they can contribute to storage and could contribute to the geothermal system if connected to the fracture network. The MH-2 borehole was drilled on the Mountain Home Air Force (MHAF) Base outside of Mountain Home, Idaho (Figure 1-1). It is in the western Snake River Plain (SRP) and was drilled into the low-volume basalt flows typical of the central and eastern SRP (Shervais et al., 2013) but not before passing through ~700 ft of Pleistocene to Recent surface basalts that overlie ~2,000 ft of Pleistocene lake bed sediments from the ancient Lake Idaho (Bonnichsen and Godchaux, 2002; Wood and Clemens, 2002).

The nature, orientation, and distribution of natural fractures in the SRP are likely a result of cooling and inflation during basalt emplacement and brittle failure in response to the in situ stress conditions. Observations of core samples from MH-2 indicate that the majority of fractures exhibit Mode I failure (Engelder, 1987; Kattenhorn and Schaefer, 2007; Pollard and Aydin, 1988). The presence of slickenlines on a smaller percentage of fracture faces indicate shear offset that are representative of faults or fault systems at depth. In the one-dimensional data set, the amount of offset along the shear surfaces cannot be determined but the number of shear surfaces and clustering of shear surfaces indicates the presence of a fault zone. Cooling and inflationary fractures form during the

deposition of lava as the low-volume flows cool, are inflated by subsequent input of lava to the system, and eventual complete cooling. Those fractures tend to be function of the aspect ratio (width to height) of the individual lava flow as described in Kattenhorn and Schaefer (2007). Fractures that form in response to local stress conditions develop in rocks that compensate for the applied stresses by undergoing brittle failure. Rocks that do not experience brittle failure compensate for the stress by undergoing ductile deformation. The mode of deformation can be predicted by knowing the elastic properties and the compressive strength of the rocks and understanding the stress tensor through calculation of the principal stress magnitudes and measurement of the principal stress orientations. Rocks in the MH-2 borehole below a depth of ~945 m (~3,100 ft) are primarily basalt with sections of highly altered basalts, hyaloclastite, and reworked basaltic sediments. The rock types possess a range of mechanical properties that are measured from core samples to contribute to a geomechanical model that will be used to predict fracture development at depth. A high-temperature, artesian flow zone was encountered in MH-2 at 1,745 m (5,726 ft) bgs with fluid temperatures in excess of 140 °C making it a viable prospect for geothermal energy exploration. Prediction of fracture network connectivity is a fundamental approach to determining the commercial potential of the geothermal resource.

A number of methods have been developed to measure and calculate the elastic properties in the laboratory, on outcrop, and in boreholes (Laubach et al., 2009; Zoback et al., 2003). Here we use unconfined uniaxial compressive stress (UCS) experiments on core samples from the MH-2 borehole near Mountain Home, Idaho. The experiments took place at the Experimental Geophysics Group laboratory at the University of Alberta

in Edmonton, Canada. The UCS experiments provide a method to measure the strain of core samples as a load is applied. From the experimental data, we calculate uniaxial compressive strength (UCS), Young's modulus (E), and Poisson's ratio (ν). Those properties define the failure envelope that is used to predict which rock units in the MH-2 borehole are most likely to experience brittle failure under a given stress state and those that will undergo ductile deformation and will not experience brittle failure. The distribution of fractures with depth in the borehole and their relationships, if any, to stratigraphic boundaries, defines fracture stratigraphy (Laubach et al., 2009; Lorenz et al., 2002; Nelson, 2001). The distribution of elastic and physical properties of the rocks defines mechanical stratigraphy (Laubach et al., 2009). A conceptual geomechanical model can then be used to predict fracture density through the correlative spatial relationships between lithology, fracture stratigraphy, mechanical stratigraphy, and stress conditions.

Uniaxial compressive stress experiments conducted on core samples provide static elastic properties and unconfined compressive strength (ASTM, 2010). The experiments provide the information required to determine the static elastic properties of the samples that experience brittle failure and those that compensate stress load through ductile deformation. In this paper, we present the results of the compressive stress experiments, core descriptions, and fracture measurements from core and acoustic televiewer data in order to: describe the basic lithological stratigraphy, characterize fractures in the borehole and core, define the fracture stratigraphy, examine the correlative stratigraphic and fracture relationships, interpret the mechanical stratigraphy,

and provide the geological foundation for prediction of fracture networks for future exploration work.

This paper provides the geological and mechanical descriptions of rocks at moderate depths in the subsurface of the SRP. This is the first field-based study on rocks at these depths in the Mountain Home area and provides insight into the depths and thicknesses of strong, elastic rock and weak rocks that usually do not undergo brittle deformation and the relationship of the stratigraphy to fractures. A companion paper (Chapter 3) couples this work with borehole log data to develop a method to predict the physical, lithological, and dynamic elastic properties when core, time, or budget are not available for experimental work to measure static properties. This work provides the basis for which further geothermal exploration will advance to assess the potential for commercial geothermal energy development in the western SRP.

Geologic Setting

The MH-2 borehole was drilled in the western SRP (latitude-43.069°, longitude-115.893°; Figure 1-1) and was cored between June 2011 and February 2012 on the Mountain Home Air Force Base outside Mountain Home, Idaho. Whole-rock core was recovered from the entire depth of the borehole with greater than 90% recovery. A large set of fracture data and core samples are available for analysis. A zone of interest (ZOI) for geothermal resources is identified from ~ 1,280 m (~4,200 ft) below ground surface (bgs) to a total depth (TD) of 1,821 m (5,976) ft bgs that includes the artesian thermal zone that flowed 140°C water at the surface in January 2012. For our experimental program, we collected 110 core-sized samples over the ZOI at 55 depth locations. Two

samples were collected at each location in order to determine the reproducibility of the test results to measure mechanical properties and describe the variability of mechanical properties between adjacent samples. The static elastic properties calculated from results of the UCS experiments provide the foundation for a subsequent in-depth geomechanical analysis that will compare the static elastic properties to dynamic elastic properties calculated from wellbore geophysical log data, describe the in situ principal stress directions and magnitudes from breakout and tensile induced fractures, and define the Mohr-Coulomb failure envelopes for the sample locations used in the UCS experiments.

The SRP volcanic province (Figure 1-1) consists of thick sections of mantle-derived basalts that erupted in the axial portions of the plain over the past 6 - 8 million years and are similar in composition to oceanic island basalts like those forming the Hawaiian island chain (Bonnichsen et al., 2008; Bonnichsen and Godchaux, 2002; Shervais et al., 2002) Thick sequences of felsic rhyolite caldera complex deposits are present along the margin of the plain as a result of melting of continental crust during intrusion of basalts from the hotspot melting source (McCurry et al., 1996; Pierce and Morgan, 1992). The volcanic sequences record a complete record of volcanism from ~17 Ma to 200 ka in the west and 2 ka in the east (Shervais, 2010). The SRP is a region of very high heat flow (Blackwell, 2012) sourced from emplacement of a large amount of basaltic magma in the deep to intermediate-depth crust (Shervais, 2010).

The eastern SRP is a northeast-southwest oriented downwarped plain formed from lithospheric thinning and subsidence as a result of passage over the Yellowstone hotspot that currently underlies the Yellowstone Plateau (Blackwell, 1989). The oblique-extension, fault-bounded basin of the western SRP is a result of a complex interaction

with the hotspot ~17 Ma and western extension of the Basin and Range beginning ~11 Ma (Benford et al., 2010; Shervais et al., 2002; Wood and Clemens, 2002). The horst and graben complex of the Great Basin extends from the south to the west-northwest into eastern Oregon and includes the western SRP. The western SRP is bounded by northwest-striking, high-angle normal faults that are almost orthogonal to the hotspot track and the eastern SRP (Wood and Clemens, 2002). The northeastern boundary of the basin is defined by range-front faults that strike in two clusters. Faults near the MH-2 borehole (blue faults in Figure 1-1), as mapped by Shervais (2002), are oriented N60°W and are truncated by younger faults that strike N85°W. The regional faults to the northeast are generally oriented consistently with the N60°W cluster (Figure 1-1; Breckenridge et al., 2003). The basin is bounded to the southwest by high-angle normal faults that define the boundary of the Owyhee Plateau (Benford et al., 2010; Bonnichsen et al., 2008). The plateau boundary faults are consistent with the range-front faults and are oriented N60W while faults on the plateau are oriented more northerly at N20W and are consistent with faults mapped in the Idaho Batholith to the northeast (Breckenridge et al., 2003).

High permeability zones are found in fracture networks and at rubble zones at the boundaries of the lava flows that are conduits for rapid transport of groundwater in the SRPA (Smith, 2002) and geothermal fluids at greater depths. The aquifer is present in the central SRP below the base of the vadose zone at around 60 m (200 ft) to a potential depth of 900 m (3,000 ft) (Sant, 2012; Shervais, 2010; Wood and Low, 1986). Recharge for the aquifer is sourced in the mountains formed by the Idaho batholith. The main drainages that recharge the aquifer include Birch Creek, Little Lost River, and Big Lost

River (Smith, 2002) along with the Snake River itself and irrigation canals used for agricultural purposes on the SRP.

The MH-2 borehole penetrated ~215 m (700 ft) of Pleistocene basalts and ~730 m (2,400 ft) of Pleistocene lacustrine sediments (Figure 2-1), deposited in the lake bed of the ancient Lake Idaho (Ruez, 2009), before entering a series of alternating layers of Miocene basalt, altered basalt, and hyaloclastites to a TD of 1,822 m (5,976 ft).

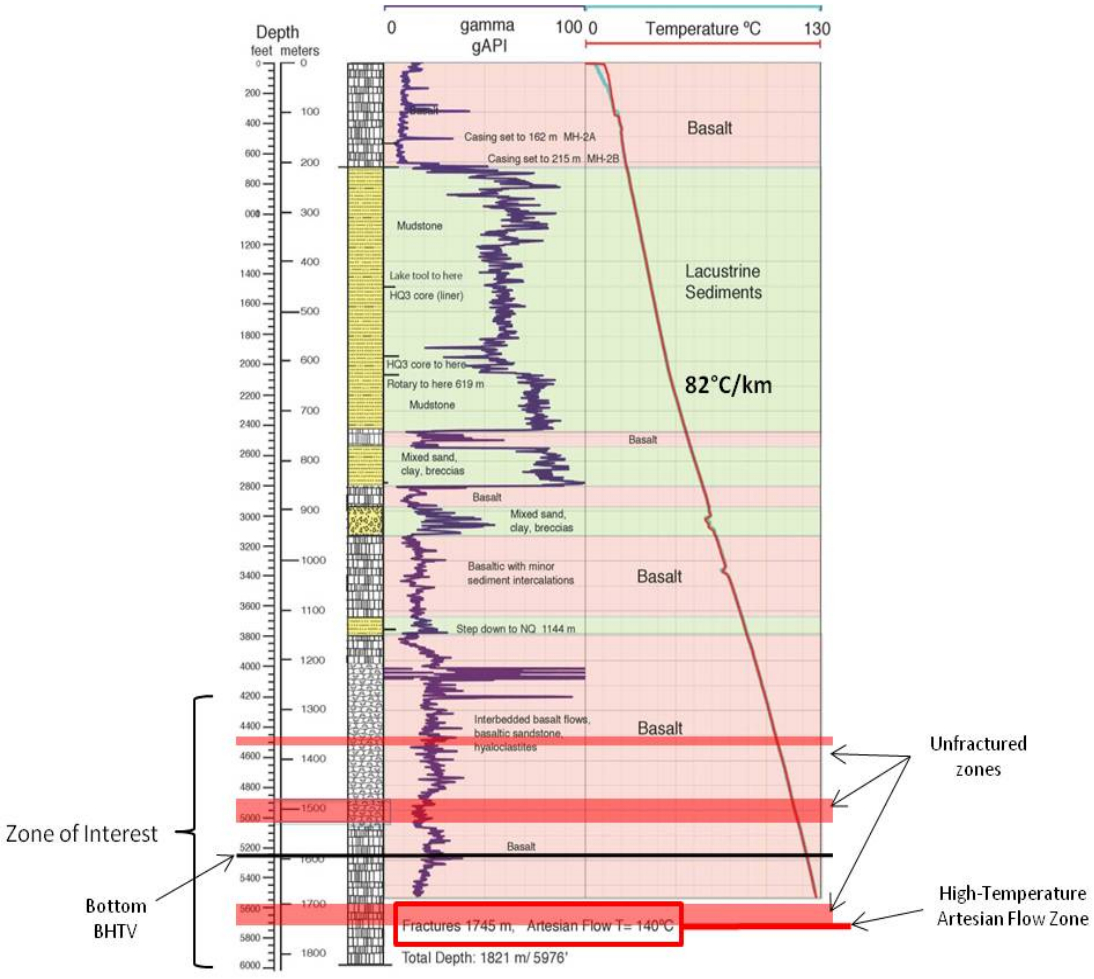

Figure 2-1. Lithological log of the MH-2 borehole with gamma ray and temperature log.

The samples collected here are from the lower Miocene rocks (Shervais, 2002). Large fracture and fault zones exhibit evidence for fluid flow in the form of secondary mineralization, alteration, and brecciation in the deeper portions of the borehole**.** Highly altered basalt is present and is interbedded with hyaloclastite in places (Figure 2-2) demonstrating the interaction of young basalts with fluids. Thermal gradients in the MH-2 borehole are high (~85° C/km) and the equilibrated bottom-hole temperature (BHT) is ~140° C (Blackwell, 2012)**.** The high subsurface temperatures and the potential for subsurface fluid flow through networks of fractures and other discontinuities indicate a potential for geothermal energy development in the western SRP.

Figure 2-2. Examples of samples collected for this study

The drill site was partially chosen based on the Bouger gravity anomaly map by Liberty (2010) from State of Idaho gravity data (Keller et al., 2002), and from the results

of an earlier drilling 10 km to the ESE also on the MHAFB. The gravity model shows an elliptical gravity high that is sub-parallel to the axis of the plain (Figure 2-3). The drill sites were selected at the boundary of a gravity high interpreted as a possible buried caldera in the vicinity of Kimama. Fractures zones around the boundary of the caldera were expected to be zones of high fluid conductivity and convective heat flow. The gravity anomaly could be a result of underplating of the crust from the intrusion of dense mantle material (Glen and Ponce, 2002; Shervais, 2010).

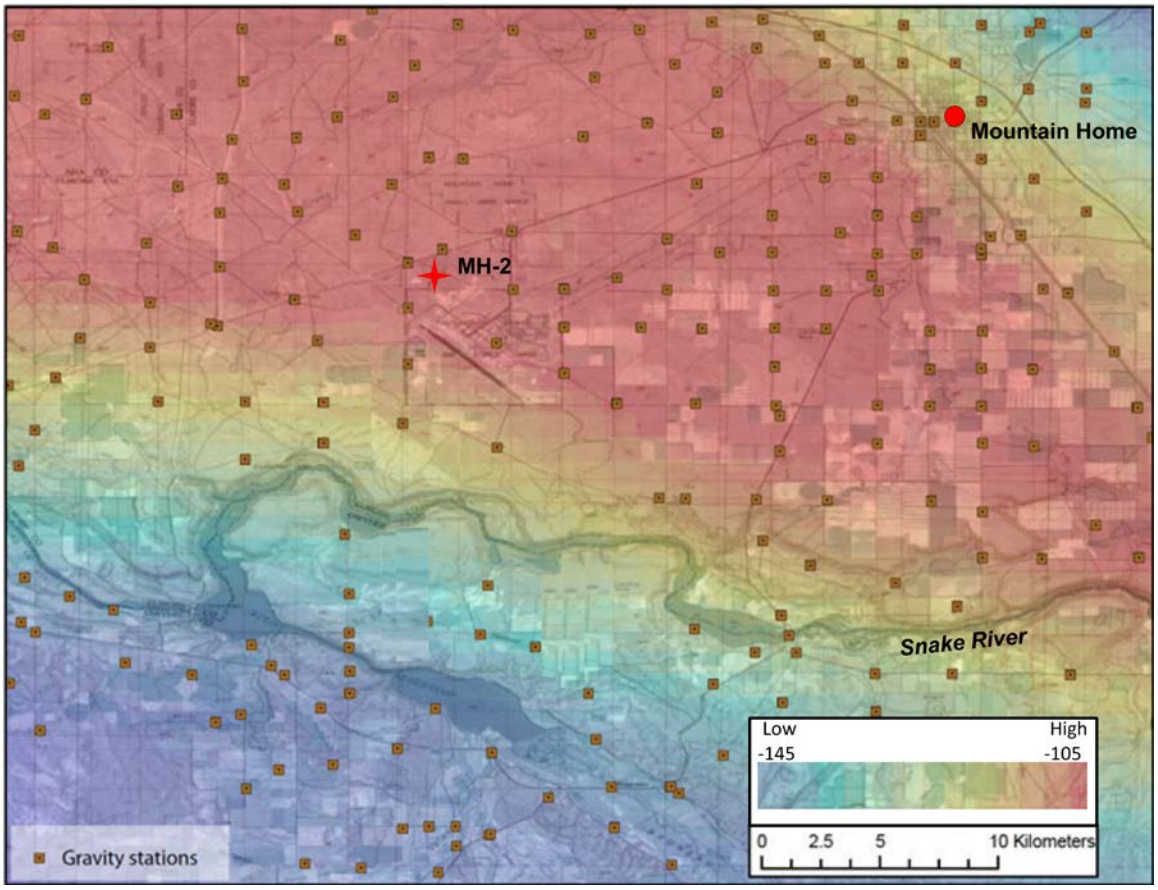

Figure 2-3. Bouger gravity anomaly map (modified from Shervais et al., 2011)

The site was also partially chosen based on the results of the MH-1 well drilled to 1,342 m (4,403 ft) bgs on the MHAFB roughly 3 km (1.9 mi) to the east-northeast of MH-2. That borehole penetrated dominantly silty sands, sandy silts, and clays interbedded with relatively minor basalt flow to a depth of 590 m (1,936 ft). Below that depth the lithology is almost entirely basalt flows with a few interbedded sediment layers. Eleven faults were identified (Lewis and Stone, 1988). That assessment measured a quasi-equilibrated geothermal gradient of 78°C/km and indicated a commercial geothermal resource if drilled to 2,000 m (6,562 ft) depth or more. In the MH-2 borehole, a 140°C artesian hydrothermal system was discovered at 1,745 m (5,726 ft) bgs with a geothermal gradient of 73°C/km. We assume that temperature is equilibrated to drilling mud and that the in situ reservoir temperature could be higher based on preliminary data from clay alteration data (Walker, personal communication). The MH-2 borehole did not penetrate the bottom of the potential geothermal reservoir and the total thickness of the potential reservoir is unknown. It did penetrate several lithological units that we interpret as a reservoir structural/stratigraphic trap system for a potential hydrothermal reservoir that may have the potential for commercial geothermal energy development.

Methods

The zone of interest (ZOI) in the MH-2 borehole is defined by the interval in which we have collected borehole acoustic televiewer (BHTV) data down to TD in the borehole and includes virgin basalt units, altered basalt units and fractured zones down through the high temperature, artesian flow zone. The top of the interval of the BHTV data is 1,286 m (4,220 ft) bgs and TD is 1,821 m (5,976 ft) bgs defining the zone of

interest as a 530 m (1,739 ft) interval at the bottom of the borehole. Sample selection was limited by the practical number of samples that could be prepared and tested in the timeframe that the laboratory was accessible. The goal of sample selection was to obtain a sample set that is distributed over the interval enough to define the mechanical stratigraphy and also be diverse enough to compare samples taken from near fracture zones and those in relatively intact rock. Two samples were intentionally selected because they contained sealed fractures with the goal to test the strength of those previously fractured rocks and compare the results to unfractured samples. The final sample set included 110 individual samples from 55 depth locations. Two samples were taken at each depth location do determine the variability between adjacent samples. A 15 cm (6 in) sample was collected at each depth location and was subdivided into two 5 cm (2 in) samples with the remainder designated for x-ray diffraction (XRD) and x-ray fluorescence (XRF) analyses to be examined in subsequent papers.

The ZOI is within the NQ interval of the borehole and core samples are 4.47 cm (1.85 in) in diameter. Each sample was ground to a tolerance of 0.025 cm (0.010 in) in parallel between the two ends of the sample and within 0.025 cm (0.010 in) of perpendicular between each end and the long side of the core. Size and shape can have a significant effect on the results of strength and elastic moduli calculations (Thuro et al., 2001). In most instances, the vertical sides of the core samples were straight enough to achieve the tolerance thresholds when grinding the ends. In some cases, the sides of the core were not straight and these were noted during analysis of the results. In most cases, however, the samples met the tolerance in parallel and perpendicular and often well exceeded them. Each sample was fitted with a strain gauge aligned parallel to the axial

direction of the load and another oriented perpendicular to the axial load to simultaneously measure strain in the axial and lateral directions in the sample during loading.

Prior to destruction in the press, each sample was measured for dry bulk density, grain density, and pneumatic permeability. Dry bulk density was measured with high-precision calipers and a high precision scale. The diameter and length was measured and used to calculate volume and mass was measured with the scale. Grain density was measured using a He pycnometer. Due to the low matrix porosity and low matrix permeability the values for both dry bulk density and grain density are considered overestimates due to the likelihood of disconnected and isolated pore space within the sample. Pneumatic permeability was measured parallel to the long axis of each sample with a TinyPerm II permeameter. Pneumatic permeability measurements are considered a first-order estimate to evaluate the variability amongst the samples. The complexity of measuring permeability in basalt renders the permeability measurements more of a relative measurement than a true measure of matrix permeability.

Each sample was loaded into the uniaxial press and the strain gauges were wired to a bus connected to a desktop computer for data collection. The press consists of horizontal and parallel upper and lower platens, a hydraulic cylinder connected to a hand pump, a lower riser, a 50,000 lb load cell, and an upper riser. The sample was placed centered on the upper riser between it and the upper platen. The load was applied through the hand pump and hydraulic cylinder. The load cell was also connected to the desktop computer and the load data were recorded during the experiments. A load was applied as continuously as possible to the sample until it reached failure. The strain gauges

measured axial and lateral strain continuously throughout the experiment. Output included the load in pounds, the force applied to the sample from the hydraulic cylinder, the excitation voltage of the power source, and the axial and lateral strain in change of voltage across the strain gauge that are later converted into strain values.

Experimental Data Interpretation

Stress was measured as a function of the force from the hydraulic cylinder applied to the area of the core sample. Strain was measured during each experiment with two foil strain gauges, one aligned in the axial orientation on the core sample and the other oriented perpendicular to that and aligned with the lateral axis of the core sample. The stress and strain data were used to determine uniaxial compressive strength, Young's modulus, and Poisson's ratio for each sample run. Axial compressive strength was determined from identifying the stress load at absolute failure from a plot of the stress-(axial) strain data (Figure 2-4). Young's modulus was determined from plotting a tangent line on the stress-strain curve and identifying the linear portion of the curve. A maximum and minimum limit of the linear portion of the curve was chosen where the stress-strain curve deviated from the tangent (Figure 2-5). Young's modulus was then calculated for each data point along in the range of the linear portion of the curve. A histogram of the results (Figure 2-5) shows the population of Young's modulus values for the linear range. The largest grouping was then chosen as the estimate of Young's modulus for that sample. A similar exercise was undertaken to estimate Poisson's ratio from the lateral strain-axial strain relationship. In order to maintain a reasonable relationship between

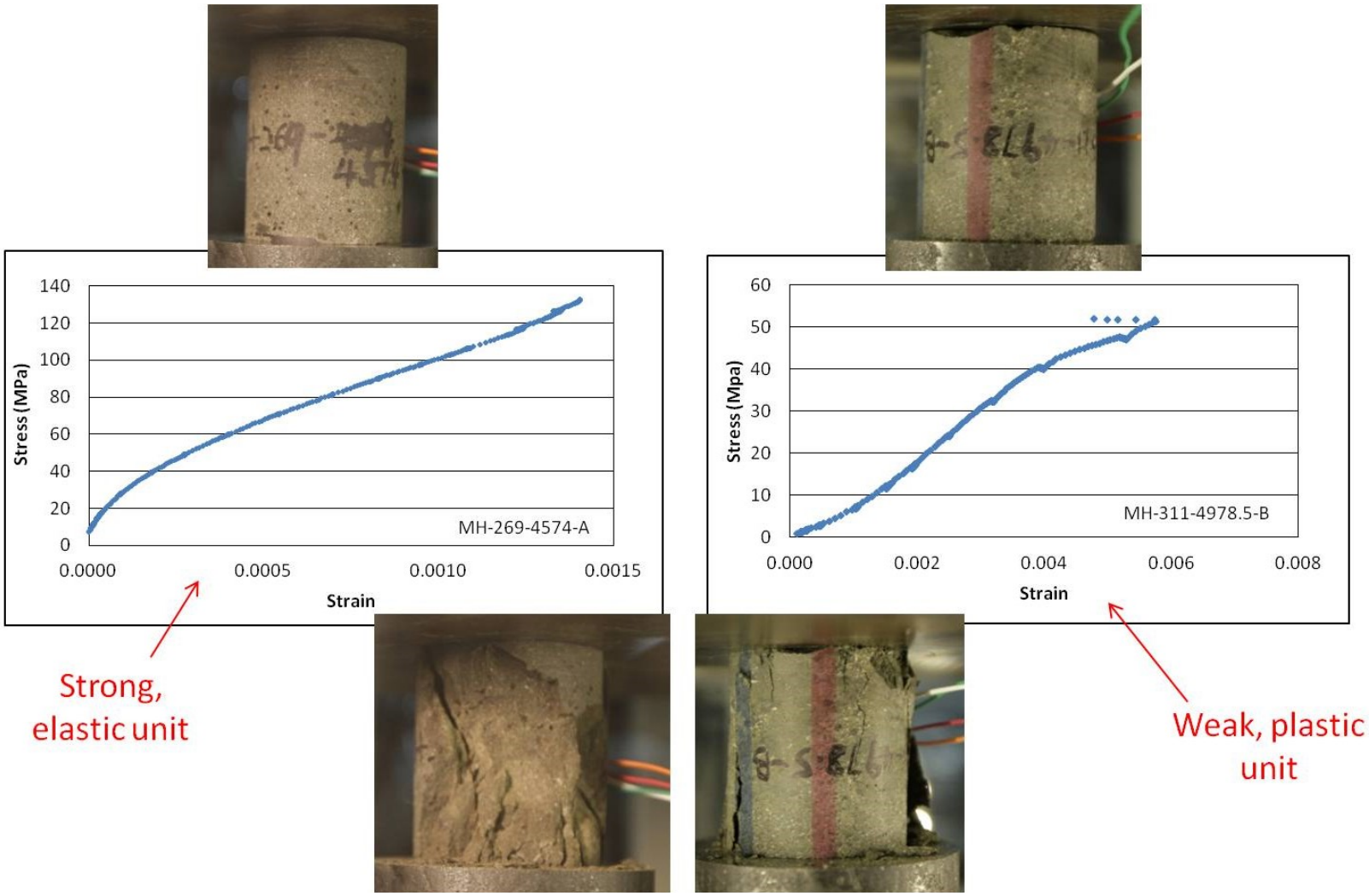

Figure 2-4. Stress-strain relationship showing final failure and the sample compressive strength. Note the magnitudes of stress and strain in both samples.

Young's modulus and Poisson's ratio, we ensured that the upper and lower limits identified from the curves were similar or the same.

Fracture Data from BHTV Log

We measured azimuth, dip and aperture and calibrated the logged fracture to core samples that showed a matching fracture at the same depth. WellCAD© (Rockware, Inc.) was used to map the sinusoids of fractures on the oriented BHTV log. Bedding is not easily identified with the relatively low resolution of the acoustic travel time log, and given the stratigraphy is often thick, relatively homogenous basalt flows, fractures are not often confused with bedding planes. The styles of the fractures in basalt are diverse, however, and the challenge lies in identifying a natural, open or closed, fracture from induced fractures. In the MH-2 borehole, many induced tensile fractures exist that are not linear features at 90° apart, but rather have a morphology similar to a petal-centerline fracture in core. While mapping fractures in the BHTV data, we correlated the logged fractures with the same fractures found in core samples. In the majority of cases, we could match the fracture in the BHTV log with the fracture in the core with a high degree of certainty.

The aperture measurements are taken from the acoustic televiewer data. The apertures are measured as fracture thickness on the logs. A number of challenges exist in interpreting the aperture data. The first being that, at best, aperture is relative aperture since the thickness is measured as the vertical opening of the fracture on the borehole wall rather than perpendicular to the fracture plane. Other challenges include the likelihood that damage to the borehole wall at the edges of the fractures has artificially

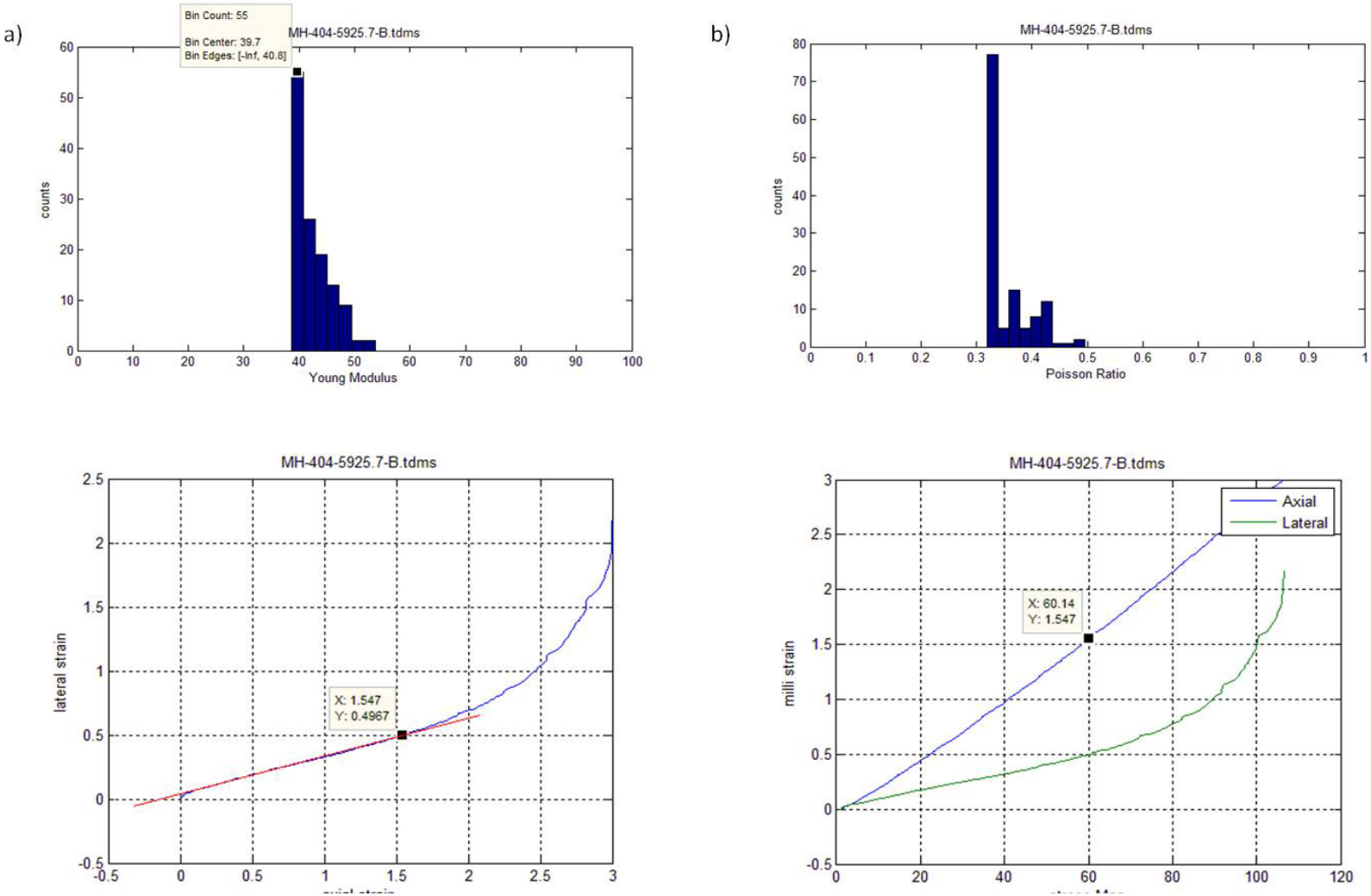

Figure 2-5. Histograms of the population of E and v values calculated from the linear portion of the stress-strain and strain-strain curves, respectively.

widened the fracture aperture at the borehole wall and the fracture width is not representative of the actual fracture aperture. We consider these data to be a measure of relative aperture to help identify the largest fractures but caution using the aperture data as absolute aperture values.

Results

We observe a systematic distribution of dry bulk density, elastic rock properties, rock strength, fracture density, and pneumatic permeability over the ZOI in the MH-2 borehole. We define nine mechanical stratigraphic units based on common groupings between all data sets (Figure 2-6). The mechanical units are defined by the distribution of these properties with respect to depth. The mechanical units are grouped into three categories that we define as: Category 1) very strong, elastic rocks that experience little ductile deformation before undergoing brittle failure at the highest stress loads we could apply; Category 2) moderately strong, elastic rocks that experience a moderate amount of ductile deformation before undergoing brittle failure at moderate stress loads; and Category 3) weak, low-elasticity rocks that experience a high degree of ductile deformation and either undergo brittle failure at very low stresses or do not experience brittle failure at all under the stresses applied in our experiments (Table 2-1). We define the three categories based on the stress-strain behavior of the samples during the UCS experiments. During the UCS experiments, the Category 1 samples experienced a relatively small amount of ductile deformation after exceeding the elastic limit and before failure compared to the other samples. The Category 1 samples also sustained the largest stress loads. The Category 2 rocks demonstrated a larger amount of ductile deformation

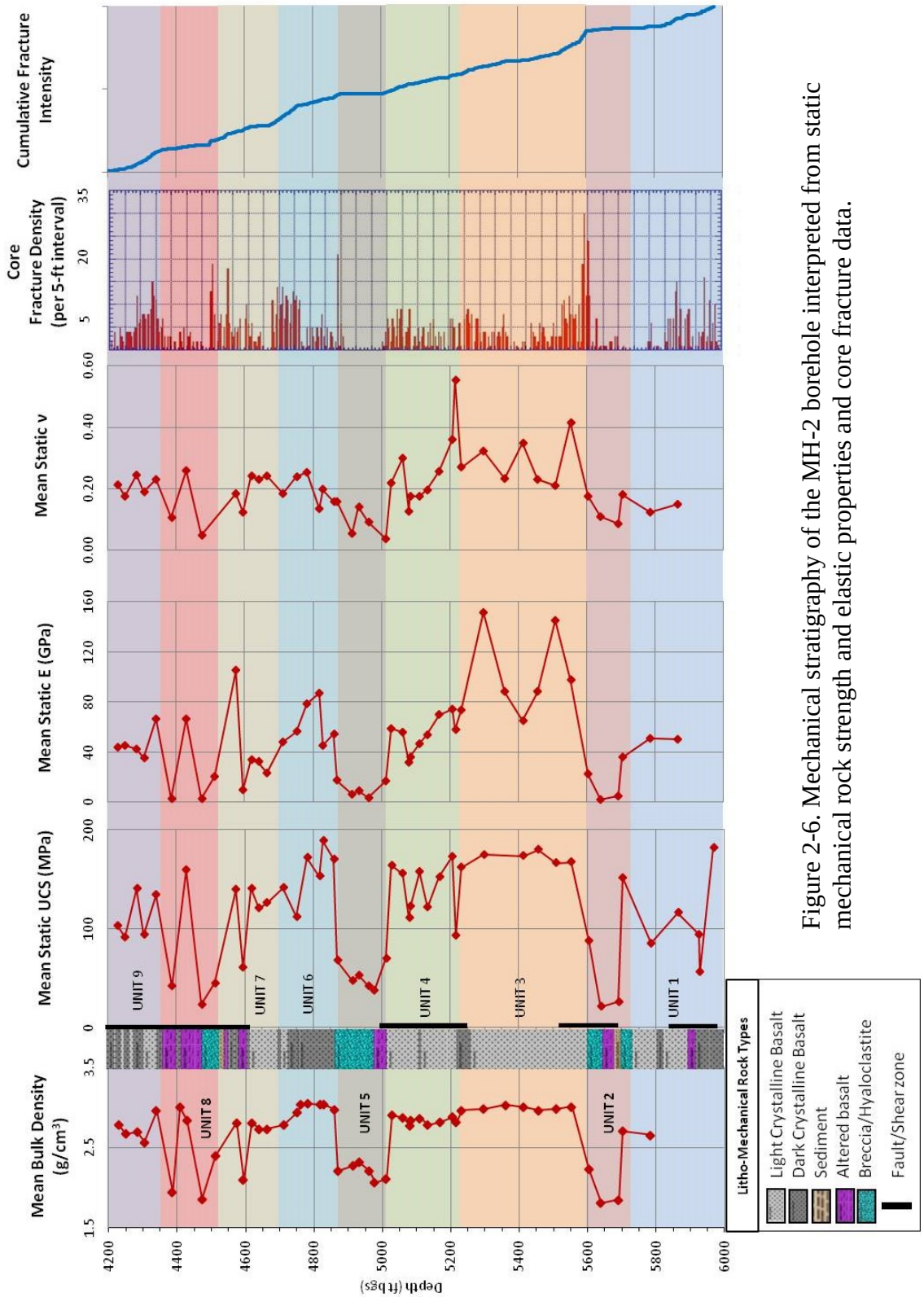

Figure 2-6. Mechanical stratigraphy of the MH-2 borehole interpreted from static mechanical rock strength and elastic properties and core fracture data.

Mechanical Unit	Top Depth (ft)	Bottom Depth (ft)	Top Depth (m)	Bottom Depth (m)	Density (g/cc)	Density Range	Mean Uniaxial Compressive Strength (Mpa)	UCS Range	Mean Young's Modulus (Gpa)	Young's Modulus Range	Mean Poisson's Rati (L/L)	Mean Poisson's Ratio Range	Mean Pneumatic Permeability (μD)
9	4,220	4,450	1,286	1,356	2.68 ± 0.31	1.94 – 3.00	108.6 ± 36.2	41.4 – 158.6	43.0 ± 20.0	2.5 – 66.5	0.20 ± 0.05	0.11 – 0.26	3.8 ± 1.5
8	4,450	4,540	1,356	1,384	2.12 ± 0.27	1.86 – 2.39	33.6 ± 10.8	22.7 – 44.4	11.3 ± 8.7	2.6 – 20.0	0.05		5.3 ± 2.3
7	4,540	4,700	1,384	1,433	2.63 ± 0.27	2.10 – 2.81	117.1 ± 29.4	60.4 – 140.4	40.6 ± 33.2	9.7 – 104.8	0.20 ± 0.05	0.12 – 0.24	2.8 ± 0.4
6	4,700	4,865	1,433	1,483	2.98 ± 0.09	2.78 – 3.05	155.7 ± 24.7	111.7 – 188.4	61.3 ± 15.6	45.2 – 86.9	0.19 ± 0.04	0.14 – 0.25	3.6 ± 0.7
5	4,865	5,020	1,483	1,530	2.19 ± 0.09	2.06 – 2.31	52.4 ± 12.3	36.8 – 69.4	10.2 ± 5.6	3.0 – 17.0	0.10 ± 0.05	0.04 – 0.16	10.4 ± 8.4
4	5,020	5,220	1,530	1,591	2.84 ± 0.04	2.77 – 2.90	138.5 ± 26.0	92.2 – 172.6	53.6 ± 13.2	31.6 – 73.9	0.26 ± 0.12	0.18 – 0.55	3.3 ± 1.2
3	5,220	5,553	1,591	1,693	2.99 ± 0.02	2.96 – 3.03	170.3 ±6.0	161.7 – 179.5	101.0 ± 31.3	64.9 – 151.1	0.29 ± 0.07	0.21 – 0.41	2.6 ± 1.0
2	5,553	5,705	1,693	1,738	1.96 ± 0.19	1.80 – 2.23	44.4 ± 30.3	20.6 – 87.1	9.4 ± 8.9	2.0 – 22.0	0.12 ± 0.04	0.09 – 0.18	4.1 ± 1.9
1	5,705	5,976	1,738	1,821	2.68 ± 0.11	2.53 – 2.90	113.7 ± 42.1	31.8 – 50.8	44.3 ± 7.7	31.8 – 50.8	0.19 ± 0.04	0.12 – 0.24	4.8 ± 1.6

Table 2-1. Summary of results from unconfined uniaxial compressive stress experiments

than Category 1 rocks but with a comparable elastic window. Category 2 samples also failed at stresses that were lower than Category 1 rocks. We assume that the strain rate was consistent enough during all the experiments so that the rate of change in elastic properties during the experiments is directly comparable between each sample. The change in mechanical rock properties and fracture density between Category 1 and Category 2 rocks is significant enough to distinguish them. The larger implication for this study, however, is identification of the Category 3 units. Compared to the stronger, more elastic and brittle units, Category 3 rocks show a small elastic window and experience a relatively long period of ductile deformation before fracture, if the sample fractured at all before loss of function of one or both of the strain gauges. Category 3 units likely play a vital role in establishing the potential geothermal reservoir by trapping hydrothermal fluids in the underlying fractured units. While the categories are not quantitative, they suffice to describe the fundamental differences in the physical and mechanical nature of the units.

Lithological Descriptions of Mechanical Units

The lowermost unit (Unit 1) is a Category 2 unit that contains the potential geothermal reservoir (Figure 2-7a). Fracture density is high and cores indicate the presence of large vugs that may be contributing to fluid storage. The rocks are strong, elastic, aphanitic basalt rich in feldspar (labradorite) with some minerals (Table 2-2) indicating hydrothermal alteration including sulphides and smectite clay (saponite) (Walton and Shiffman, 2003). Some minor vesiculation is present and sealed fractures are seen near the bottom 10 m (33 ft) of the unit with a montmorillonite/chlorite fill. The

intermediate nature of the elastic properties is a result of low-grade hydrothermal alteration as indicated by the mineralogical analysis. The samples underwent brittle failure more often near the bottom of the unit. The variations in mineralogy and elastic properties indicate that hydrothermal alteration could be gradational from top to bottom.

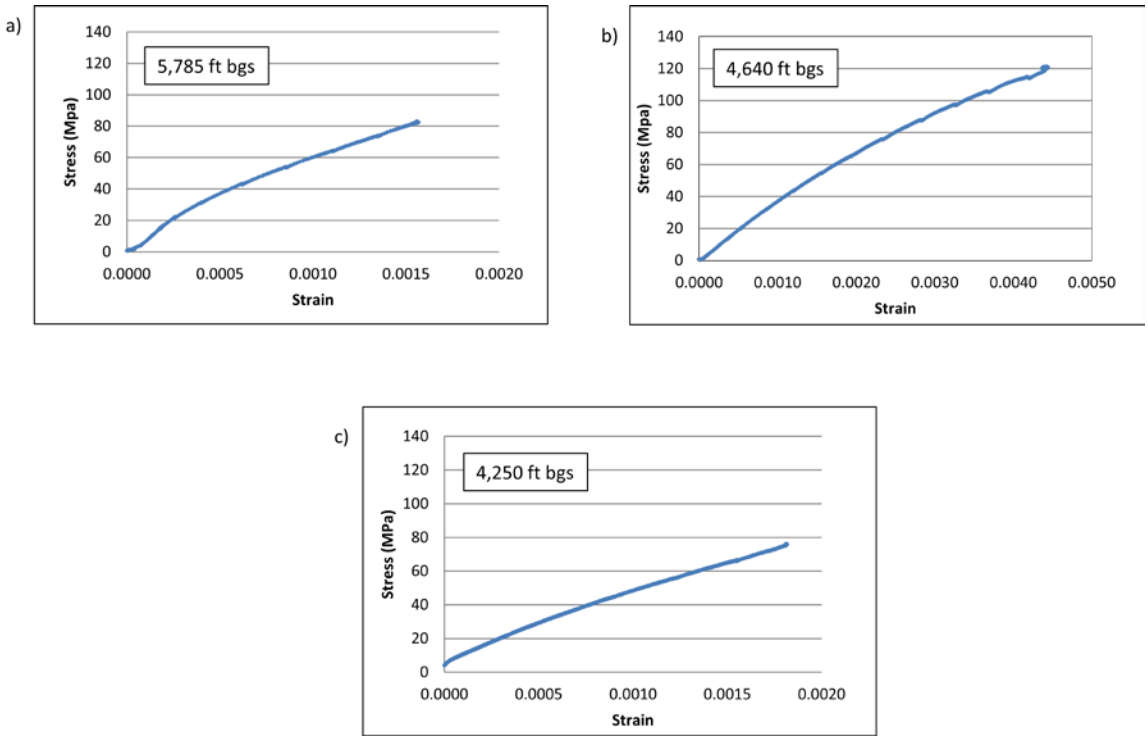

Figure 2-7. Stress-strain relationships for samples from the Category 2 units. a) Unit 1, b) Unit 7, c) Unit 9

Unit 2 is the lowermost Category 3 unit and lacks fractures (Figure 2-8a). The core samples show fine-grained, highly altered basalt with minor silica-filled voids (Figure 2-8a). The presence of smectite clays (saponite) indicates hydrothermal alteration and the presence of feldspar (labradorite) and other silicates (stishovite) may indicate the preservation of original material that has been reworked and redeposited in this unit.

Some samples contain reworked basaltic sediments that appear to have been deposited in a secondary environment from their original volcanic deposition. The unit may be acting as a cap rock to the underlying geothermal reservoir by limiting the propagation of fractures and acting as a seal to contain hydrothermal fluids in the reservoir.

Mechanical Unit	Top Depth (ft)	Bottom Depth (ft)	Top Depth (m)	Bottom Depth (m)	Major Minerals
9	4,220	4,450	1,286	1,356	anorthite, chalcopyrite
8	4,450	4,540	1,356	1,384	quartz, calcite, sulphides
7	4,540	4,700	1,384	1,433	silicates
6	4,700	4,865	1,433	1,483	feldspar, montmorillonite
5	4,865	5,020	1,483	1,530	silicates, montmorillonite, saponite
4	5,020	5,220	1,530	1,591	feldspar, lautite, saponite
3	5,220	5,553	1,591	1,693	anorthite, nontronite
2	5,553	5,705	1,693	1,738	feldspar, silicates, and smectite clay
1	5,705	5,976	1,738	1,821	feldspar, sulphides, and smectite clay

Table 2-2. Summary of x-ray diffraction (XRD) mineralogical results by mechanical unit

This stress-strain relationship shows that the sample exhibited ductile deformation until a fracture developed late in the experiment. This unit had one sample fail during prep due the weak nature of the rock and the reduced strength and cohesion when it got wet during the grinding process.

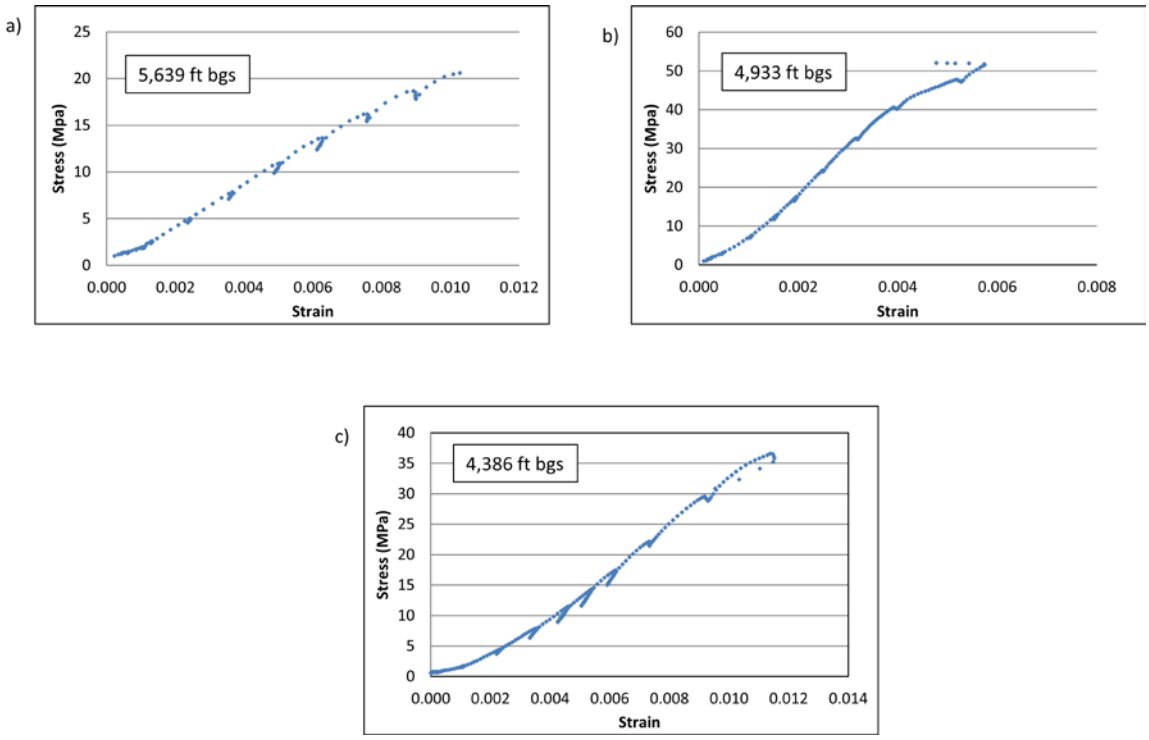

Figure 2-8. Stress-strain relationships for samples from the Category 3 units. a) Unit 2, b) Unit 5, c) Unit 8

Unit 3 is a Category 1 unit that is the strongest unit in the ZOI (Figure 2-9a). The core samples here reveal this unit to be a massive, fine-grained, aphanitic, crystalline, greenish-gray, and dense basalt. The mineral assemblage shows an abundance of anorthite. The presence of nontronite gives the samples a greenish-gray color. This unit contains one sample that did not fail up to a maximum load of 34,000 kg (75,000 lbs).

Unit 4 is a very similar Category 1 rock to Unit 3 (Figure 2-9b) in texture with the exception of having zones of larger grains along with the presence of sporadic mineral-filled vesicles and vugs. The mineral assemblage includes an abundance of feldspar (labradorite, anorthoclase) and minor amount of sulphides (lautite) and clay (saponite). The strength measurements of the rocks in this unit are similar in magnitude to Unit 3 but

individual samples vary more. This is likely the result of vugs or vesicles present in any given sample indicating that the texture is driving local variability more than the lithology.

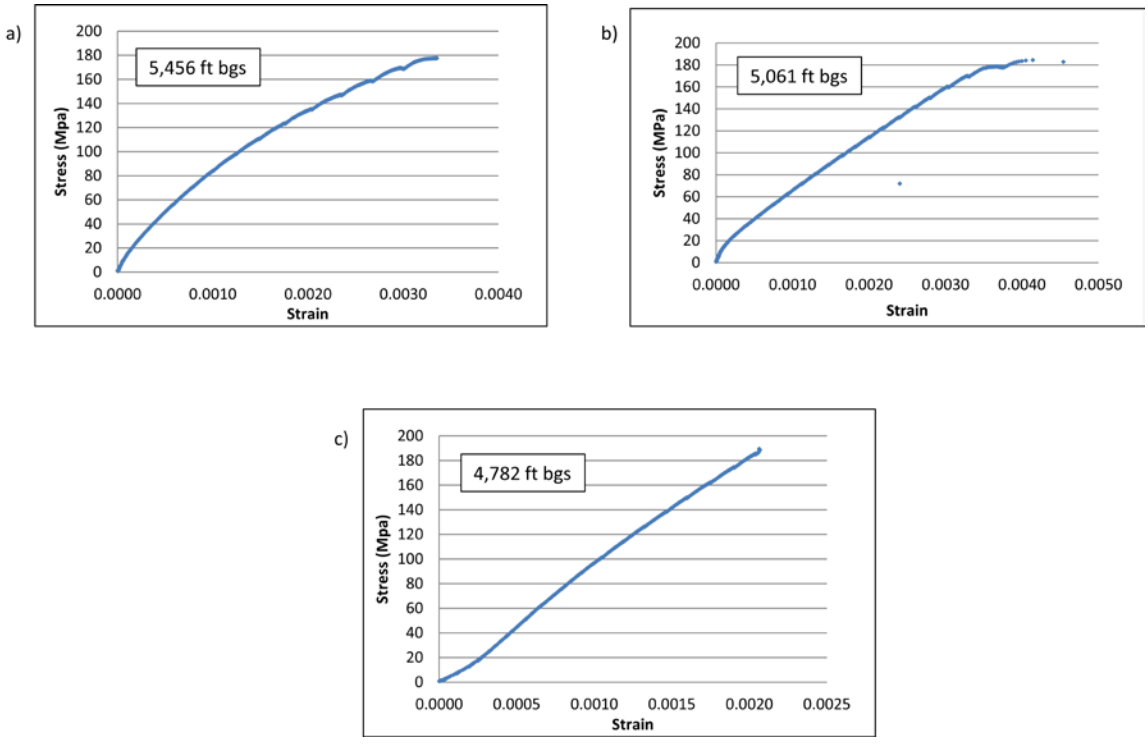

Figure 2-9. Stress-strain relationships for samples from the Category 1 units. a) Unit 3, b) Unit 4, c) Unit 6

Unit 5 is a Category 3 unit very similar to Unit 2 (Figure 2-8b) in elastic properties (Table 2-1) and mineralogical assemblage (Table 2-2). The core samples have a mottled texture with <0.5-cm sized fragments of basalt or altered basalt in a silica "matrix". The mineral assemblage consists of clays formed during hydrothermal alteration (montmorillonite and saponite) as well as silicates (tremolite). Three samples from this unit failed during preparation, indicating the loss of strength and cohesion when wet and during the grinding process. Unit 5 shows no natural fractures in core or in

borehole data indicating that the rocks are sustaining the stress load through ductile deformation and may contribute to the unit acting as a cap to underlying fluids and heat.

Unit 6 is the uppermost Category 1 unit and is very comparable to Unit 3 and Unit 4 in strength and elastic properties (Figure 2-9c). Core samples are gray aphanitic basalt rich in feldspar (labradorite) with some hydrothermally altered clay (montmorillonite). Near the upper boundary, filled vesicles are present. The XRD sample is taken from a section devoid of vesicles but is near minor filled fractures which might explain the presence of montmorillonite in the mineralogical analysis. This unit is the second strongest unit in the ZOI and has some of the closest fracture spacing in the ZOI as indicated by the cumulative fracture intensity curve.

Unit 7 is a Category 2 unit (Figure 2-7b) with moderate and varying strength and elastic properties as demonstrated by the large standard deviation for each property. The core shows slightly more alteration than the strongest units with consistent filled vesiculation throughout. In places, voids and/or vugs are present and filled with silica. A discrete of more highly altered basalt is present at ~1,402 m (~4,600 ft) bgs

Unit 8 is the uppermost Category 3 unit and very few fractures exist in the unit (Figure 2-8c). The core samples are highly altered, light gray, mottled basalt with silica fill that acts partially as a matrix supporting the altered basalt fragments. Parts of the unit may be hyaloclastite but with small (<1 cm) fragments in the silica matrix. The mineral assemblage indicates strong hydrothermal alteration based on the presence of calcite and sulphides (stilleite). Quartz in the analysis could be secondary silica fill. Only one sample from this unit provided a reliable value for Poisson's ratio. The boundaries of this unit are gradational between the intermediate units 7 and 9. The samples vary widely in elastic

properties and the fracture density decreases from the top of Unit 9 to Unit 8 and increases from Unit 8 to the bottom of Unit 7. The boundaries of Unit 7 here are defined by the lack of fractures but it could be argued to adjust them based on the other properties.

Unit 9 is the uppermost Category 2 unit (Figure 2-7c) and is variable down through Unit 8 and into Unit 7. It is similar in color and texture to Unit 1. The unit is gray, fine-grained, aphanitic, basalt with minor silica fill in the lower half of the unit. The mineralogical analysis indicates the presence of original basalt feldspar (anorthite) and secondary alteration sulphides (chalcopyrite). The upper half of the unit displays open and filled moderately-sized (~0.5 – 1.0 cm) vesicles. The variation in elastic properties mimics the variation in texture in this unit but overall it possesses intermediate level strength and elastic properties.

Fracture Characterization

Oriented natural fracture data are logged over the interval from the top of the ZOI to the bottom of the acoustic televiewer log at ~1,596 m (5,235 ft) bgs (Figure 2-10). The fractures sampled by the MH-2 borehole tend to cluster in three groups with dip azimuths clustered between 342º - 45º, 115º - 190º, and 135º - 155º (Figures 11a and 11b). They all dip between 40º and 80º from horizontal (Figure 2-11c). The discrete cluster orientations indicate unique and predictable causes for the fracture orientations. Changes in rock type, rock properties, elastic properties, stress orientations, and stress magnitudes can affect fracture orientation, aperture, and spacing (Cooke et al., 2006; Hanks et al., 1997; Lorenz

et al., 2002; Petrie et al., 2012). Units 1, 2, and essentially all of Unit 3 lack oriented fracture data due to the temperature limits of the slimhole acoustic televiewer instrument.

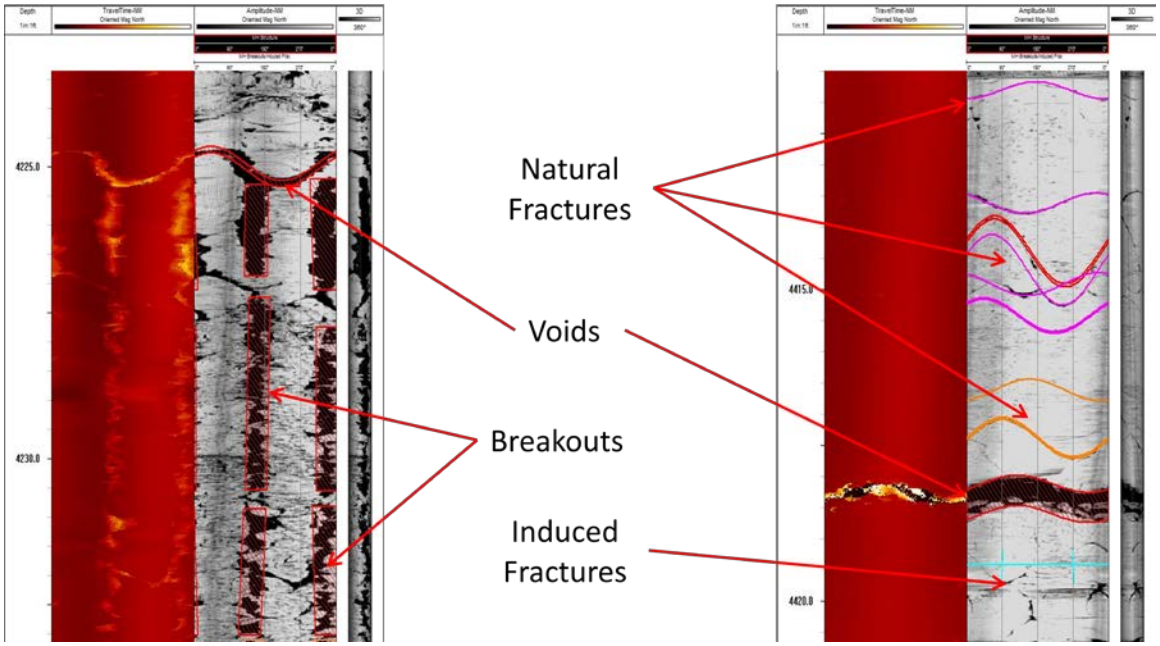

Figure 2-10. Example of acoustic televiewer log from 4,220 – 5,235 ft bgs

We examined the fracture population according to mechanical unit subdivisions to determine if fracture orientation, aperture, or density/spacing is a function of lithology, rock strength, or elastic properties. Each unit has unique fracture orientations (Figure 2-12). For example, the number of fractures is similar in each of the strong, elastic units (4, 6, 7, and 9) but the way the fractures are distributed and oriented is unique for those units above and below Unit 5. Fractures in Unit 3 and Unit 4 seem to be more scattered in orientation, and dip more shallowly than the fractures in the units above Unit 5. Fracture orientations appear to become more organized into conjugate sets of fractures upsection from Unit 5 (Figure 2-12). This may be a function of the variability in lithology so that

thicker lithologic units may fracture more consistently compared to a section of interbedded units that vary in mechanical properties. The implications of this observation are that fracture complexity may be higher in more lithologically variable units. It may also impact hydrofracture design in the case of stimulation in a well. Unit 8 and Unit 9 indicate only one set of the conjugate pair which could indicate a change in faulting style. Fracture aperture may be a function of mechanical stratigraphy and depth (Figure 2-13). The fracture density histogram (Figure 2-14) and cumulative fracture intensity curve show that fracture density and spacing is also unique for each unit. Here we describe the fracture orientation, aperture, and density/spacing, for four strong, elastic units in the ZOI.

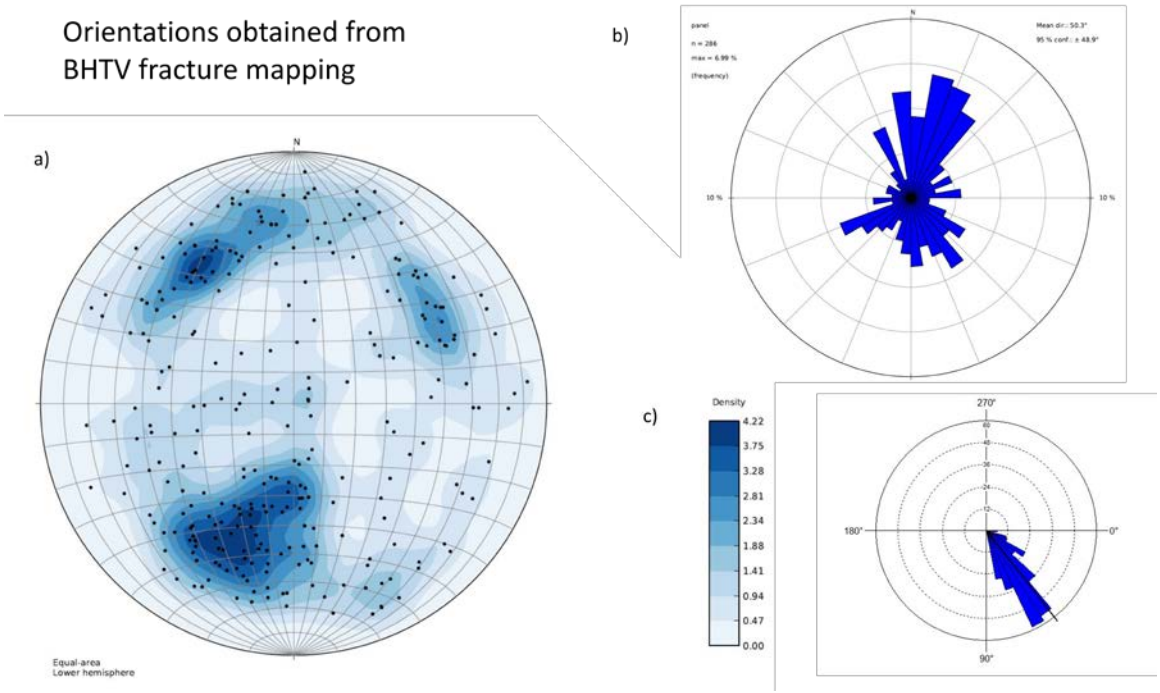

Figure 2-11. Fracture orientation data for the whole population of fractures in the ZOI in the MH-2B borehole. a) stereonet of contoured poles to plane, b) azimuths of dip direction, c) dip angles from horizontal

Upon inspection of fracture data segregated to mechanical unit (Figure 2-12), we can see that there seems to be a fundamental difference between the fracture populations in the strong, elastic units above and below the weak Units 5 and 8. The weak units contain few or no fractures from the televiewer log or from core. Units 3 and 4 seem to have more scatter in the fracture population with more low-angle fractures than Units 6 and 7, and Unit 9 that is separated from Units 6 and 7 by Unit 8. The high angle fractures in Units 3 and 4 have similar strike directions as the dominant populations in the strong, elastic units above Unit 5 but have antithetical dip directions. Two of the stronger groupings in Units 3 and 4 also strike NW-SE and NE-SW. The fractures in Units 6 and 7 seem to have a dominant dip that is > 45° and are striking in two general directions, WNW-ESE and NE-SW. Unit 9 has essentially one dominant grouping of fractures that also strikes NW-SE but is dipping between 30° and 40° so are not as steeply dipping as those in Units 6 and 7 but are steeper than those in Units 3 and 4. The common strike directions among all the strong, elastic units indicate that the fractures are in response to a common stress field. The variation in dip directions could be a result of local perturbations in the differential stress caused by variations in the bed thickness, lithology, degree of alteration, or physical undulation of individual lava flows that are difficult to determine from a single borehole.

Fracture aperture also appears to be a function of mechanical stratigraphy defined from the experimentally derived values (Figure 2-13). We see that most fracture aperture measurements are < 5 mm for all the strong, elastic units that have measurable fracture aperture. There is a clear distinction between the aperture measurements in Units 4 and 6 compared to Units 7 and 9. The uppermost strong, elastic units have a greater number of

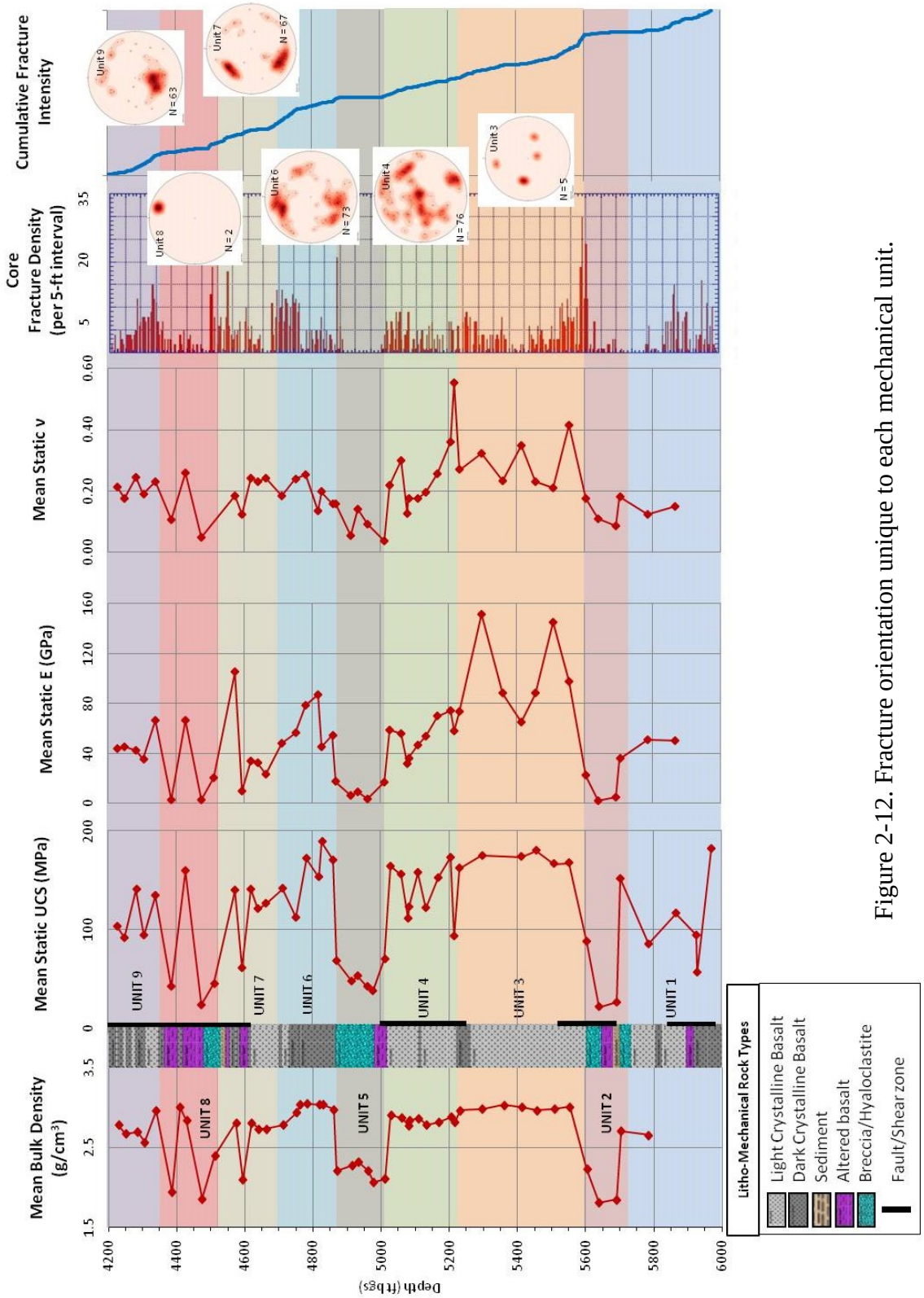

Figure 2-12. Fracture orientation unique to each mechanical unit.

fractures with apertures > 5mm. The patterns are consistent with the mechanical units. Here we rely on the relative aperture change between mechanical units. Most fractures in the acoustic televiewer interval are sealed but we suspect some washout has taken place at the borehole wall that might give a false indication of fracture aperture and we might be overestimating the aperture in that case. Despite that possibility, there is still an apparent relationship between fracture aperture and mechanical stratigraphy. The strong variability in the rock strength and elastic properties in Units 7 and 9 (Figure 2-12) may be a cause for the presence of large aperture fractures as well. A considerable amount of high temperature alteration has taken place and the change in rock properties is a gradual one from the base of Unit 7 to the top of Unit 9 with Unit 8 being the highest altered rock that exhibits ductile deformation.

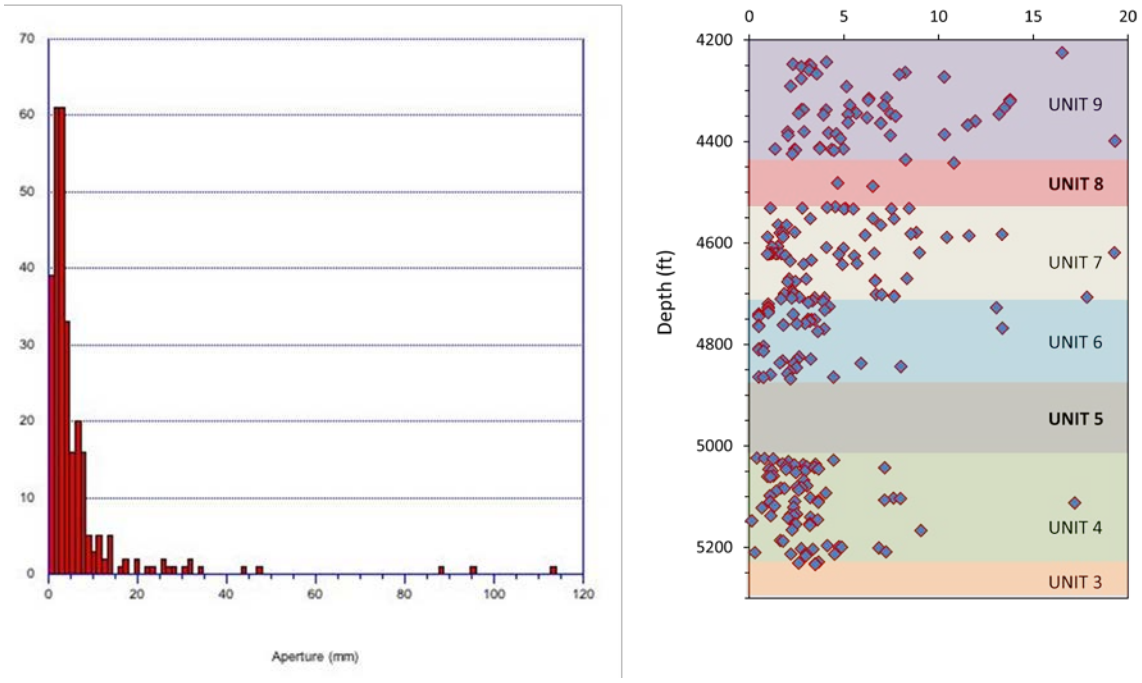

Figure 2-13. Total fracture aperture and fracture aperture with depth in the MH-2 borehole.

Unit 4 has a consistently spaced fracture density throughout the unit with the exception of two to three sections that have few or no fractures (Figure 2-14). These sections are also visible on the fracture density histogram.

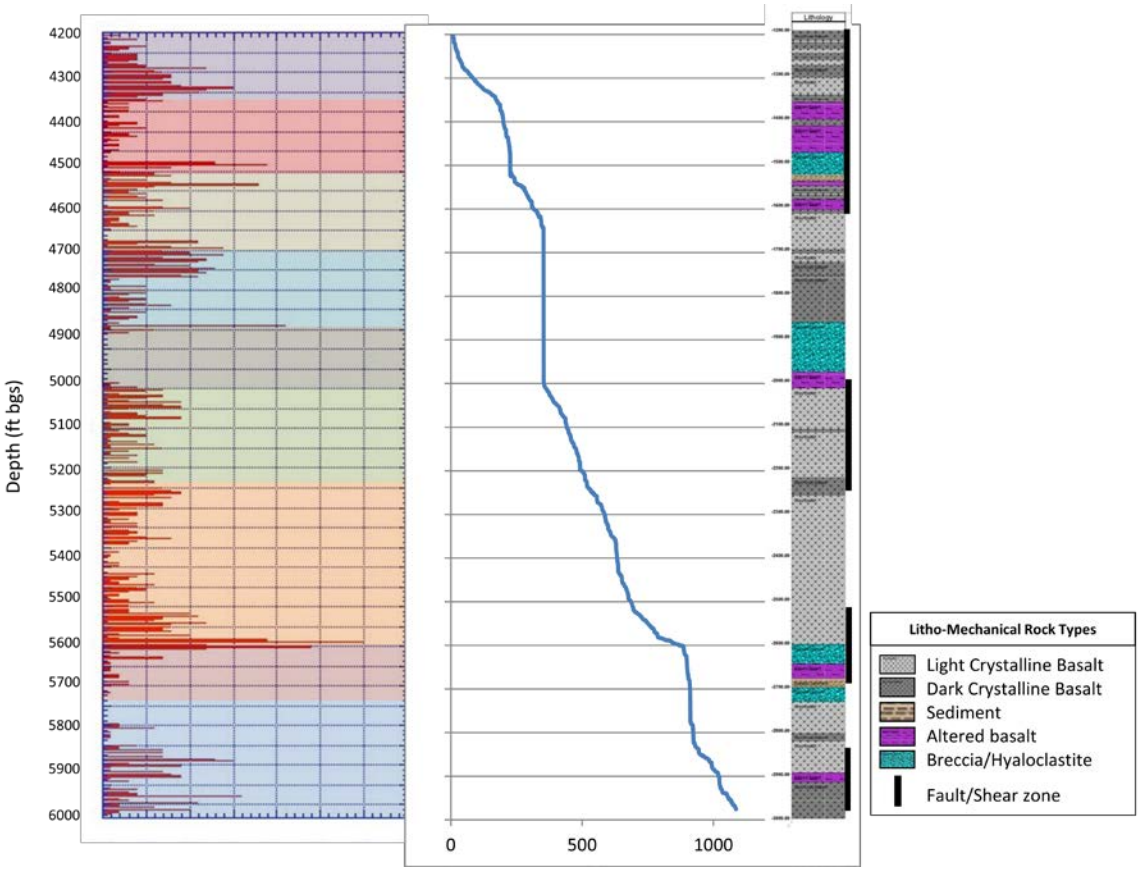

Figure 2-14. Fracture density and cumulative fracture intensity in the ZOI in the MH-2 borehole. Black bars are shear zones delineated by clusters of slickenlines on fracture surfaces.

Unit 6 has a very consistent fracture population with the only obvious variation taking place at the change in slope of the cumulative intensity curve. The change shows a decrease in the fracture density but the section is not devoid of fractures for much of that interval and we see in the fracture density histogram that there are not many empty bins.

The cumulative fracture intensity curve for Unit 7 is quite different in that it has as many as seven or more sections that are devoid of fractures. Unit 9 is similar to Unit 7 in that it has as many as four or more sections that are devoid of fractures and this supports the interpretation that Unit 7 and Unit 9 have properties that are similar and are gradational around Unit 8. While there are many possible explanations for the distribution of fractures in the ZOI, they appear to be coincident with the distribution of rock properties and elastic properties defined by the mechanical stratigraphy.

Cap Rock-Reservoir Interface

We observe over 100 shear plane surfaces identified by the presence of slickenline slip indicators (Figure 2-15) in the MH-2 borehole. We group these into four general shear zones based on the distribution of slip surfaces throughout the borehole. The large number of shear surfaces and an apparent lack of order in the slip directions is an indication that the borehole was drilled into or near a fault zone at the depths of the ZOI. The small faults could also be a result of tectonic strain in the area without being a direct result of a larger organized fault system. We discern that faulting is a contributing mechanism for emplacement of hydrothermally altered basalt, hyaloclastite, and reworked basaltic sediments in sharp contact with unaltered crystalline basalt.

Discussion

We utilize whole rock core, ultrasonic acoustic televiewer logs, unconfined uniaxial stress experiments, and physical rock properties from a borehole drilled into a potential geothermal reservoir to describe the variation in rock lithology, physical

properties, elastic properties, and rock strength. We show that there are at least three zones of altered basalt, reworked basaltic sediments, or hyaloclastite in the ZOI of MH-2 that correspond to a decrease in uniaxial compressive strength and bulk density while there is a nominal increase in the pneumatic permeability measurements in these zones. We also show that Young's modulus and Poisson's ratio correspond to the degree of alteration, lithology as seen in core, and in the mineralogical analysis. Young's modulus and Poisson's ratio also decrease considerably in the altered zones. Gurocak and Kilic (2005) show that the degree of weathering and alteration in basalts is related to

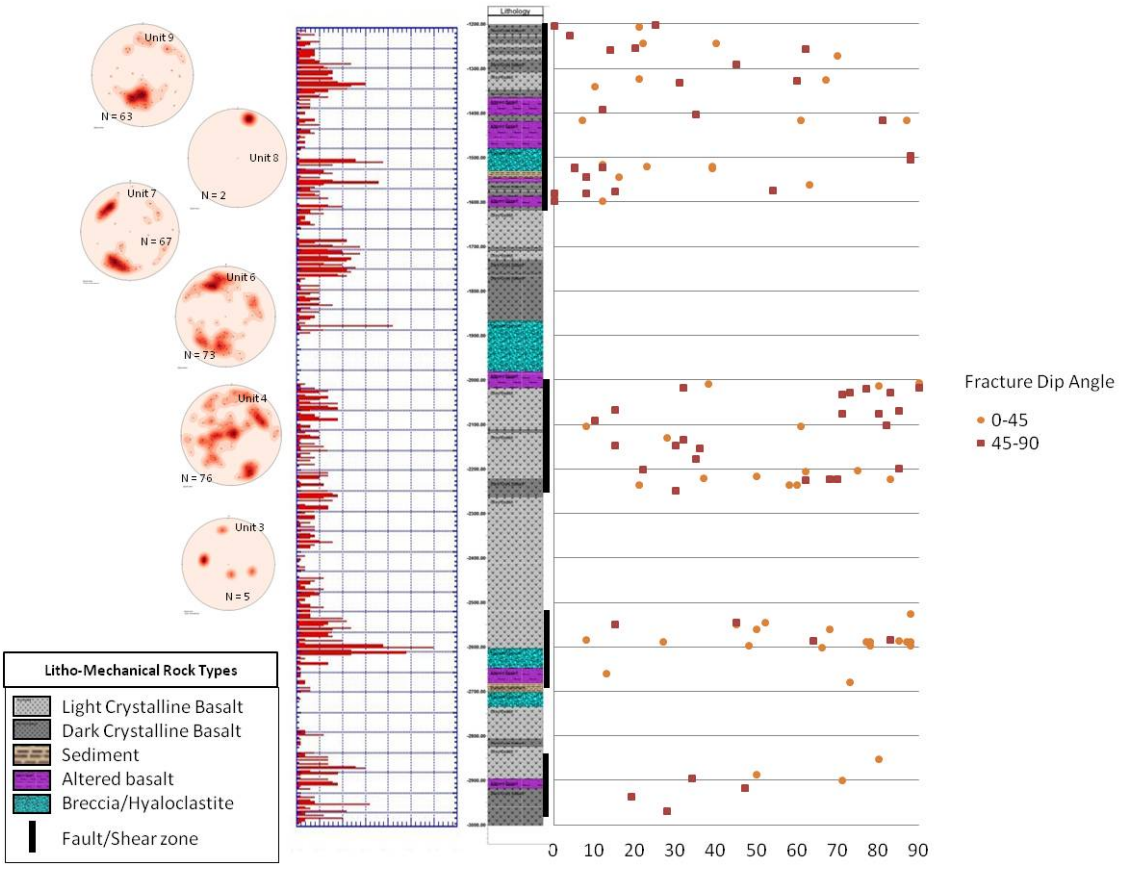

Figure 2-15. Slickenline dip relative to fracture dip, with fracture density, orientations by mechanical unit, and lithology; black bars are shear/fault zones

the geomechanical properties. Among other properties, the uniaxial compressive strength decreases with the degree of weathering while porosity increases and bulk density decreases. We have observed the change in lithology and mechanical properties to be a result of emplacement of altered basalt, basaltic sediments, and/or hyaloclastite onto strong, elastic units through faulting. We interpret the resulting stratigraphy to form a trap for hydrothermal fluids in the underlying fractured geothermal reservoir.

In our interpretation, the material and mechanical contrast at the Unit 1/Unit 2 boundary control fluid and heat flow within the potential geothermal reservoir in Unit 1. The mechanical differences between Unit 1 and Unit 2 effectively make Unit 2 a cap rockcap rock that traps heat and high-temperature fluids within the fractured Unit 1. The importance of the Unit 2 cap rock to trapping heat and fluids means the strong rock-weak rock pairing of Unit 1 and Unit 2 can be used as a target in future exploration wells. The sharp contact between Unit 1 and Unit 2 may be related to a set of shear failure planes that may indicate that the stratigraphic relationship between Unit 1and Unit 2 may be structurally controlled and they have been juxtaposed through faulting. In a one-dimensional data set, we cannot determine if the spatial relationship is a purely structural trap but our observations indicate that both structure and stratigraphy are important to making Unit 2 a competent cap rock.

Research that examines the relationship between fractures and the mechanical properties in fine-grained sedimentary rocks (Cooke et al., 2006) and crystalline rocks (Guddmunsson et al., 2002; LaPointe, 1987) has shown that the mechanical properties of these rocks controls the distribution of fractures that form the primary storage and permeability in subsurface fluids systems. Our data show considerable scatter between

fracture density and rock properties (Figure 2-16). However, there appears to be some predictable relationships between uniaxial compressive strength, Young's modulus, bulk density, and Poisson's ratio. While there is a large degree of scatter in the data for all four properties, we can see a general trend of increasing fracture density with increasing UCS and Young's modulus. Bulk density and Poisson's ratio seem to correlate to higher fracture density within particular ranges. Fracture density is highest in the bulk density range between 2.807 and 2,956 g/cm^3. The range of fracture density within this range of bulk density indicates that bulk density is representative more of the degree of alteration rather than the fracture density. The range of Poisson's ratio with increased fracture density is between 0.18 and 0.24.

Our interpretation is that the uncertainty in the Poisson ratio measurements renders that property a weak predictor of fracture density. Fracture orientation appears to become more organized in mechanical units above Unit 5 than those in the strong, elastic units between Unit 2 and Unit 5 (Figure 2-12). The systematic change in orientation upsection is an indication that fracture orientation is independent of mechanical rock properties. The amount of scatter in the data can be explained by the nature of the experiments through the limited control on load rate and sample preparation and that we represent a range of rock properties from a single sample. However, we are able to interpret the results, supported by core samples, to demonstrate that the mechanical properties of the altered and reworked basalt rocks in the MH-2 borehole can be used to predict the presence of fracture networks and, more definitively, the weak units that act as a seal to the underlying geothermal reservoir.

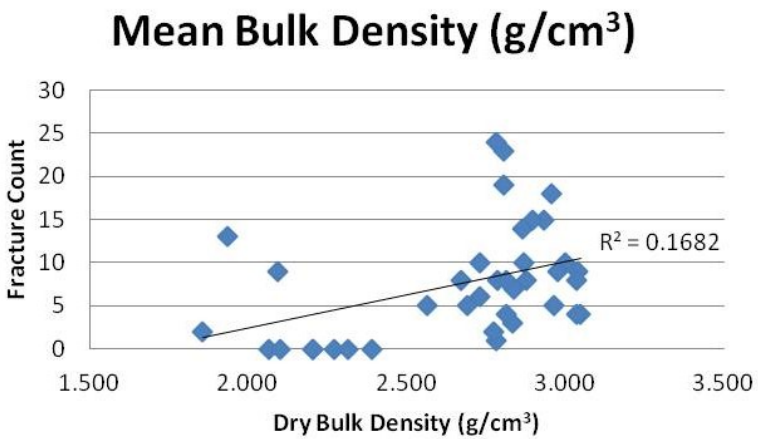

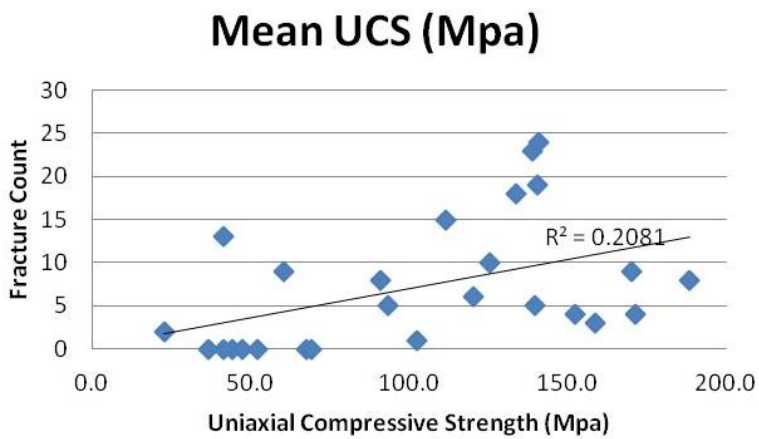

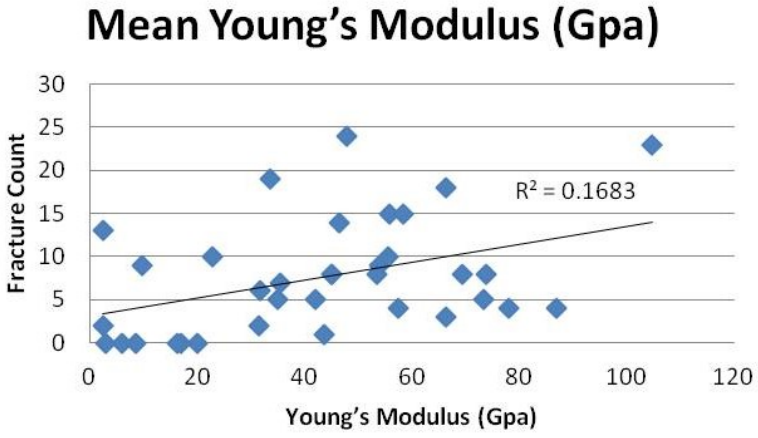

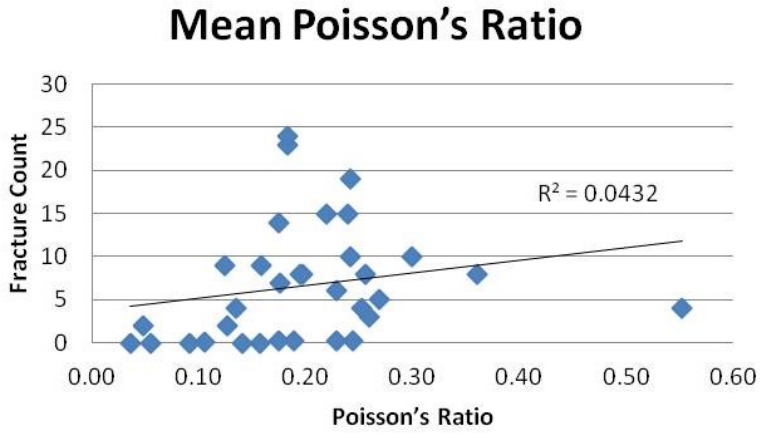

Figure 2-16. Correlation between fracture density and mechanical properties

We would not expect basalt that had been hydrothermally altered to have a sharp, distinct contact with the original basalt. We would expect that contact to be gradational and over a considerable interval of depth. Instead, we observe a distinct contact and the presence of multiple shear surfaces. We are limited to a one-dimensional dataset so cannot speculate to the spatial relationship of the stratigraphy and structure in three-dimensions. We can conclude, however, that both structure and stratigraphy are important contributors to the development of the weak, plastic cap rock/strong, elastic reservoir pair that we identify here as a potential target for future exploration wells. Wood and Clemens (2002) and Shervais et al. (2002) describe simplified models of the structure of the western Snake River Plain with large basin-bounding normal faults and fault zones along with intrabasinal antithetical normal faults offsetting the Miocene basalts at depth. The location of the intrabasinal faults are inferred from unit thicknesses and depths from several boreholes drilled in the western SRP (Arney et al., 1980; Lewis and Stone, 1988; McIntyre, 1979; Wood and Anderson, 1981). A detailed description of the intrabasinal structure in the western SRP remains unavailable but our observations from the MH-2 borehole support some faulting in the basin the result of which is a complex set of stratigraphic relationships and a complex geothermal system.

The fracture patterns (Figure 2-12) show a relationship between the degree of organization in fracture orientation and the mechanical unit from which they were measured. The fractures above weak unit 5 appear to cluster into two main orientations with generally consistent conjugate sets of fractures, particularly in Unit 6 and Unit 7. The fractures in Unit 8 and Unit 9 are unimodal but are consistently oriented with the fractures in Unit 6 and Unit 7 varying only slightly in dip angle. In some cases only one

set develops or the two sets form at different times (Lorenz, personal communication, 2014). While the dip angles vary slightly the fracture orientations are consistent with strong stress anisotropy. The fractures measured in Unit 3 and Unit 4 are more randomly oriented than the fractures in the units above. The physical and elastic rock properties are comparable with the units above that have well organized fracture orientations. As discussed above, fracture density appears to be a function of rock properties to some extent. However, we observe that rocks with similar properties develop fractures with very different orientations. The orientations of those fractures are apparently independent of rock properties. The organized fracture sets in the upper units are an indication that they formed under similar stress fields and that the stress orientation is the primary control of fracture orientation. Less organization in fracture orientation is an indication of multiple modes of failure and could be a combination of fracturing from far-field stresses, local stress perturbations, or cooling of lava (thermal cracks).

In our interpretation, the independence of fracture orientation from mechanical or lithological stratigraphy means that fracture orientations are a function of the regional structural geology and the far-field stresses acting on the rock in the borehole. We discuss the stresses and structural interpretations in detail in a companion paper (Chapter 3). Here we infer from the presence of a relatively large number of faulted shear surfaces (Figure 2-15) that the faults are controlling the fracture orientations to some extent in the mechanical units above Unit 5. The relative lack of faulted surfaces in Unit 3 and Unit 4 is an indication of a fundamental change in the way rocks respond to the far-field stresses above and below Unit 5. Fracture orientations in Unit 6 and Unit 7 show that fractures appear to develop orientation clusters of fracture density moving up section away from

Unit 5. The decrease in scatter from Unit 6 to Unit 7 is an indication that the method of deformation in Unit 5 in response to the stress field is affecting a portion of the fractures in Unit 6. We interpret that relationship to be a function of local stress perturbations caused by ductile shearing in Unit 5. Where it is in contact with the lower rocks of Unit 6, ductile deformation distorts the stress field locally and causes scatter in a portion of the fractures formed in Unit 6. If we assume that the vertical stress is the maximum principal stress, then Unit 3 and Unit 4 could both be affected by the weak units above and below. Being sandwiched between two weak units that undergo ductile shear could be affecting the way that the strong, elastic rocks fracture under the maximum principal stress direction. The conceptual model is that much of the strain is accumulated in ductile deformation in Unit 2 and Unit 5 above and below Unit 3 and Unit 4.

An additional source of the fracture and fault orientation discrepancy is that the fractures in the units above Unit 5 are shear plane faults and fail according to the regional stress field while the fractures in Units 3 and 4 are hydraulic fractures that formed under overpressure conditions at some point in the past. If Unit 2 and Unit 5 act as flow barriers, they could have prevented fluid loss until pore pressures exceeded the minimum principal stress and fractured the rocks. Overpressured conditions can produce hydraulic fracturing that would be oriented parallel to the maximum principal stress at the time of fracturing and may not necessarily be related to the current-day stress field. Any variation in orientation from fractures created by faulting would increase the scatter in the fracture orientation data. The orientations would be a function of timing, which cannot be determined from the available data.

Regardless of the method dominating the fracture orientation, our interpretation is that the fracture orientation is a function of regional geology and far-field stresses and less a function of physical and elastic rock properties while fracture density is more controlled by rock properties. In the MH-2 borehole, fracture density is more dependent on rock properties and fracture orientation is dependent on the stress field. The implication for geothermal exploration from these data is that both mechanical properties of the rocks and the stress orientations and magnitudes must be known to predict a connected fracture network well enough to exploit the geothermal resource.

Conclusions

Whole rock core recovery and borehole acoustic televiewer data provide an excellent opportunity to study the lithology, physical properties, and elastic properties in the MH-2 borehole and relate those properties to the natural fracture systems. Results of unconfined uniaxial compressive stress experiments on core samples provide measurements of uniaxial compressive strength, static Young's modulus, and static Poisson's ratio. Core samples provided the opportunity to measure physical properties: dry bulk density and pneumatic permeability. We examined the variability of those properties and correlated the variations to fracture density and spacing, or cumulative fracture intensity, measured from both core and borehole acoustic televiewer data. Through interpretation of the correlations of all the data sets we identified nine unique mechanical stratigraphic units. Three of those units (2, 5, and 8) exhibit ductile deformation under uniaxial compressive stress and did not demonstrate significant brittle failure in the UCS experiments. Fracture measurements from core and acoustic

televiewer data indicate little to no natural fractures in Units 2, 5, and 8. The six other units exhibit a range of brittleness and fracture density but all exhibited brittle failure during the UCS experiments and were the stiffest samples tested. Fracture density is highest in these units. Unit 1 hosts the potential geothermal reservoir and its permeability is primarily fracture-dominated. The stratigraphic relationships between the weak units and the strong, elastic units indicate a combination of structural emplacement of the ductile units over the strong, elastic units and some combination of fault sealing and lithological cap rock that act as a seal for the underlying reservoir.

Unit 2 overlies a high-temperature, artesian, flow zone that may hold the potential for commercial geothermal energy development. Under the assumption that fracture porosity represents the majority of storage and permeability in the crystalline rocks, then Unit 2 may be acting as a cap rock or seal to the underlying geothermal reservoir if the unit is extensive and cohesive on the reservoir scale. Units 2, 5, and 8 appear to be arresting fracture propagation and are instead experiencing ductile deformation under the past and current stress regimes. The lack of fractures and unique physical and elastic properties of these units make them prime targets during exploration and make them easily identifiable in an otherwise uniform lithology. This interpretation can be the foundation of the geothermal play concept if the reservoir proves to be extensive. The resource is the high-temperature fluids that are present, the fractures in strong, elastic rocks are the porosity and permeability in the reservoir, and the weak, non-elastic, unfractured rocks are the cap and seal.

The mineralogy of the strong, elastic units is very similar and the weak, plastic units show the presence of hydrothermal alteration in the form of clays. In this case, the

smectite mineral assemblage can be used as a proxy for identification of the weak units and the potential reservoir cap rocks or seals. The unique presence of clays may allow for the use of wireline borehole logs to identify the weak units based on the log signatures of the weak units without the expense and time it takes to collect core, analyze the samples, and test the samples for static elastic properties. Wireline logs may allow us to calculate dynamic elastic properties in lieu of static elastic properties and use in combination with lithologic signatures in wireline logs to identify the weak units and potential seals more quickly and efficiently.

This study provides the basis for which we can utilize data collected from core samples and compressive tests to compare to the results from wireline log analysis, structural geology, and the regional stress field. In companion papers, we test this idea by comparing the dynamic elastic properties with static elastic properties to examine the effectiveness of traditional geomechanical and lithological analyses on crystalline basalt as well as hydrothermally altered or reworked basalt rocks. A full suite of wireline log data are available in addition to acoustic televiewer data from the MH-2 borehole so we have the unique opportunity to test the effectiveness of traditional borehole analysis methods in a unique and uncommon geological environment to assist future exploration efforts. We also analyze what we have learned about the regional stress field and the structural conditions at depth in the western Snake River Plain.

References

Arney, B. H., Boyer, J. H., Simon, D. B., Tonani, F. B., Weiss, R. B., 1980. Hot dry rock geothermal site evaluation, western Snake River Plain, Idaho. Geotherm. Res. Counc. Trans. 4, 197-200.

American Standards for Testing and Materials (ASTM), 2010. Standard E111-04.

Benford, B., Crowley, J., Schmitz, M., Northrup, C.J., Tickoff, B., 2010. Mesozoic magmatism and deformation on the northern Owyhee Mountains Idaho: Implications for along-zone variations for the western Idaho shear zone. Lithosphere, 2, 93-118.

Blackwell, D.D., 2012. Geothermal heat flow map of the U.S. (http://www.smu.edu/~/media/Site/Dedman/Academics/Programs/Geothermal%20Lab/Graphics/SMU2011USHeatFlowMap.ashx?la=en).

Blackwell, D.D., 1989. Regional implications of heat flow of the Snake River Plain, Northwestern United States. Tectonophysics 164, 323-343.

Bonnichsen, B., Leeman, W.P., Honjo, N., McIntosh, W.C., Godchaux, M.M., 2008. Miocene Silicic Volcanism in Southwestern Idaho: Geochronology, Geochemistry, and Evolution of the Central Snake River Plain. Bull. of Volc. 70, 315 – 342.

Bonnichsen, B., Godchaux, M.M., 2002. Late Miocene, Pliocene, and Pleistocene geology of southwestern Idaho with emphasis on basalts in the Bruneau-Jarbidge, Twin Falls, and western Snake River Plain regions. In: Bonnichsen, B., White, C.M., McCurry, M., (Eds.), Tectonic and Magmatic Evolution of the Snake River Plain Volcanic Province. Idaho Geol. Surv. Bull. 30, 233–312.

Breckenridge, R.M., Lewis, R.S., Adema, G.W., Weisz, D.W., 2003. Miocene and younger faults in Idaho. Idaho Geol. Surv. Moscow, Idaho. (http://www.idahogeology.org/pdf/Maps_(M)/m-08-m.pdf)

Cooke, M.L., Simo, J.A., Underwood, C.A., Rijken, P., 2006. Mechanical stratigraphic controls on fracture patterns within carbonates and implications for groundwater flow. Sed. Geol. 184, 225-239.

Engelder, T., 1987. Joints and shear fractures in rock. In: Atkinson, B.K., (Ed.), Fracture mechanics of rock. London, Academic Press, pp. 27 – 69.

Glen, J.M.G., Ponce, D.A., 2002. Large-scale fractures related to inception of the Yellowstone hotspot. Geology, 30, 647–650.

Gudmundsson, A., Fjeldskaar, I., Brenner, S.L., 2002. Propagation Pathways and Fluid Transport of Hydrofractures in Jointed and Layered Rocks in Geothermal Fields. J. Volc. Geotherm. Res. 116, 257 – 278.

Gupta, H., and Roy, S. 2007. Geothermal Energy: An alternate resource for the 21st century. Elsevier, Amsterdam, The Netherlands. pp. 292.

Gurocak, Z., Kilic, R., 2005. Effect of weathering on the geomechanical properties of the Miocene basalts in Malatya, Eastern Turkey. Bull. Eng. Geol. Env. 64, 373-381.

Hanks, C.L., Lorenz, J., Teufel, L., Krumhardt, A.P., 1997. Lithologic and Structural controls on natural fracture distribution and behavior within the Lisburne Group, northeastern Brooks Range and North Slope subsurface, Alaska. Am. Assoc. Petrol. Geol. Bull. 81, (10), 1700-1720.

Kattenhorn, S.A., Schaefer, C.J., 2007. Thermal-Mechanical Modeling of Cooling History and Fracture Development in Inflationary Basalt Lava Flows. J. Volc. Geotherm. Res. 170, 181 – 197.

Keller, G.R., Hildenbrand, T.G., Kucks, R., Roman, D., Hittelman, A.M., 2002. Upgraded gravity anomaly base of the United States. Leading Edge (Tulsa, OK), 21, (4), 366-367+387.

LaPointe, P.R., 1987. A method to characterize fracture density and connectivity through fractal geometry. Int. J. Rock Mech. Mineral Sci. and Geomech. 25, (6), 421-429.

Laubach, S.E., Olson, J.E., Gross, M.R., 2009. Mechanical and Fracture Stratigraphy. Am. Assoc. of Petrol. Geol. Bull. 93, (11), 1413-1426.

Lorenz, J.C., Sterlin, J.L., Schechter, D.S., Whigham, C.L., Jensen, J.L., 2002. Natural fracture in the Spraberry Formation, Midland basin, Texas: The effects of mechanical stratigraphy on fracture variability and reservoir behavior. Am. Assoc. of Petrol. Geol. Bull. 86, (3), 505-524.

Lewis, R.E., Stone, M.A.J., 1988. Geohydrologic data from a 4,403-foot geothermal test hole, Mountain Home Air Force Base, Elmore County, Idaho. U.S. Geol. Surv. Open-File Rep. 88-166.

McCurry, M., Watkins, A.M., Parker, J.L., Wright, K., Hughes, S.S., 1996. Preliminary volcanological constraints for sources of high-grade rheomorphic ignimbrites of the Cassia Mountains, Idaho: Implications for the evolution of the Twins Falls volcanic center. Northwest Geology, 26, 81–91.

McIntyre, D.H., 1979, Preliminary description of Anschutz Federal No. 1 drill hole, Owyhee County, Idaho. U. S. Geol. Surv. Open-File Rep. 79-651.

Nelson, R., 2001. Geologic Analysis of Naturally Fractured Reservoirs, Gulf Publishing Co., Houston, TX, 352.

Petrie, E.S., Jeppson, T.N., Evans, J.P., 2012. Predicting rock strength variability across stratigraphic interfaces in cap rock lithologies at depth: Correlation between outcrop and subsurface. Env. Geosciences, 19, (4), 125-142.

Pierce, K.L., Morgan, L.A., 1992. The track of the Yellowstone hotspot: Volcanism, faulting, and uplift. In: P.K. Link, M.A. Kuntz, L.B. Platt, (eds.), Regional Geology of Eastern Idaho and Western Wyoming. Geological Society of America Memoir 179, 1-53.

Pollard, D.D., Aydin A., 1988. Progress in understanding jointing over the past century. Geol. Soc. Am. Bull. 100, 1181-1204.

Ruez Jr., D.R., 2009. Framework for stratigraphic analysis of Pliocene fossiliferous deposits at Hagerman Fossil Beds National Monument. Idaho, Rocky Mtn. Geol. 44 (1), 33-70.

Sant, C.J., 2012, Geothermal Alteration of Basaltic Core from the Snake River Plain, Idaho. Master's Thesis, Utah State University, Logan, Utah.

Shervais, J.W., Schmitt, D.R., Nielson, D., Evans, J.P., Christiansen, E.H., Morgan, L., Shanks, W.C.P., Prokopenko, A.A., Lachmar, T., Liberty, L.M., Blackwell, D.D., Glen, J.M., Champion. D., Potter, K.E., Kessler, J.A., 2013. First results from HOTSPOT: The Snake River Plain Scientific Drilling Project, Idaho. U.S.A. Sci. Drill. 15, 36 – 45.

Shervais, J.W., Evans, J.P., Christiansen, E.J., Schmitt, D.R., Liberty, L.M., Blackwell, D.D., Glen, J.M., Kessler, J.A., Potter, K.E., Jean, M.M., Sant, C.J., Freeman, T.G., 2011. Hotspot: The Snake River Geothermal Drilling Project – An Overview. Geothermal Res. Counc. Trans. 35, 995 – 1003.

Shervais, J.W., 2010. Phase 1 Report: The Snake River Geothermal Drilling Project – Innovative Approaches to Geothermal Exploration. Report to the Dept of Energy DE-EE0002848.

Shervais J.W., Shroff, G., Vetter, S.K., Matthews, S., Hanan, B.B., McGee, J.J., 2002. Origin and evolution of the western Snake River Plain: Implications from stratigraphy, faulting, and the geochemistry of basalts near Mountain Home, Idaho. In: Bonnichsen, B., White, C.M., McCurry, M., (Eds.), Tectonic and Magmatic Evolution of the Snake River Plain Volcanic Province. Idaho Geol. Surv. Bull. 30, 343-361.

Smith, R., 2002. Geologic Setting of the Snake River Plain Aquifer and Vadose Zone. Vadose Zone Journal, 3, 47 – 58.

Thuro, K., Plinninger, R.J., Zah, S., Schutz, S., 2001. Scale effects in rock strength properties. Part 1: Unconfined compressive test and Brazilian test. In: ISRM Regional Symposium, EUROCK 2001: Rock Mechanics a Challenge for Society, Helsinky University of Technology.

Walton, A.W., Schiffman, P., 2003. Alteration of hyaloclastites in the HSDP 2 Phase 1 Drill Core 1. Description and paragenesis. Geochem. Geophys. Geosys. 4, (5), doi: 10.1029/2002GC000368.

Wood, S.H., Anderson, J.E., 1981. Chapter 2: Geology. In: Mitchel, J.C. (Ed.), Water Information Bulleting No. 30: Geothermal Investigations in Idaho, Part II. Idaho Department of Water Resources, under Department of Energy contract DE-AS07077ET28407.

Wood, S.H., Clemens, D.M., 2002. Geologic and tectonic history of the western Snake River Plain, Idaho and Oregon. In: Bonnichsen, B., White, C.M., McCurry, M., (Eds.), Tectonic and Magmatic Evolution of the Snake River Plain Volcanic Province. Idaho Geol. Surv. Bull. 30, Ê69-103.

Wood, W.W., Low, W.H., 1986. Aqueous geochemistry and diagenesis in the eastern Snake River Plain aquifer system, Idaho. Bull. Geol. Soc. America, 97, 1456-1466.

Zoback, M.D., Barton, C.A., Castillo, D.A., Finkbeiner, T., Grollimund, B.R., Moos, D.B., Ward, C.D., Wiprut, D.J., 2003. Determination of stress orientation and magnitude in deep wells. Int. J. Rock Mech. Mining Sci. 40, 1049 – 1076.

CHAPTER 3

DYNAMIC AND STATIC ELASTIC PROPERTIES OF BASALTS IN A POTENTIAL GEOTHERMAL RESERVOIR: CORRELATING *IN SITU* BOREHOLE MEASUREMENTS, CORE DATA, AND RESULTS OF UNIAXIAL COMPRESSIVE STRESS EXPERIMENTS[2]

Abstract

Fluid flow in crystalline geothermal reservoirs commonly occurs through connected fracture networks in low matrix permeability rocks, making fracture characterization and the rock properties that can control fractures, paramount to prediction of fluid flow. We compare two methods of measuring elastic parameters to interpret rock strength and elastic properties that we use to define the mechanical stratigraphy that can control the distribution of fractures in a geothermal reservoir. Dynamic elastic properties and rock strength are commonly calculated from bulk density and dipole sonic logs to interpret mechanical stratigraphy. While properties measured in static tests on rock samples are considered a more accurate measure of in situ properties, rarely is enough core available to use static properties for interpretation over a large variable sequence of rocks. We compare independent interpretations of mechanical stratigraphy from static properties and dynamic properties from a zone of geothermal interest and perform a quantitative correlation of each rock property. We develop an empirical power function that describes

---

[2] Chapter to be coauthored by:
J. A. Kessler[a], M. A. Strange[a], X. Chen[b], D. R. Schmitt[b], J. P. Evans[a]
[a] Dept of Geology, Utah State University, 4505 Old Main Hill, Logan, Utah 84322 USA
[b] Dept of Physics, University of Alberta, 4-181 CCIS, Edmonton, AB T6G 2E1 Canada

the relationship between static uniaxial compressive strength and dynamic Young's modulus that can be used to calculate dynamic uniaxial compressive strength in these rocks. We demonstrate that the dynamic properties determined from wireline log analyses are sufficient to consistently interpret the mechanical stratigraphy. Dynamic Young's modulus and dynamic uniaxial compressive strength correlate well with the static properties and the precision of dynamic Poisson's ratio is improved over the static property estimated from unconfined stress experiments. In-lab acoustic velocities measured on core samples supplement borehole wireline data well in these rocks. We show that neutron porosity, sonic velocity, and magnetic susceptibility logs can be useful in testing the mechanical stratigraphic model while gamma ray and resistivity logs are likely responding to lithological variation in the rocks that may not correlate with elastic properties at the appropriate scale. We interpret a reservoir/cap rock boundary at the interface between the lower strong elastic fractured reservoir unit and the overlying weak,plastic seal and recommend this boundary be a target in future wells.

Introduction

Elastic properties (Young's modulus, E, Poisson's ratio, ν), compressive strength (UCS), and the primary physical properties of rocks, including density, porosity, permeability, are routinely used to describe or model the possible mechanical responses to the effective deviatoric stress field in the subsurface or to determine fluid stresses in the rocks during reservoir stimulation (Zoback et al., 2003). The distribution of physical properties, rock strength, and elastic properties describes the mechanical stratigraphy that can have an impact on fracture propagation and the distribution of fracture density in

stratified rock sequences (Laubach et al., 2009). We use the concepts of fracture and mechanical stratigraphy in the analysis of Mountain Home core (Chapter 2) to predict the zones in the lithological stratigraphy that are likely to host connected fracture networks and will effectively increase fracture permeability during hydraulic fracture stimulation. In crystalline reservoirs, Type I fractures (Nelson, 2001) act as the primary storage and permeability in a low permeability protolith so that fracture density and fracture connectivity are the major controls on fluid storage and flux in the reservoir (Ferno, 2012). Natural Type I fractures are often confined to discrete geomechanical units defined by changes in rock type, strength, and elasticity (LaPointe, 1987; Petrie et al., 2012). In order to minimize the amount of fluids and proppants required during stimulation, boreholes are oriented parallel to the minimum principal horizontal stress to best take advantage of the principal horizontal stress orientations and maximize fracture propagation in the most easily fractured rocks and in the direction of maximum horizontal stress. Those tend to be the rocks that exhibit the least ductile deformation before brittle failure and usually have large Young's modulus (E), small Poisson's ratio (v), and moderate uniaxial compressive strength (UCS) that is less than the minimum compressive stress. Large values of UCS may prevent the rock from fracturing under natural or practical stimulation scenarios.

Whole-rock core was collected with 90% recovery from the MH-2 borehole on the Mountain Home Air Force Base near Mountain Home, Idaho (Figure 1-1; Shervais et al., 2013). Samples over a zone of interest (ZOI) from 1,280 m (4,200 ft) to TD at 1,821 m (5,976 ft) were collected for unconfined uniaxial compressive strength (UCS) experiments as reported in Chapter 2. The zone of interest is the lower 541 m (1,775 ft)

of rock around and above the depth at which artesian water with temperature of 140° C flowed. We tested 110 samples from 55 depths in UCS experiments (Chapter 2). Two samples were collected at each location in order to determine the reproducibility of the test results to measure mechanical properties and describe the variability of mechanical properties between adjacent samples. The static elastic properties calculated from results of the UCS experiments were interpreted to show nine mechanical units in the ZOI and provide the basis for comparison between that interpretation and an independent interpretation using only borehole wireline log data.

The full suite of borehole geophysical logs available from MH-2 includes total gamma ray, spectral gamma ray, full wave train sonic, neutron porosity, deep and shallow resistivity, and magnetic susceptibility (Shervais et al., 2013). The borehole logs measure or respond to the physical properties of the rocks and fluids in the ZOI. The wireline data are available down to 1,708 m (5,605 ft). The wireline logs do not extend to TD due to temperature limits of the instruments. To supplement the dynamic data set, acoustic velocities were measured on the UCS samples in the Experimental Geophysics Group's laboratory at the University of Alberta in Edmonton, Canada. The acoustic velocities from wireline logs and laboratory measurements are used to calculate an independent set of dynamic elastic properties and rock strength. It is generally thought that dynamic elastic properties are two to ten times the magnitude of static elastic properties (Fjaer et al., 2013; Plona and Cook, 1995). The possible sources of the discrepancies include the presence of microcracks, voids, time effects, temperature effects, variations in stress loading and magnitudes, and saturation (Devorak, 1970). For the purposes of this study, we focus on the relative changes in static and dynamic elastic

properties and rock strength. A quantitative geomechanical model will require a rigorous analysis of the discrepancy in magnitudes between the static and dynamic values and is beyond the scope of this study. Here the relative changes in magnitude suffice for the purpose of identifying unique mechanical units.

We use the data from these two methods to test for correlations between elastic and physical rock properties and the distribution of fracture density. The test is reinforced with a comparison of two sets of dynamic elastic properties to static elastic properties. One set is calculated from shear and compressional sonic velocities from wellbore wireline log data and another from shear and compressional sonic velocities measured in pressure vessels in the laboratory. A comparison of how each mechanical stratigraphic interpretation best predicts fracture density. Static measurements are generally interpreted to be a closer representation of in situ rock properties due to the frequency sensitivity of dynamic properties and the common overestimate of mechanical rock properties from the calculations from high-frequency sonic data (Fjaer et al., 2013). Just as high strain rate, or fast stress loading, UCS experiments can cause an overestimate of rock strength and Young's modulus, high frequency sonic data have a tendency to overestimate rock strength and elastic properties that can be orders of magnitude too high compared to static estimates (Zoback, 2010). In this paper, we compare the fracture stratigraphy from core and borehole image data developed in Chapter 2, and determine the mechanical stratigraphy interpreted from dynamic and static properties, test for correlations of dynamic elastic properties and static elastic properties, examine the effectiveness of modeling elastic properties with in-lab acoustic velocities, and evaluate wireline log response to geomechanical properties in basalt.

This paper describes the method to evaluate the effectiveness of mechanical stratigraphy interpreted from dynamic data to assist us in fracture prediction. We identify strong, elastic units that may host connected fracture networks that provide the storage and permeability for commercial geothermal energy development. We also identify weak, plastic units that may act as thermal and hydrological cap rocks for geothermal reservoirs. We demonstrate that the method can be used in conjunction with analysis of other borehole log data to identify the weak, plastic cap rock units and underlying strong, elastic units that may contain a potentially connected fracture network. The fractured strong, elastic unit and accompanying cap rock pair that constitute the potential geothermal reservoir in MH-2 can be identified from relative changes in rock properties and physical properties of the cap rock and reservoir rock in future exploration wells. If the units prove to be extensive enough to constitute a commercially viable reservoir, then successful implementation of the method presented here will allow us to readily identify the target units to maximize efficiency in well drilling and design. If successfully implemented, the method will save the time and expense of coring the borehole and analyzing the core samples in future wells and will contribute significantly to the successful economic development of the geothermal resource.

Study Area

The MH-2 borehole is in the western SRP (Figure 1-1) and was cored between June 2011 and February 2012 on the Mountain Home Air Force Base outside Mountain Home, Idaho (Shervais et al., 2013). Whole-rock core was recovered from the entire depth of the borehole with greater than 90% recovery. A zone of interest (ZOI) is defined

from ~ 1,280 m (~4,200 ft) bgs to a total depth (TD) of 1,821 m (5,976) ft bgs that includes a high-temperature, artesian hydrothermal zone near the base of the zone. The thickness of the potential geothermal reservoir is unknown because the MH-2 borehole did not penetrate the bottom of the hydrothermal zone. The reservoir is potentially greater than 76 m (250 ft) thick if the strong mechanical unit that contains the hydrothermal zone also hosts a fully connected fracture network.

The regional geology is a result of complex interaction between passage of the North American tectonic plate over the Yellowstone Hotspot and initiation of extension associated with the Basin and Range in the Miocene (Bonnichsen and Godchaux, 2002; McCurry et al., 1996; Pierce and Morgan, 1992; Shervais, et al., 2002). The details of the study area and regional geology are described in Chapter 2. The oblique extension in the western Snake River Plain has generated a basin bound by high-angle normal faults with large amounts of offset up to ~ 1,200 m (~ 4,000 ft) to the north and south of the study site. The basin is bounded by the Idaho batholith to the north/northeast and the Owyhee Mountains, comprised of Tertiary volcanics, to the west/southwest. The northwest-oriented graben held the ancient Pleistocene Lake Idaho (Ruez, 2009). Hundreds of feet of lakebed sediments were deposited over Miocene volcanic rocks and are overlain by Pleistocene basalts that erupted from the end of Lake Idaho time to the present. High heat flow in the area and the potential for fluid storage and permeability in connected fracture networks make the western Snake River Plain a target for exploration for commercially viable geothermal energy (Blackwell, 2012).

The MH-2 borehole passed through ~215 m (700 ft) of Pleistocene basalts and ~730 m (2,400 ft) of Pleistocene lacustrine sediments (Figure 2-1) that were deposited in

the lake bed of the ancient Lake Idaho (Ruez, 2009) before entering a series of alternating layers of Miocene basalt, altered basalt (Figure 3-1a and 3-1d), reworked basaltic sediments (Figure 3-1c) and hyaloclastites (Figure 3-1b and 3-1e) to a TD of 1,821 m (5,976 ft). The high-temperature artesian zone is in the lower Miocene rocks at 1,745 m (5,726 ft).

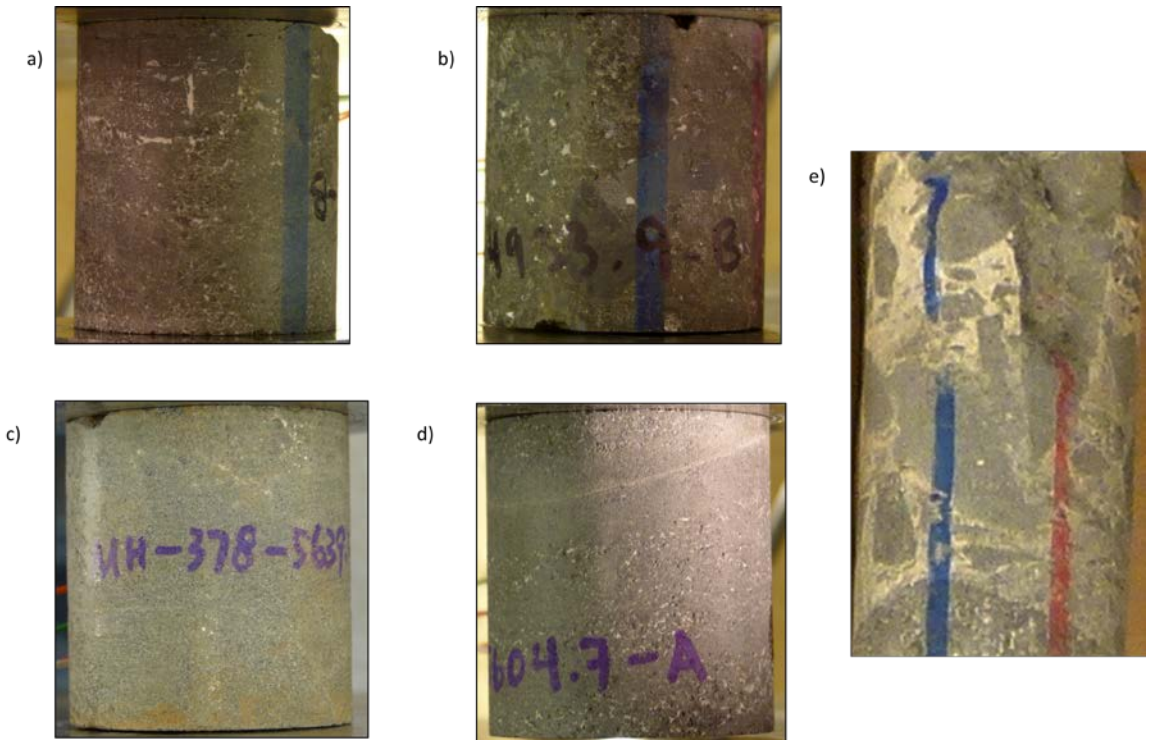

Figure 3-1. a) highly altered basalt from Unit 5, b) hyaloclastite from Unit 5; c) reworked basaltic sediment from Unit 2, d) hydrothermally altered basalt from Unit 2, e) hyaloclastite from Unit 2.

Large fracture and fault zones are found in the MH-2 borehole (Chapter 2) with evidence for fluid flow in the form of secondary mineralization, alteration, and brecciation in the deeper portions of the borehole. Hydrothermally altered basalt is present and is interbedded with hyaloclastite in places that demonstrates the interaction of young basalts with both high-temperature fluids in the case of altered basalt and low-

temperature fluids in the case of hyaloclastites. Thermal gradients in the MH-2 borehole are high (~73° C/km) and the equilibrated bottom-hole temperature (BHT) is ~140° C. The high subsurface temperatures and the potential for subsurface fluid flow through connected fracture networks and other discontinuities indicate a potential for geothermal energy development near the Mountain Home, Idaho area.

Methods

Static elastic properties were calculated and uniaxial compressive strength was determined from stress and strain data measured during unconfined uniaxial compressive stress experiments conducted on 110 samples from 55 depth locations in the MH-2 borehole as described in Chapter 2. We interpreted the distribution of static elastic rock properties, rock strength, bulk density, and pneumatic permeability to define nine mechanical units (Chapter 2) in the section (Figure 2-6). The mechanical interpretation is at a scale appropriate to identify the cap rock unit (Unit 2) and strong unit (Unit 1) that hosts the potential geothermal reservoir. Based on our interpretation from the static properties, we identified three strong, elastic units (units 3, 4, and 6), three weak, plastic units (units 2, 5, and 8), and three intermediate units (units 1, 7, and 9) (Chapter 2). The high-temperature, artesian flow zone at 1,745 m bgs (5,726 ft) coincides with the boundary between weak unit 2 and strong unit 1, and with a change in clay types that indicate an increase in temperature and water availability in Unit 1 that causes basalt to alter to corensite clay instead of smectite clay (Walker et al., pers. comm. 2013). Unit 2 represents a potential cap rock to the underlying reservoir in Unit 1. We analyze the method used to identify the rock properties of the mechanical units solely from dynamic

data to assess the effectiveness in predicting the mechanical stratigraphy that was previously interpreted from static data.

Here we use dynamic elastic properties and rock strength data to determine if our method can be used in lieu of UCS experiments to describe similar values and types of mechanical units. We first intentionally ignore the lithological data that we acquired in Chapter 2 in order to objectively interpret the dynamic properties independently so that the dynamic-static correlations can then be tested by the lithological data and other wireline borehole data. Due to temperature limitations of the wireline instruments, we use ultrasonic acoustic velocity data from wireline logs from the top of the ZOI to ~1,670 m (5,480 ft) bgs. Below 1,670 m (5,480 ft) to TD, we use ultrasonic pulse velocities from laboratory measurements taken on samples that are the same as those in the UCS experiments described above. We lack bulk density logs in the wireline log suite so we use bulk density measured on the UCS samples in lieu of continuous log density data. The combination of V_p, V_s, and bulk density is used to calculate Poisson's ratio (ν), Young's modulus (E), and uniaxial compressive strength (UCS). Dynamic ν and E values are calculated with the following (Lucier et al., 2006; Potter and Foltinek, 1997):

$$\nu = (V_p^2 - 2V_s^2)/(2(V_p^2 - V_s^2) \quad (1)$$

$$E = 2\rho_b V_s^2(1 + \nu) \quad (2)$$

Dynamic uniaxial compressive strengths are calculated from a statistical model (Figure 3-2) based on the empirical correlative relationship between static UCS and dynamic E (Zoback, 2010).

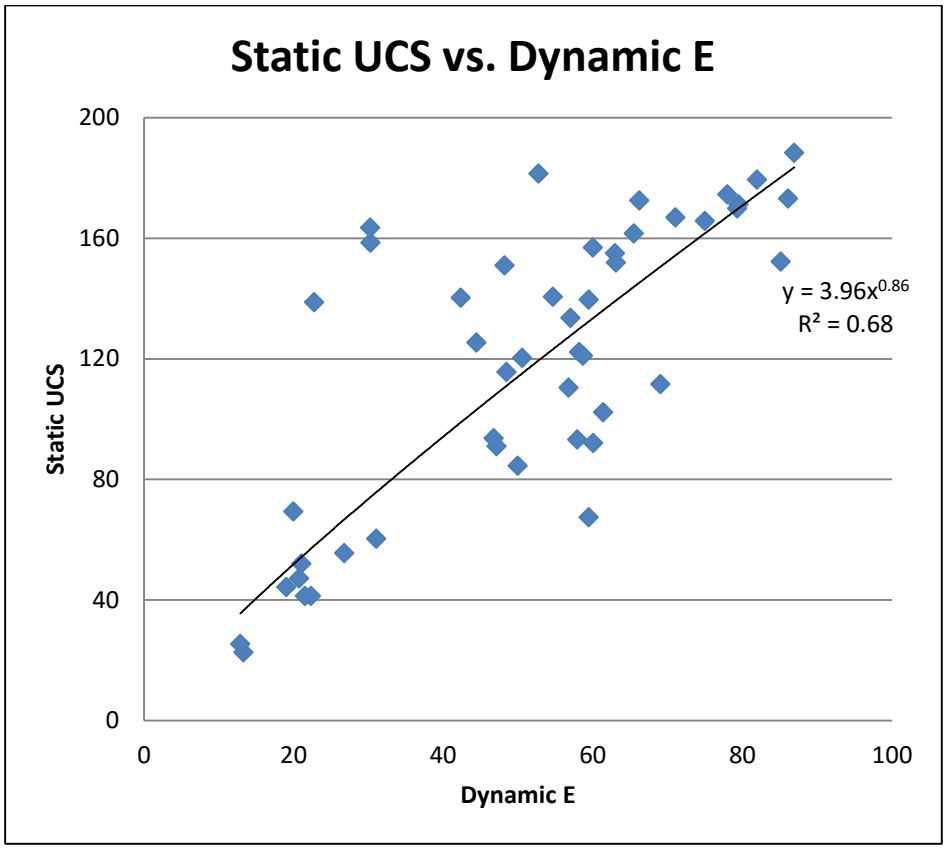

Figure 3-2. Power model fit to the correlation between static UCS results from compressive stress experiments and dynamic Young's modulus calculated from wireline log data.

Static UCS is often considered a more precise measurement of rock strength so that the relationship between static UCS and dynamic E is strong enough to predict dynamic UCS from the power function fit to the correlation between static UCS and dynamic E. That relationship between UCS and E is important because core is often not available from most wells drilled for a project. If the model can be built from core recovered from a well in a field, then the model can be used to estimate UCS in future wells for that particular field. The relationship is empirical and models are available for typical rock types in the case that no core is available to test for UCS and build an

empirical model for a particular field. The correlation and the power function used to calculate dynamic UCS as a function of Young's Modulus from basalts in MH-2 is:

$$UCS = 3.9602(E^{0.86}) \quad (3)$$

The dynamically derived E values are sampled are from the same locations as those used in the UCS experiments. Each sample is loaded into the vessel and velocities are calibrated by measuring velocities traveling through the instrument without the presence of a rock sample. A sample is then loaded into the instruments at atmospheric pressure and temperature. The sample is subjected to incremental increases in pressure and temperature and velocities are measured. The calibrated velocity is subtracted from the measured velocity in the sample and the result is the final shear and compressional velocity for each sample. This kind of measurement was conducted on 11 samples over the ~150 m (500 ft) interval. We used these velocity measurements in lieu of sonic log data for this interval of the borehole in the same manner as described above.

The logs used in this study to measure the physical properties of the rock and the fluids are the total gamma ray, compressional and shear acoustic velocities (sonic), neutron porosity, deep and shallow resistivity, and magnetic susceptibility. Gamma ray logs are typically used to identify shale in oil and gas wells by measuring the gamma ray emission from clays in the formation. Here we use the same technique to identify highly altered, clay-rich basalts. The technique is complicated by the fact that basalts alter to clay under a variety of conditions and may not necessarily be a proxy for temperature or mechanical properties that may affect fracture propagation. However, we expect that more clays will be present in more highly altered basalts that may help us identify weak,

plastic units in future exploration wells, even if the signature is subtle in the data. Neutron porosity logs are a measure return of neutrons emitted from the tool that bounce off hydrogen atoms in water molecules in the formation and is a proxy for porosity. The challenge with these logs is most interpretation techniques are based in formations with high matrix to fracture porosity ratio. In this case, matrix porosity is low in most of the units so that we can interpret the neutron logs as fracture porosity. Resistivity logs are used to identify permeability in the near-borehole environment by measuring the ability of drilling fluids to permeate the formation and measuring the difference in resistivity of the drilling muds and the formation fluids. The typical application of this method is in hydrocarbon-bearing formations so that the resistivity of the drilling muds and the formation fluids is distinct and easily identifiable on deep, intermediate, and shallow resistivity logs. Here, the challenge is to identify infiltration of drilling fluids in discrete fracture zones and separate the signal from the formation fluids. Magnetic susceptibility is used here to help identify native, unaltered basalt that has not been highly altered to clays. These units may have a tendency to be undergo brittle failure and the MS logs could be used to support an interpretation of strong, elastic units.

Results

Our interpretation of unconfined uniaxial compressive strength experiments defined nine mechanical stratigraphic units over the ZOI in the MH-2 borehole using measured and calculated values of static UCS, E, ν, and fracture density (Figure 2-6). Unit 1 and Unit 2 represent the reservoir/cap rock contact for the potential geothermal reservoir. Unit 1 is a strong, elastic unit that hosts connected fracture networks. Unit 2 is

a weak, plastic unit that may arrest fracture propagation and acts as a hydraulic and thermal cap rock that prevents the loss of high-temperature fluids from escaping the reservoir in Unit 1 (Chapter 2). While UCS experiments are an effective method to identify mechanical stratigraphy from static strength and elastic properties, the tests are time consuming and resource intensive including the man hours and expense of collecting continuous whole-rock core. Here we test a more commonly used method using ultrasonic velocity data and bulk density to calculate dynamic elastic properties and rock strength and compare the results of the interpretation made from the static data (Figure 3-3). A quantitative analysis of the static and dynamic data was performed using independent correlations and demonstrates that dynamic measurements for Young's modulus and the power model used to estimate UCS are very similar and can be used to calibrate dynamic values of UCS and E from future wells.

The mechanical stratigraphy interpreted from dynamic properties (Figure 3-4) reveals the presence of three weak, plastic units (Category 3 rocks, (Chapter 2) 45 m – 57 m (150 ft – 190 ft) thick based on low UCS, low E, and low ν. Unit 2, Unit 5, and Unit 7 show the lowest values of these properties. Based on the physical and elastic properties, we predict that these three units would undergo more ductile deformation before brittle failure, if they experience brittle failure at all. Unit 2 only shows one data point on the curve but there are two other samples in that interval with attenuation that is too high to produce reliable velocity measurements. While we cannot use these data points quantitatively, we

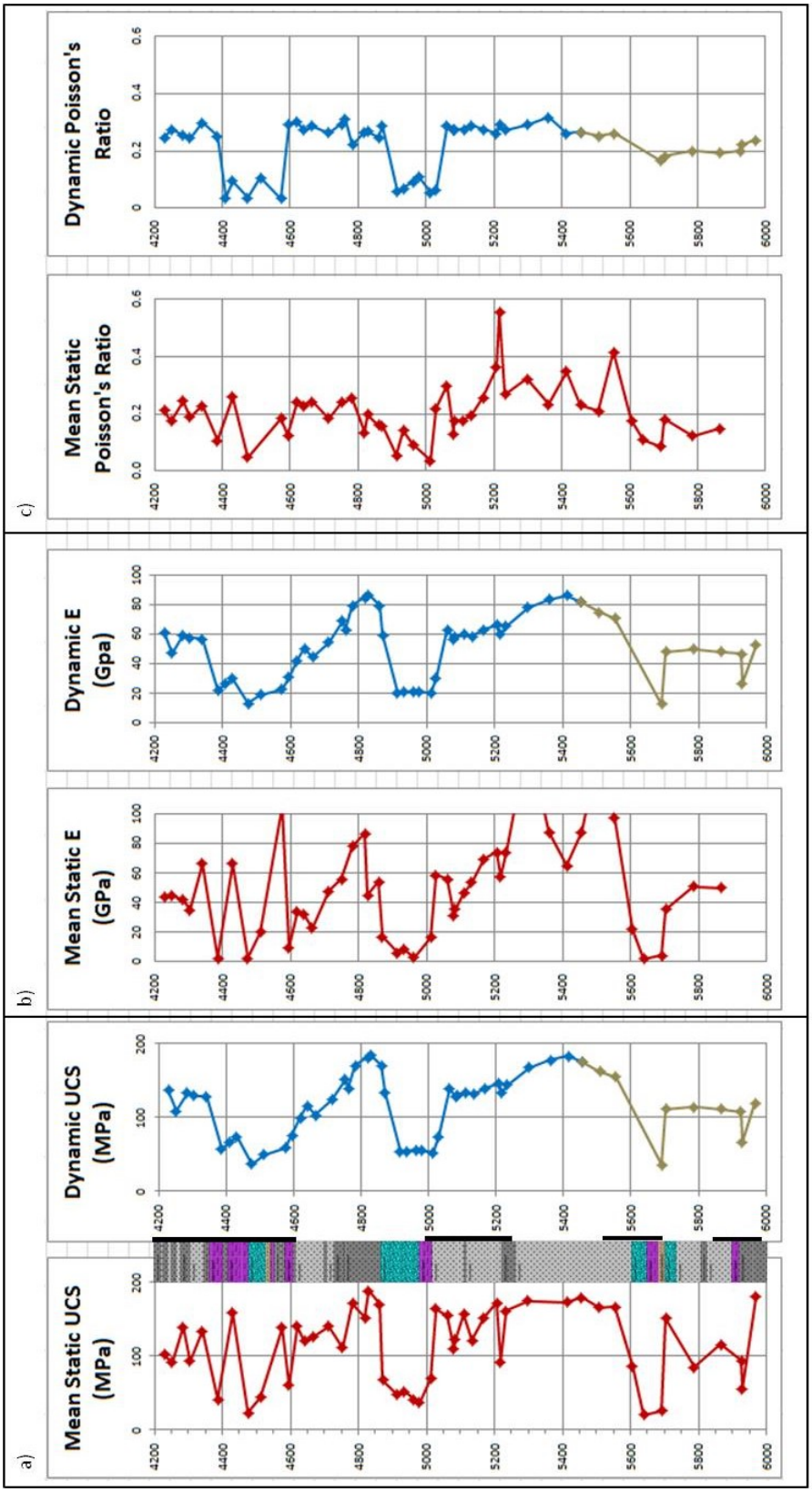

Figure 3-3. Comparison of static and dynamic data. a) unconfined compressive strength, b) Young's modulus, c) Poisson's ratio.

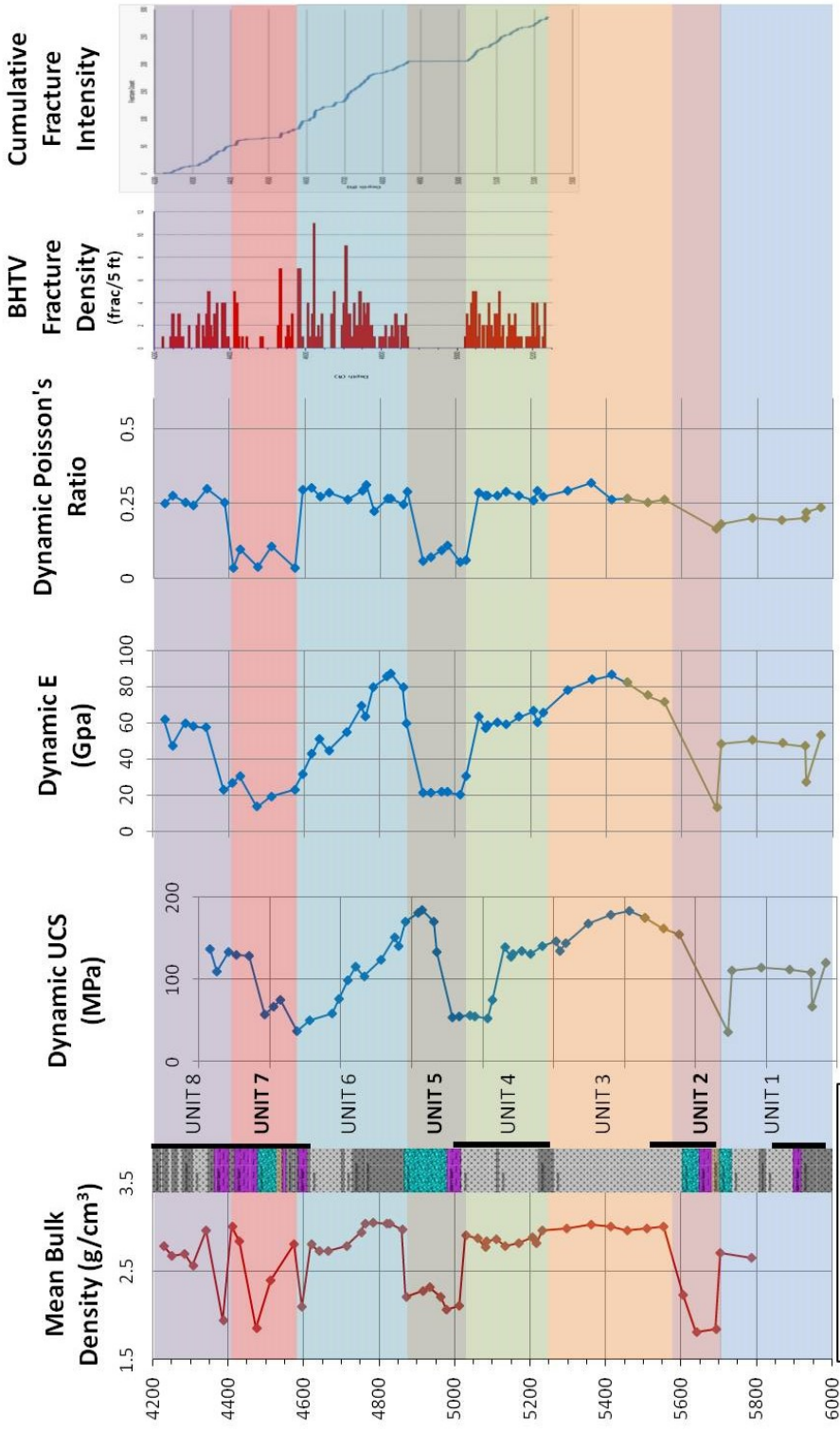

Figure 3-4. Mechanical stratigraphy of the MH-2 borehole interpreted from dynamic mechanical rock strength and elastic properties.

interpret the high attenuation as a result of the elastic properties of the samples and assume they would plot low on the scale. The weak, plastic units all overlay strong, elastic units (Category 1 rocks, Chapter 2). In the case of Unit 7, it overlies Unit 6 that is a transitional unit that is very strong and elastic at the base but transitions to moderately strength at the top. Unit 1, Unit 4, and Unit 8 are all elastic units with moderate strength (Category 2, Chapter 2). The UCS and E data for the interval that includes Unit 6, Unit 7, and Unit 8 appear to indicate that this interval is a transitional interval from a maximum strength at the base, to weak and plastic in the center and increasing strength and elasticity to the top. The Poisson's ratio curve (Figure 3-4), however, shows distinct decreases in Unit 5 and Unit 8 and apparently corresponds to decreases in fracture density. Those distinct boundaries are the primary basis for interpreting the upper and lower boundaries of Unit 5 and Unit 7. The boundary between Unit 3 and Unit 4 is gradational in the Poisson's ratio curve but can be seen in the UCS and E curves (Figure 3-4). Since we lack fracture data from BHTV below ~1,595 m (5,233 ft), we cannot used the borehole data to confirm whether these changes are significant in the fracture density in the borehole. There does appear to be a unique change in UCS and E at ~1,600 m (~5,250 ft) where the smooth curve in Unit 3 with high values for both appears to flatten and this is the basis for distinguishing between Unit 3 and Unit 4. The interpretation defines eight mechanical stratigraphic units of varying thickness with a repeating stacked pattern of a unit of moderate strength and elasticity overlain by a weak, plastic unit, which is then overlain by a very strong, elastic unit. The exception to this pattern is Unit 8 but since it is at the top of the ZOI, we cannot define its upper boundary and cannot definitively confirm that its strength does not increase upsection. The stacking pattern

may indicate that regional structural features control the stratigraphy in the ZOI and this is the subject of the subsequent chapter/paper.

Correlation of Rock Strength and Elastic Properties

A comparison of dynamic and static UCS curves (Figure 3-3a) shows that the rock strength stratigraphy is well represented by the dynamic data compared to the static model. The variability in the static curve compared to the dynamic curve can be accounted for by the discrete sampling of the UCS samples. Inspection of the lithology log (Figure 2-1) shows the presence of a high degree of variability in rock types in the upper 120 m (400 ft) of the ZOI. We account for the variability in the static curve by acknowledging the alternating, relatively thin beds of crystalline and altered/reworked basaltic units in the interval of the borehole. The dynamic curve is smoother due to the 2-meter resolution of the sonic logging instrument that washes out the effect of the thin, alternating beds in that part of the zone. Despite the differences in resolution, both curves show enough variability to identify the weak, plastic units and distinguish them from the strong, elastic units. We can see in both curves that the moderate values are around the 100- 130 MPa area, the maximum values are > 150 MPa and the minimum values are < 50 MPa at similar depths. The quantitative analysis (Figure 3-5) demonstrates that the dynamic model does a good job of simulating the quantities that are calculated from the static data. A strong correlation ($R^2 = 0.69$) shows that the dynamic data, in this case, do not significantly overestimate the magnitude of uniaxial compressive strength. The trendline (Figure 3-5) is a power function but is almost linear and closely follows the 1:1 line, indicating a strong independent correlation between static UCS and dynamic UCS.

The outlying points are samples from Units 7 and 9. These are units with thin beds and alternating rock types and explain the variability from sampling. The implications of these results are that rock strength can be quantifiably estimated from wireline log data and can be used in geomechanical models, discrete fracture network models, and completions and stimulation designs.

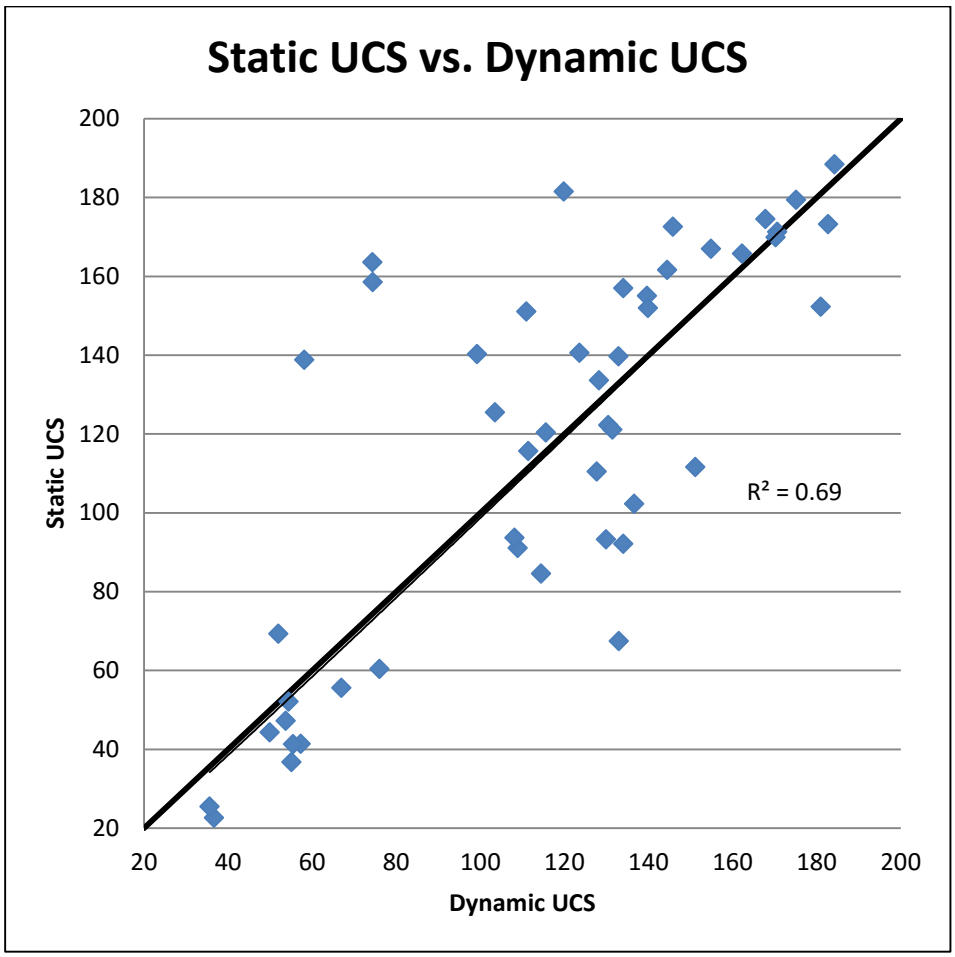

Figure 3-5. Independent correlations of uniaxial compressive strength. Thick black line is the one-to-one line and the thin black line is the regression line corresponding to the R^2 value.

The static and dynamic curves for Young's modulus show two important characteristics (Figure 3-3b). First, variability is much higher in the static data than in the

dynamic curve. Secondly, the general trends of low E between 1,341 and 1,402 m (4,400 and 4,600 ft), 1,493 and 1,523 m (4,900-5,000 ft), and 1,706 and 1,737 m (5,600 – 5,700 ft), a transitional trend between 1,280 and 1,462 m (4,200 ft and 4,800 ft), and peak E values between 1,447 and 1,485 m (4,750 and 4,875 ft) and 1,615 and 1,676 m (5,300 and 5,500 ft) is represented well in both curves. The dynamic curve is much smoother and is likely a result of the resolution of the sonic logging instrument compared to discrete sampling done in the UCS experiments. As with the UCS data, the mechanical units are not lithologically homogenous so variability from one sample to the next has the potential to be high as is evident in the static curve. The dynamic data are calculated from sonic data that average the velocity of sonic waveforms in the formation over an interval the length of the tool. An independent correlation analysis indicates a strong relationship between the quantities produced by both methods (Figure 3-6). With an R^2 of 0.59, we can see that the dynamic data mimic the static data well both from a relative rock type perspective and in the effectiveness of the dynamic data to quantify the rock properties produced in the UCS experiments. The dynamic data do show a slight trend towards an overestimate of the magnitude of E but by a factor of 2-3, not 10 or more. Expecting this discrepancy, we interpret these data to be a good reproduction of the static properties. We would advise applying a correction to the dynamic data before use in quantitative geomechanical models and completion designs. In this case, an empirical function could be developed from the data presented here or many published functions exist for the general conversion of dynamic E data to a static E scale that can be found in the literature.

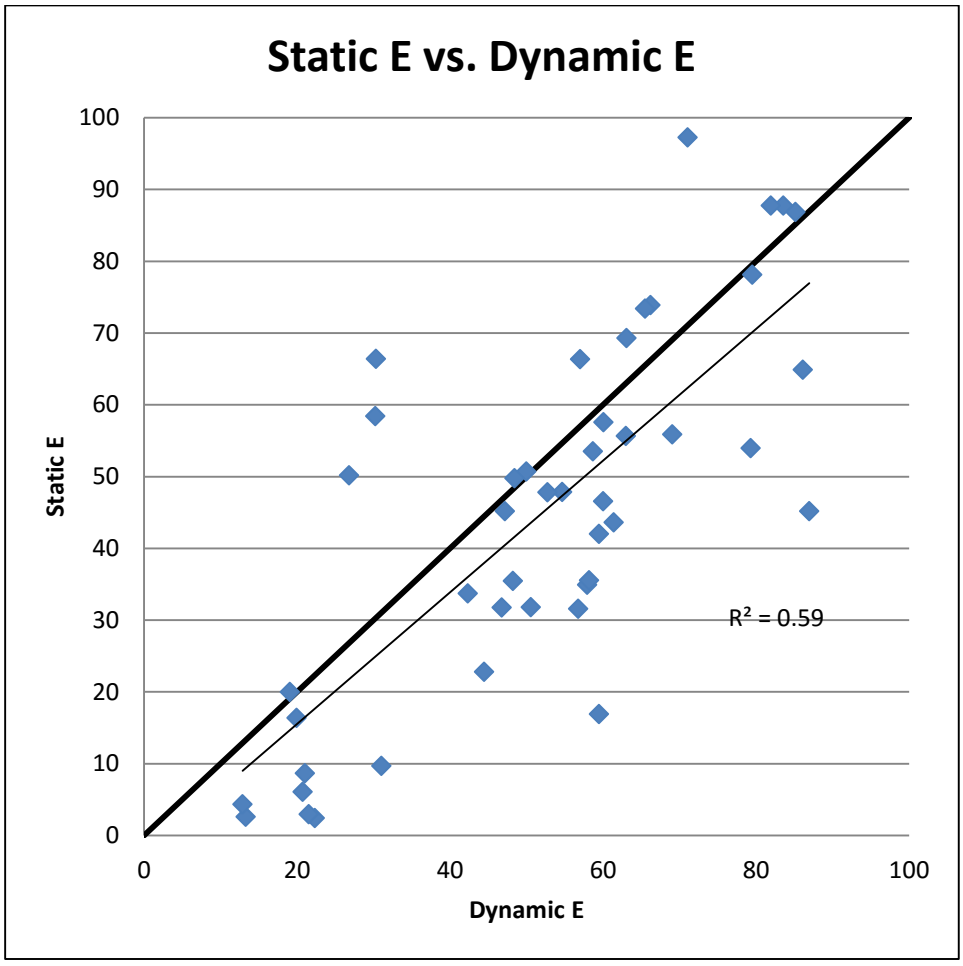

Figure 3-6. Independent correlations of Young's modulus. Thick black line is the one-to-one line and the thin black line is the regression line corresponding to the R^2 value.

The curve produced from the dynamic Poisson's ratio data (Figure 3-3c) has the same smoothing effect from the sonic tool averaging an interval of the borehole that is equivalent to the length of the tool. There is much less variability from point to point compared to the static curve (Figure 3-3c). The dynamic curve follows the static curve at the upper and lower limits. That is, where the static curve is high, the dynamic curve is high. Where the static curve is low, the dynamic curve is low. The intermediate v magnitudes show a smaller range in the dynamic data compared to the static data. Instead

of relatively gradual changes in the curve like the static data, the dynamic data show abrupt changes, particularly between 1,341 and 1,395 m (4,400 and 4,580 ft), and between 1,493 and 1,539 m (4,900 and 5,050 ft) bgs. Again, due to high attenuation, ultrasonic velocity in two samples at 1,708 and 1,718 m (5,604 and 5,639 ft) could not be measured accurately and are not shown on the plot. We suspect that the curve would drop in this interval based on the properties of these samples measured previously. The correlation plots (Figure 3-7) shows a weak correlation for the whole population of v measurements ($R^2 = 0.23$).

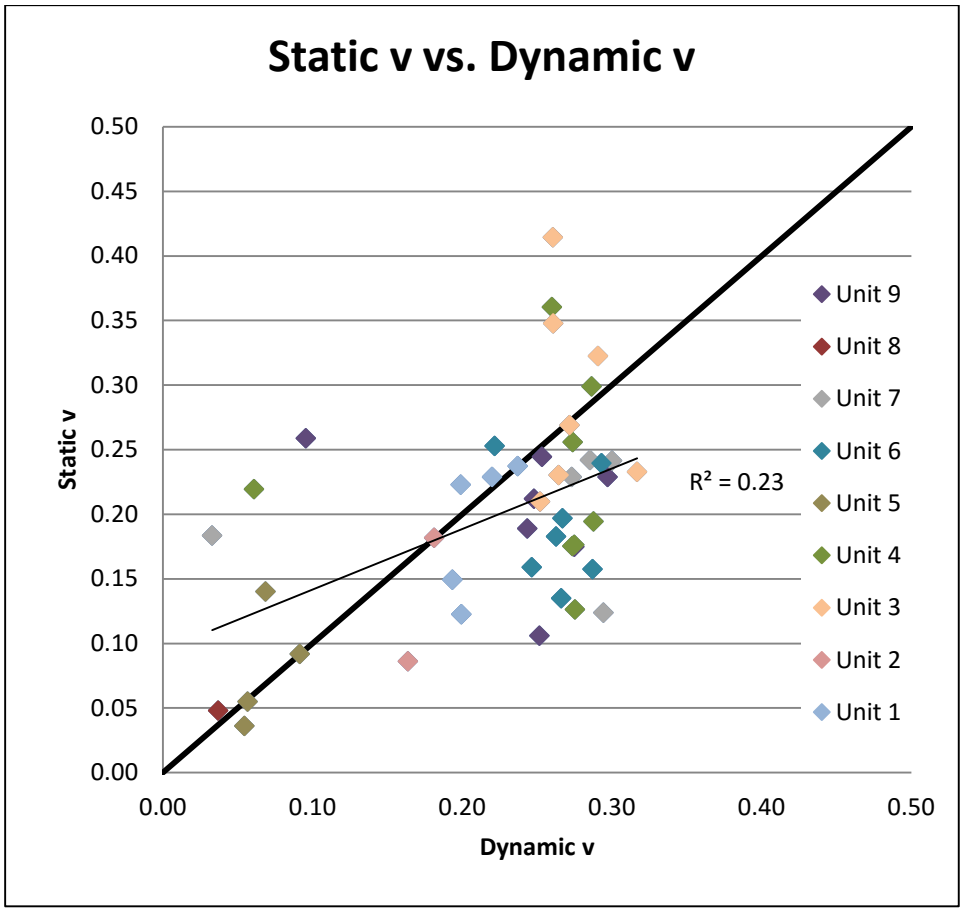

Figure 3-7. Independent correlations of Poisson's ratio. Thick black line is the one-to-one line and the thin black line is the regression line corresponding to the R^2 value.

The trend line is a measure of the fit of the whole data set. The data points are also plotted by mechanical unit as described in Chapter 2 and this distribution shows that the source of the scatter is from the unconfined UCS experiments that provided no restraint to lateral strain under applied stress. No confining pressure means each sample could undergo lateral strain that would be unrealistic under in situ conditions and is a drawback of unconfined compressive tests. For each mechanical unit, the set of dynamic v data are scattered along the y axis and have a very narrow range along the x axis. This relationship shows that the source of uncertainty is from the UCS experiments and that the precision of the dynamic data is high. We cannot test the accuracy of the dynamic data due to the scatter in the static data but we can say that the dynamic data are measured consistently. When we inspect the static and dynamic curves, we see that values for v are above the 0.2 line for the strong, elastic units and at or below the 0.1 line for the weak, plastic units in both curves. So the dynamic curve does produce a qualitative effective representation for the maxima and minima even though we may look skeptically at the quantitative reproduction of the elastic property on the whole.

Fracture Data from Core and BHTV Log

We measured fracture density in core and in the wellbore using wireline ultrasonic acoustic borehole image data (Figure 3-8). In this study, the fracture density interpreted from core data are generally double the number of fractures per 1.5-m (5-ft) interval compared to the fracture density interpreted from BHTV data. This phenomenon has been noted previously as being the source of common discrepancies between core and BHTV (or other borehole image) data (J. Lorenz, personal communication), although

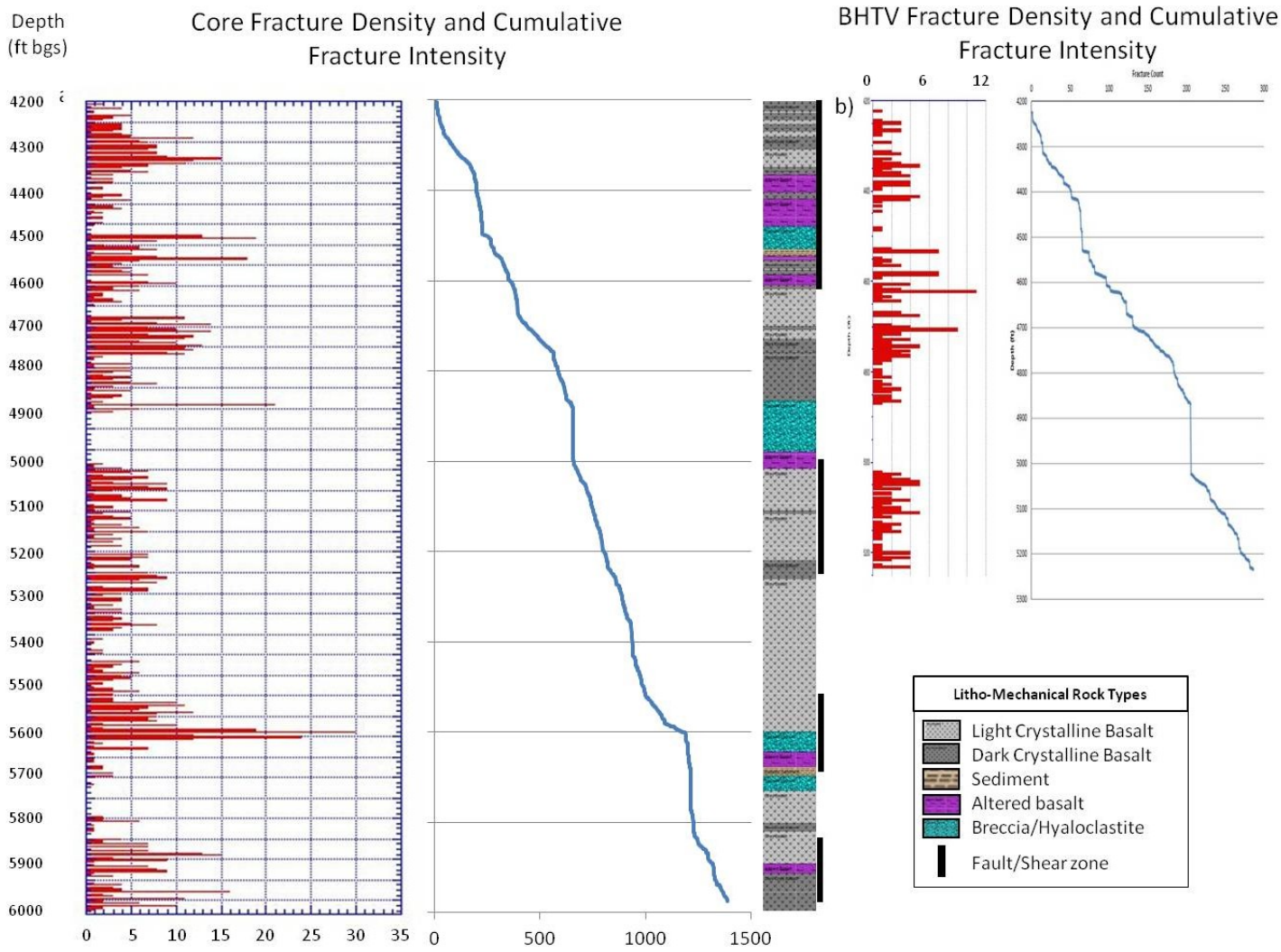

Figure 3-8. Comparison of core fracture data to BHTV fracture data. a) fracture density and cumulative intensity from core, b) fracture density and cumulative intensity from borehole televiewer data.

undersampling also happens in core in some cases. Despite the discrepancy in the magnitudes of fracture density distributions, the general pattern of the fracture density is comparable (Figure 3-8). For example, the the core fracture data in Unit 4 shows a large cluster of fractures near the bottom of the unit, few directly above that cluster and a general increase to maximum density in the unit near the top around 1,523 m (5,000 ft) bgs. Observation of the image log data shows a very similar pattern with a large cluster at the bottom, very few directly above that cluster and a general increase to a maximum near the top of the unit. Similar comparisons can be made for all of the other units as well. Unit 8, in both core fracture data and BHTV fracture data, has nearly zero fractures at the bottom but generally increases in fracture density up to the top of the unit.

Another notable pattern in the fracture density plots that could play an important role in future exploration wells is the tendency for fracture density to decrease sharply near the transition from the bottom of a crystalline lithology into the top of a zone of altered basalt and/or hyaloclastite. The most notable of these patterns can be seen in the core fracture density histogram at ~1,706 m (5,600 ft). The same relationship can be seen ~1,478 and ~1,325 m (4,850 and 4,350 ft) in both core fracture and BHTV fracture density plots. The challenge in evaluating the effectiveness of the BHTV data to test the interpretation of the mechanical stratigraphy is that data do not exist below ~1,595 m (5,235 ft) so we cannot analyze the results from the lower ~225 m (740 ft) including the target near the bottom of the borehole.

Borehole Wireline Logs

We compare the mechanical stratigraphic model from the dynamic properties with a suite of wireline borehole logs (Figure 3-9). The two main logs that are proxies for porosity, neutron and sonic velocitiy, appear to track each other closely and are likely responding to similar changes in porosity in the borehole. With the exception of Unit 7, the neutron log response is highest in the very strong, elastic units and lowest in the weak, plastic units and an intermediate response in the units with moderate strength and elasticity. Generally speaking, the higher response in the strong, elastic units could be interpreted as a result of higher fracture density and higher fluid flow in those units. A close inspection of the log and fracture density will reveal that the log does not respond exactly to fracture density in this way. However, not all fractures are open conduits for fluid flow and the neutron log is likely responding to those fractures that conduct fluids. The neutron log in Unit 7 is erratic and inconsistent with abrupt changes in counts and some flatlining on the boundary between Unit 7 and Unit 6. Unit 7 is highly altered and brecciated in places and the log could be responding to large vugs or washouts in the vicinity of the borehole wall.

Sonic velocities are highest in the crystalline rocks and lowest in the altered and weak units (Figure 3-9). Local variations in sonic velocities could be the result of the presence of fractures. Fractures are likely to decrease sonic velocity, especially if they are open and unfilled with secondary minerals. The neutron porosity tool measures at the borehole wall so disruption of the borehole wall in Unit 7 would explain the discrepancy between the neutron count response and the sonic velocities. The image log shows a very

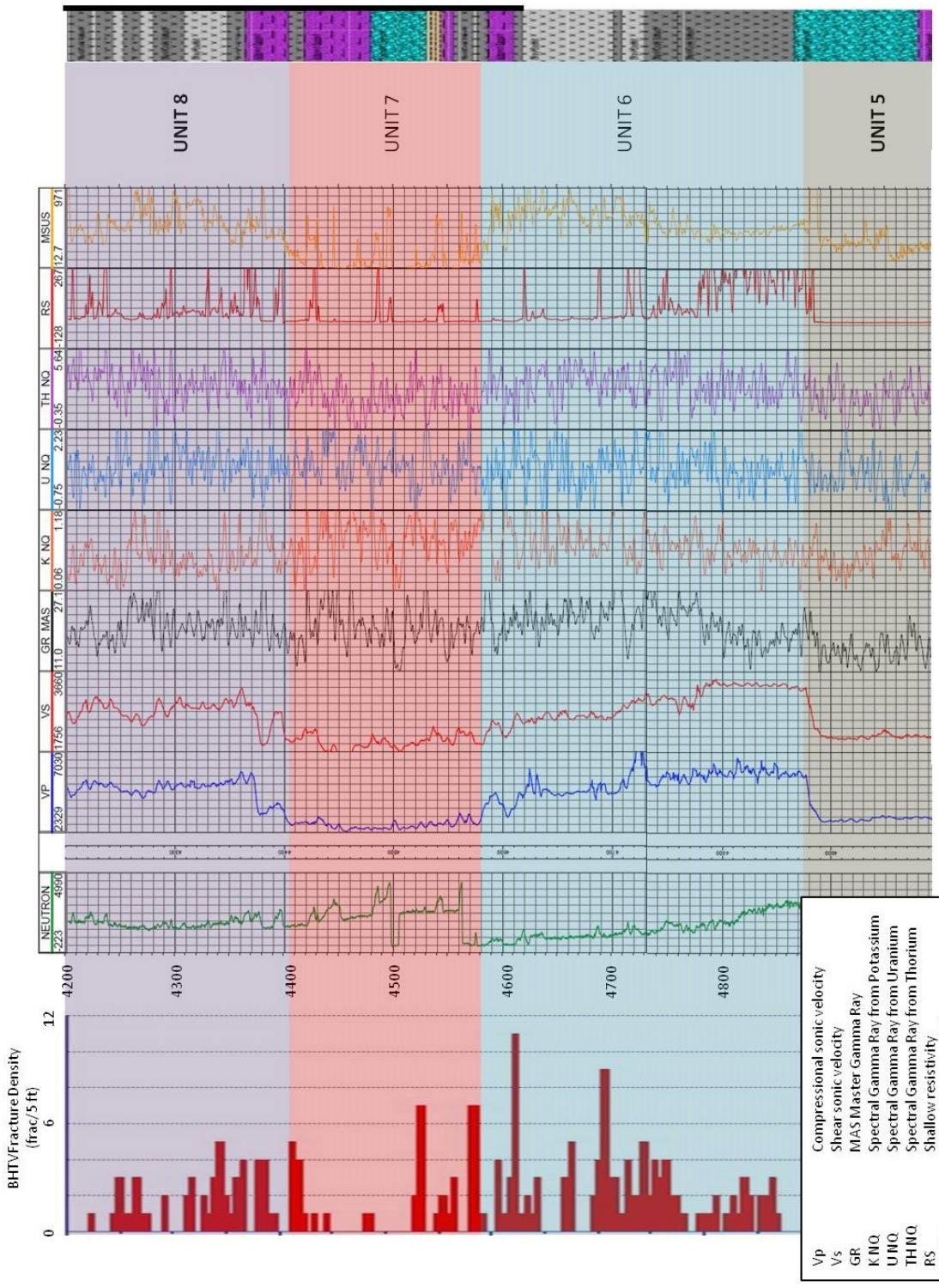

Figure 3-9. Borehole wireline geophysical log suite.

low-end amplitude response over the same interval of the erratic response in the neutron log and supports the interpretation that the borehole is highly distorted with washout, cave-in, breakouts, etc. over the interval 1,334 m (4,380 ft) to 1,392 m (4,570 ft). The sonic velocities are highest in the very strong units, intermediate in the moderate strength zones, and drop to very low velocities abruptly at the weak unit boundaries. Sonic logs appear to give the clearest indication of mechanical properties and could be used as a proxy for fracture density and fracture permeability in crystalline volcanic rocks.

The four gamma ray logs do not exhibit a strong response to the rocks on the scale of the mechanical stratigraphy, but do appear to have responded to details in the lithology on the sub-meter scale (Figure 3-9). The total gamma log has the strongest response and the potassium gamma ray log appears to mimic it the most and is likely the cause of the variation in the total gamma ray log. A potassium response is an indication of the presence of phyllosilicates with high potassium content. Many fractures are filled with secondary clay minerals so it might be tempting to use the potassium response to identify fractured zones that have fractures that are filled or partially filled with clay. However, many vesicles or altered zones have a large clay content. The gamma ray response in Unit 5 the lowest and is most distinct in the log, and the gamma counts are highest in the very strong units (Figure 3-9). The log signatures are subtle and we question the usefulness of using gamma ray logs as a tool to identify mechanical units objectively. The resistivity logs in Track 8 (Figure 3-9) show no separation between the shallow and deep resistivity that demonstrates little to no penetration of drilling mud into the formations. The logs do show unique absolute responses that seem to be unique for some lithological units but not necessarily a function of mechanical properties. The lower 38 m (125 ft) of Unit 6 is a

single, relatively unfractured lithological unit that has a unique resistivity compared to the overlying lithological unit that is part of the same mechanical Unit 6. The resistivity log responds similarly in Unit 7 as it does in the upper ~45 m (150 ft) of Unit 6, which is an indication that resistivity is a more a function of lithology in these rocks that mechanical properties and should be used with caution when interpreting mechanical stratigraphy. The strong units seem to have the highest resistivity whereas the weak units exhibit mostly baseline resistivity values (Figure 3-9). The magnetic susceptibility log seems to subtly respond to the mechanical units with the lowest measurement in the weak units. The logs could be used to support an interpretation as a proxy for the degree of alteration and, presumably, a corresponding change in mechanical properties. The magnetic susceptibility logs do show a distinct change at the boundaries of the weak units so could be used to support an interpretation of weak units in future exploration wells.

Discussion and Interpretation

A comparison of the independent interpretations of mechanical stratigraphy from static and dynamic data (Figure 3-10) shows that the calculations of dynamic properties are very effective for predicting rock strength and elastic properties for the purpose of identifying the same mechanical stratigraphic units as those interpreted from static data. The dynamic data replicate the magnitude of the static data reasonably well and we show that in the case of Poisson's ratio, the dynamic data are a considerably more precise than static calculations from our unconfined compressive tests (Figure 3-7). The correlation analysis of Poisson's ratio shows that the dynamic calculations are more precise although we cannot test the accuracy due to the scatter in the static ν data set. This is not surprising

considering the lack of confining pressure in the unconfined experiments. While we cannot make a definitive conclusion for the accuracy of the magnitudes of ν, the data do show that the dynamic calculations are more consistent for each mechanical unit.

There is a slight variation in the number and thicknesses of mechanical units determined from the two methods. The Unit 1/Unit 2 pairing was modeled very similarly with

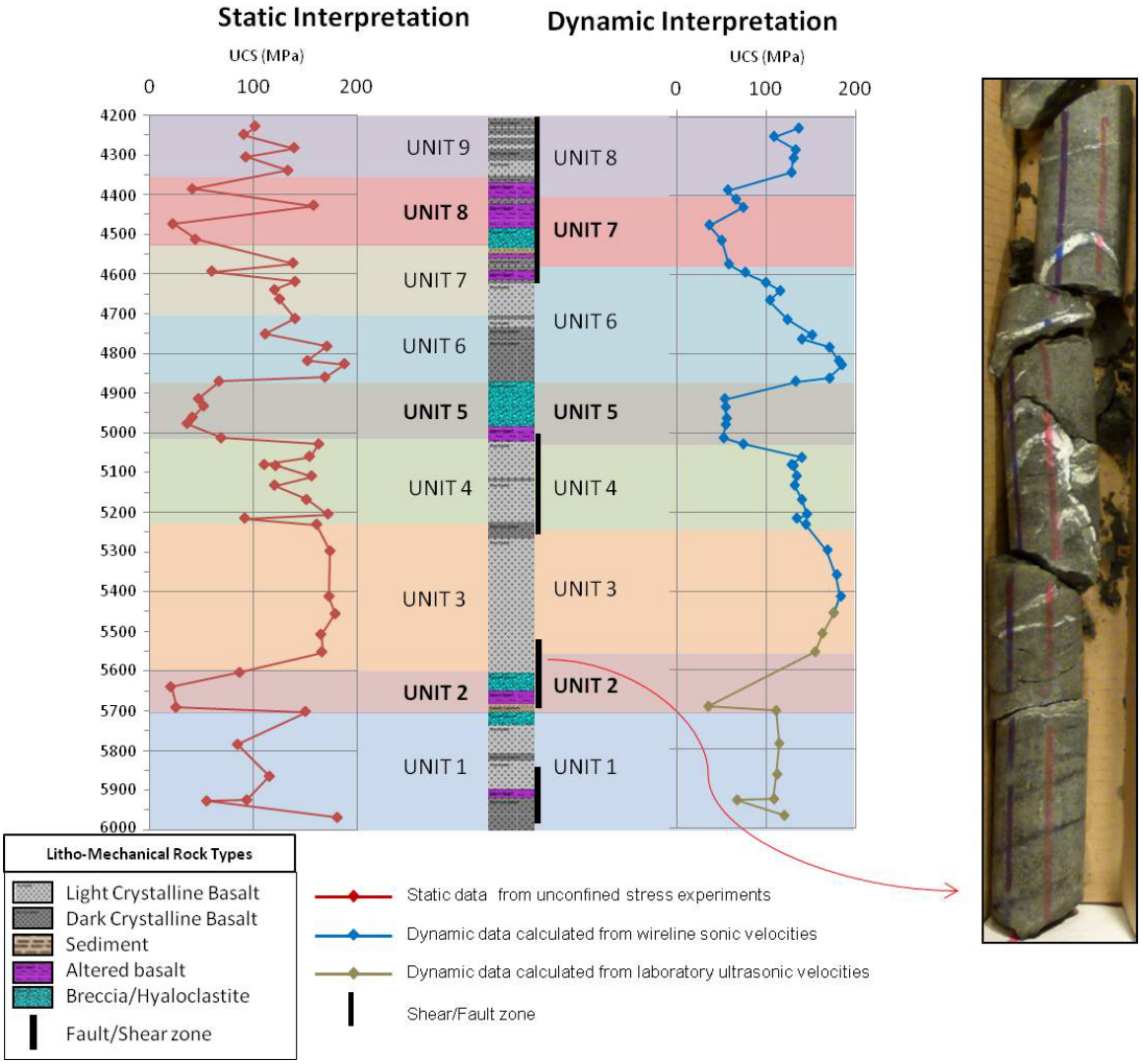

Figure 3-10. Interpretation of mechanical stratigraphy from static and dynamic data.

dynamic properties. Unit 2 was modeled about 15 m (50 ft) thick in the dynamic interpretation and corresponds to a specific lithological unit that is part of an altered and reworked section of lithology. A sample of the core from this interval shows that the section is fractured although the fractures are sealed with both clay and calcite. This discrepancy can be explained from the sparse sampling in this interval. Under most circumstances, continuous bulk density data would be available to calculate continuous logs for E, v, and UCS. This would likely indicate that 15-m (50-ft) interval as part of mechanical Unit 3 and we would avoid the ambiguity in guessing a boundary in that 15-m (50-ft) interval.

Dynamically defined Units 3, 4, and 5 are modeled as nearly identically to the static interpretation. There is a slight variation in thickness in Unit 3 and Unit 5 is almost identical and corresponds to a discrete interval of altered or reworked rocks. We determined that Unit 6 in the dynamic interpretation was a single transitional unit and it would have been difficult to justify splitting it into two units from the dynamic properties. The uppermost weak, plastic unit (8, static; 7, dynamic) is of comparable thickness but is shifted about 15 m (50 ft). Since we made these interpretations blind of lithology, we could later justify combining the two units into a single unit, if necessary. However, for the purpose of analyzing the dynamic interpretation, it shows that with a little variation, the uppermost weak, plastic unit is modeled consistently.

The implication of this work is that the wireline log data from boreholes used to calculate dynamic rock properties can allow us to effectively interpret the mechanical stratigraphy and produce reasonable magnitudes of rock strength and elastic properties. This reduces the need to invest the time and resources to collect whole-rock core samples

and executing the experiments required to make the static measurements and calculations. We have identified a weak, plastic cap rock, Unit 2, and underlying fractured (potential) geothermal reservoir in Unit 1 from the mechanical interpretation from static data and successfully replicate those data so that the same or similar could have been made without the investment in producing the static data. This contact should be the target in future exploration wells. We show that the contrast in rock properties between these two units should be visible in a number of logs and the rapid change should be used to identify the Unit2/Unit1 contact. The study demonstrates that we can use dynamic data in future exploration wells to identify the Unit1/Unit 2 contact to determine the extent of the potential reservoir and develop fairway play concepts to better understand the extent of the resource and the potential to exploit the resource for power generation.

The scale of interpretation is very important in this case. The goal is to identify mechanical stratigraphic units that are on a scale appropriate for the size of the reservoir that is being sought. In this case, the bottom of the potential reservoir is unknown but based on lithology and fracture density data we infer that the thickness of the potential reservoir is at least 30 m (100 ft) or more. We grouped mechanical units at a scale that is appropriate for the size of the reservoir. Heterogeneity within the lithological units could cause one to interpret mechanical units on the scale of around 3 m (10 ft). For example, within the upper 150 m (500 ft) there are multiple thin beds, each of which has unique mechanical properties. It would not be unreasonable to interpret the data to include many more than the three mechanical units we have interpreted here. Knowing the lithological heterogeneity allows us to explain the nature of mechanical response in the upper three units compared to the lower units that have been interpreted from much thicker units.

There is a considerable lack of variability in the dynamic data compared to the static data. The variability is a result of the resolution of the two methods. Static data are selected from individual samples and each one may be from a different lithology. The intermediate units exhibit internal values as a result of there being more variability at a finer scale than our analyses consider. Dynamic data, on the other hand, is based on an average sonic velocity between the source and the receiver in the instrument and could be as much as a 2 m (6 ft) interval. For this reason, the dynamic data do not represent the same resolution as the static data and, therefore, do not have the same amount of variability from sample point to sample point. The most obvious example of this phenomenon is in the interval of the ZOI from 1,280 m (4,200 ft) to ~ 1,408 m (4,620 ft) bgs. Over this interval the beds are much thinner so a wide variety of specific mechanical properties is averaged in the dynamic data set so that the dynamic curve is much smoother than the static curve. In the lower intervals of the ZOI, the beds are thicker and the variation in the dynamic curve mimics the static curve much more closely. Another source of the discrepancy in this case is that we are required to use bulk density measured from the core samples. In a more common application of this method, continuous bulk density log data would be used and the result would be continuous logs for E, v, and UCS. Continuous logs may show more variability than the curves in this study. The quantitative analysis of the ability of dynamic calculations to reproduce the same data that are calculated show that the method works very well for Young's modulus and uniaxial compressive strength and less so for Poison's ratio. The Poisson's ratio data are clustered strongly by strong and weak units. Nonetheless, there is an expected relationship between each property as the dynamic data increase with the increase in

static data. Factors that impact the final quantitative analysis include variability in the experimental technique, microfractures and imperfections in each sample, and limitations in getting precise bulk density measurements. In addition, limitations of the acoustic televiewer instrument need to be considered when evaluating the value of fracture data in volcanic geothermal systems. There is risk involved in relying on borehole image data for fracture analysis and the value of fracture data must be considered when weighing that risk in a well plan. For this study, we only considered fracture density from all natural fractures. We did not include drilling induced fractures in this data set but we did not distinguish between open, sealed, partially sealed, or the type of mineral fill in the fractures.

Neutron porosity, sonic velocity, and magnetic susceptibility logs provide the strongest support for interpretation of the distribution of rock strength and elastic properties in the data presented here. Neutron porosity and sonic velocity logs best model the abrupt change in mechanical properties between the strong and weak rocks. The neutron logs are susceptible to the condition of the borehole wall but are still an independent source of data since the sonic velocities are used to calculate the elastic properties. Magnetic susceptibility in basalts is likely driven by the amount of hydrothermal alteration and reworking of basalts. This is effective in supporting the interpretation because those units also are the weak, plastic units and the logs can help identify zones of crystalline basalt from basalt that has been altered or reworked. Gamma ray and resistivity showed a consistent response to lithology at a scale that was too fine to help identify mechanical units for our purposes.

We assessed the potential of dynamic data to reproduce results from UCS experiments on core samples in basalts. Due to the lack of extensive core samples in resources plays, an assessment of this kind has rarely been attempted commercially and this study can serve as a good analog for analysis of mechanical stratigraphy in unconventional petroleum systems as well. A cost- and time-effective technique for interpreting rock strength and elastic properties is required to efficiently analyze the distribution of mechanical properties to assess the potential for fracture development and connection. We demonstrate here that the method of making dynamic calculations of rock strength and elastic properties effectively reproduces results from detailed UCS experiments.

Conclusions

The MH-2 borehole on the Mountain Home Air Force Base near Mountain Home, Idaho, USA encountered a high-temperature artesian flow zone with equilibrated temperatures around 140°C at 1,745 m (5,726 ft) bgs with a high potential for commercial geothermal energy development. Whole-rock core samples from the borehole were used to conduct uniaxial compressive stress experiments to measure strain under stress loads. The data were used to calculate static uniaxial compressive rock strength and elastic properties, Young's modulus and Poisson's ratio. The results were interpreted to represent nine mechanical units in the ZOI from 1,280 m (4,200 ft) to TD at 1,821 m (5,976 ft) bgs. This study tested the more commonly used method to use sonic data and bulk density to calculate dynamic elastic properties and rock strength to test the effectiveness of the method to reproduce static results in lieu of having enough core and

resources to test enough core samples to describe the mechanical stratigraphy. Dynamic data are much more commonly collected and are usually more readily available and desirable to use to calculate rock strength and elastic properties. The method is most commonly implemented in sedimentary rock to understand the mechanics of conventional and unconventional petroleum reservoirs. As more exploration and development takes place in tights sands, shales, and crystalline reservoirs, the mechanical stratigraphy becomes more import for production of petroleum and geothermal resources alike.

This study demonstrates that dynamic elastic parameter data do effectively produce high quality data for interpretation that are as effective as detailed static data. The project shows that mechanical stratigraphy in future exploration wells in the Mountain Home area can be accomplished through the calculation of dynamic data alone, saving the time and expense required to collect continuous whole-rock core to conduct UCS experiments. It also shows that in support of sonic logs, magnetic susceptibility seems to respond to the change from weak to strong units and could be used in support of interpretation in future boreholes. Gamma ray and resistivity logs may also be helpful but should be viewed carefully. While the quantitative analysis conducted here shows a strong correlation between static and dynamic data, a more rigorous analysis should be conducted and a conversion applied to the dynamic data if the data are to be used for well bore stability, completions/stimulation designs, quantitative geomechanical modeling or discrete fracture network modeling.

References

Blackwell, D.D., 2012. Geothermal heat flow map of the U.S. (http://www.smu.edu/~/media/Site/Dedman/Academics/Programs/Geothermal%20Lab/Graphics/SMU2011USHeatFlowMap.ashx?la=en).

Bonnichsen, B., Godchaux, M.M., 2002. Late Miocene, Pliocene, and Pleistocene geology of southwestern Idaho with emphasis on basalts in the Bruneau-Jarbidge, Twin Falls, and western Snake River Plain regions. In: Bonnichsen, B., White, C.M., McCurry, M., (Eds.), Tectonic and Magmatic Evolution of the Snake River Plain Volcanic Province. Idaho Geol. Surv. Bull. 30, 233–312.

Devorak, A., 1970. Seismic and Static Modulus of Rock Masses. Proc. Int. Soc. of Rock Mech. 1, 313 – 317.

Ferno, M.A., 2012. Enhanced oil recovery in fractured reservoirs. In: Romero-Zeron, L., (Ed.), Introduction to Enhanced Oil Recovery (EOR) Processes and Bioremediation of Oil-Contaminated Sites. ISBN: 978-953-51-0629-6, InTech, DOI: 10.5772/47976., Rijeka, Croatia, May 23, 2012.

Fjaer, E., Stroisz, A.M., Holt, R.M., 2013. Elastic dispersion derived from a combination of static and dynamic measurements. Rock Mech. Rock Eng. 46, 611-618.

LaPointe, P.R., 1987. A method to characterize fracture density and connectivity through fractal geometry. Int. J. Rock Mech. Mineral Sci. Geomech. 25, (6), 421-429.

Laubach, S.E., Olson, J.E., Gross, M.R., 2009. Mechanical and Fracture Stratigraphy. Am. Assoc. of Petrol. Geol. Bull. 93, (11), 1413-1426.

Lucier, A., Zoback, M., Gupta, N., Ramakrishnan, T.S., 2006. Geomechanical aspects of CO_2 sequestration in a deep saline reservoir in the Ohio River Valley region. Env. Geo. 13, (2), 85-103.

McCurry, M., Watkins, A.M., Parker, J.L., Wright, K., Hughes, S.S., 1996. Preliminary volcanological constraints for sources of high-grade rheomorphic ignimbrites of the Cassia Mountains, Idaho: Implications for the evolution of the Twins Falls volcanic center. Northwest Geology, 26, 81–91.

Nelson, R., 2001. Geologic Analysis of Naturally Fractured Reservoirs, Gulf Publishing Co., Houston, TX, 352.

Petrie, E.S., Jeppson, T.N., Evans, J.P., 2012. Predicting rock strength variability across stratigraphic interfaces in cap rock lithologies at depth: Correlation between outcrop and subsurface. Env. Geosciences, 19, (4), 125-142.

Pierce, K.L., Morgan, L.A., 1992. The track of the Yellowstone hotspot: Volcanism, faulting, and uplift. In: P.K. Link, M.A. Kuntz, L.B. Platt, (eds.), Regional Geology of Eastern Idaho and Western Wyoming. Geological Society of America Memoir 179, 1-53.

Plona, T.J., Cook, J.M., 1995. Effects of stress cycles on static and dynamic Young's moduli in Castlegate sandstones. In: Daemen, Schultz (Eds.), Rock Mechanics. Balkema, Rotterdam, 155-160.

Potter, C.C., Foltinek, D.S., 1997. Formation elastic parameters by deriving S-wave velocity logs. In: CREWES Research Report, 9, 10-1 – 10-2.

Ruez Jr., D.R., 2009. Framework for stratigraphic analysis of Pliocene fossiliferous deposits at Hagerman Fossil Beds National Monument, Idaho. Rocky Mtn. Geol. 44 (1), 33-70.

Shervais, J.W., Schmitt, D.R., Nielson, D., Evans, J.P., Christiansen, E.H., Morgan, L, Shanks, W.C.P., Prokopenko, A.A., Lachmar, T., Liberty, L.M., Blackwell, D.D., Glen, J.M., Champion. D., Potter, K.E., Kessler, J.A., 2013. First results from HOTSPOT: The Snake River Plain Scientific Drilling Project, Idaho. U.S.A. Sci. Drill. 15, 36 – 45.

Shervais J.W., Shroff, G., Vetter, S.K., Matthews, S., Hanan, B.B., McGee, J.J., 2002. Origin and evolution of the western Snake River Plain: Implications from stratigraphy, faulting, and the geochemistry of basalts near Mountain Home, Idaho. In: Bonnichsen, B., White, C.M., McCurry, M., (Eds.), Tectonic and Magmatic Evolution of the Snake River Plain Volcanic Province. Idaho Geol. Surv. Bull. 30, 343-361.

Zoback, M.D., 2010. Reservoir Geomechanics, Cambridge University Press, New York, pp. 461.

Zoback, M.D., Barton, C.A., Castillo, D.A., Finkbeiner, T., Grollimund, B.R., Moos, D.B., Ward, C.D., Wiprut, D.J., 2003. Determination of stress orientation and magnitude in deep wells. Int. J. Rock Mech. Mining Sci. 40, 1049 – 1076.

CHAPTER 4

IN SITU STRESS AND GEOLOGY OF THE MH-2 BOREHOLE, MOUNTAIN HOME, IDAHO, USA: IMPLICATIONS FOR GEOTHERMAL EXPLORATION FROM GEOMECHANICS[3]

Abstract

The western Snake River Plain is a zone of high heat flow and is a target for commercial geothermal energy exploration. To assess the geothermal potential, the MH-2 borehole was drilled on the Mountain Home Air Force Base for the Snake River Scientific Drilling Project (Hotspot) into fractured crystalline basalt. At a depth of 1,745 m (5,726 ft) it revealed the presence of artesian hydrothermal fluids. A weak, hydrothermally altered unit with few fractures was apparently juxtaposed by faulting over the strong, elastic, fractured reservoir. The hydrothermally altered fault gouge and fault breccias act as a cap rock seal and hydrothermal barrier. Hydrothermal alteration of basalt minerals to corrensite in the reservoir below the weak, altered cap rock unit indicates a significant increase in the in situ thermal capacity of the reservoir. We characterize the state of stress based on and integrated it with detailed descriptions of lithology, fracture stratigraphy, mechanical stratigraphy, and shear slip indicators. Shear slip indicators cluster in predictable zones from an apparent variety of failure mechanisms. Our observations suggest the Mountain Home borehole was drilled into a complex structural environment

---

[3] Chapter to be coauthored by:

J. A. Kessler[a], K. Bradbury[a], D. R. Schmitt[b], J. W. Shervais[a], J. P. Evans[a]

[a] Dept of Geology, Utah State University, 4505 Old Main Hill, Logan, Utah 84322 USA

[b] Dept of Physics, University of Alberta, 4-181 CCIS, Edmonton, AB T6G 2E1 Canada

in an oblique-normal fault zone. Present-day mean stress orientations are consistent with regional Basin and Range stresses and oblique motion is consistent with recent dextral-normal oblique slip on faults in the northwesternmost extent of the western Snake River Plain. Present day strain rates are near zero and the local faults are in frictional equilibrium. A simple geomechanical model suggests that if the formations are overpressured at depth, as is common in geothermal reservoirs, differential stress and stress anisotropy are low and the system has the potential to have mixed failure mechanisms of normal motion and strike-slip motion. We suggest a structural model that shows the MH-2 borehole was drilled onto a faulted ramp between the tips of large en echelon faults along the boundary of a buried gravity high.

Introduction

The Snake River Scientific Drilling Project (Hotspot) examined the potential for commercial geothermal energy resources in the central and western portions of the Snake River Plain, Idaho, USA (Shervais et al., 2013). Three boreholes were drilled to examine the thermal gradient, in situ fluid chemistry and temperature, core geochemistry and geomechanics, and borehole conditions. The boreholes (Figure 1-1) were each drilled to a total depth (TD) near 1,800 m (6,000 ft). Borehole KA-1 was drilled at Kimama ~32 km (~20 mi) north of Burley, Idaho. KY-1 was drilled on the Idaho Agricultural Experiment Station, a University of Idaho facility in Kimberly, Idaho near Twin Falls and MH-2 was drilled on the Mountain Home Air Force Base near Mountain Home, Idaho (Figure 1-1). Temperatures in borehole KA-1 are isothermal to ~900 m (3,000 ft) due to the presence of the Snake River Plain aquifer (Sant, 2012; Shervais, 2010), a large regional aquifer

that occupies a thick section of fractured basalt and rhyolite in the eastern and central Snake River Plain (SRP). Borehole MH-2, drilled on Mountain Home Air Force Base (MHAFB), near Mountain Home, Idaho, exhibits a thermal gradient of ~73°C/km and the bottom-hole temperature is ~140°C with flowing artesian thermal water, indicating the potential for commercial geothermal energy if the resource is proven to be extensive enough for development. The work presented here is focused on fracture characterization, mechanical stratigraphy, and analysis of the stress state from the MH-2 borehole.

Geothermal reservoirs in crystalline volcanic rocks rely on connected fracture networks for fluid storage and permeability. Matrix porosity and permeability in volcanic reservoirs is low. Connected fractures provide both the volume for fluid storage and conductive heat transfer from the formation to the fluids and the permeability required for convective heat transfer as well as production from the reservoir (Wohlentz and Heiken, 1992). Typically, not all fractures contribute to porosity or permeability and in some cases as few as 10-20% of the fractures appear to provide connected pathways for flow (Morin et al., 1997). Any reservoir characterization study must identify, describe, and model the important fractures, those that contribute to porosity and permeability. In Chapters 2 and 3 we examined the distribution of rock strength, elastic properties, and fractures studied in core and wireline borehole geophysical logs. In this chapter, we review of regional geology from geological mapping and previous boreholes drilled in the region and examine stress directions and magnitudes from breakout data. We build on the mechano-stratigraphic model developed in the previous chapters and discuss the stratigraphic relationships and stress state to suggest a structural geological model based on Anderson mechanics and Coulomb frictional faulting theory that can explain our

observations of lithology, fractures, mechanical properties, and stress. This work constrains the conceptual geomechanical framework model that can serve as the foundation of quantitative geomechanical and discrete fracture network models that will: 1) estimate the distribution of critically stressed faults and fractures that could be conduits for fluid flow, 2) analyze the potential connected fracture networks in the geothermal reservoir, and 3) constrain permeability anisotropy.

The mechanical stratigraphy, fracture density, and wireline borehole geophysical logs have been described previously. In this chapter, we examine the lithology in detail including mineralogical analyses that explain the in situ bottom-hole temperatures compared to the measured equilibrated temperatures from wireline measurements. We discuss the variability between oriented fracture data measured with ultrasonic acoustic televiewer logs and fractures measured directly from core. The work done previously is put into a regional geological context and we explore the potential geological models to explain our observations. To accomplish those goals we examine:

- Lithological relationship to mechanical stratigraphy
- Fracture density, orientations, and shear slip indicators
- Indication of fault zone permeability
- Present-day state of stress
- Critically stressed fault and fracture orientations

The regional geology puts into context the detailed data revealed in the MH-2 borehole and helps us understand the nature of the stratigraphic and structural geology that controls the potential geothermal system in the western Snake River Plain. The

geological and geomechanical models presented here will be the foundation for future work derived from exploration wells and detailed modeling to predict the connected fracture network, analyze the stress field on the larger regional fracture field, predict fluid flow and thermal flux in the reservoir, and model the effects of stimulation of the reservoir.

Study Area

The Snake River Plain (SRP) volcanic province (Figure 1-1) has a thick section of mantle-derived basalts that erupted in the axial portions of the plain over the past 6 - 8 million years and are similar in composition to mafic oceanic island basalts like those forming the Hawaiian Island chain (Bonnichsen and Godchaux, 2002; Shervais et al., 2002). Thick sequences of felsic rhyolite caldera complex deposits are present along the margin of the plain as a result of melting of continental crust during intrusion of basalts from the hotspot melting source (McCurry et al., 1996; Pierce and Morgan, 1992). The volcanic sequences record a complete record of volcanism from ~17 Ma to 200 ka in the west and up to 2 ka in the east. The SRP is a region of very high heat flow (Blackwell, 2012) sourced from emplacement of a large amount of basaltic magma in the deep to intermediate-depth crust (Shervais, 2010).

The oblique-extension, fault-bounded basin of the western SRP is a result of a complex interaction with the Yellowstone hotspot ~17 Ma and western extension of the Basin and Range beginning ~11 Ma (Shervais et al., 2002; Wood and Clemens, 2002). It has generated a basin bound by high-angle normal faults with offset up to ~2,750 m (9,000 ft) (Malde, 1991). The basin is adjacent to the Idaho batholith to the northeast and

the volcanic rocks of the Owyhee mountain range to the southwest (Benford et al., 2010; Bonnichsen et al., 2008). The horst and graben complex of the Great Basin extends from the southeast to the northwest into eastern Oregon and includes the western SRP. The basin-bounding faults are almost orthogonal to the hotspot track and the eastern SRP (Wood and Clemens, 2002). The northwest oriented graben held the ancient Pleistocene Lake Idaho that extended from the central SRP in the southeast to the Idaho-Oregon border to the northwest. Approximately 600m (2,000 ft) of lake sediments accumulated over the Miocene-aged volcanic rocks and underlying Pleistocene basalts that erupted from the end of Lake Idaho time to the present (Ruez, 2009). High heat flow in the region (Figure 4-1) and the potential for fluid storage and permeability in connected fracture networks make the western Snake River Plain a target for exploration for commercially viable geothermal energy. The northeastern boundary of the basin is defined by range front faults that strike in two clusters. Faults near the MH-2 borehole (blue faults in Figure 1-1), as mapped by Shervais et al. (2002), are oriented N60°W and are truncated by younger faults oriented N85°W. Regional faults to the northeast are generally oriented consistently with the N60°W cluster (Breckenridge et al., 2003). The plateau boundary faults are consistent with the range front faults and are oriented N60°W while faults on the plateau are oriented more northerly at N20°W and are consistent with faults mapped in the Idaho Batholith to the northeast (Breckenridge et al., 2003).

Three boreholes have been drilled nearby the MHAFB previous to MH-2 and provide insight into the moderate-depth stratigraphy and structure across the western SRP (Figure 1-1). The Bostic-1A drillhole is a 2,949 m (9,676-ft) wildcat oil and gas

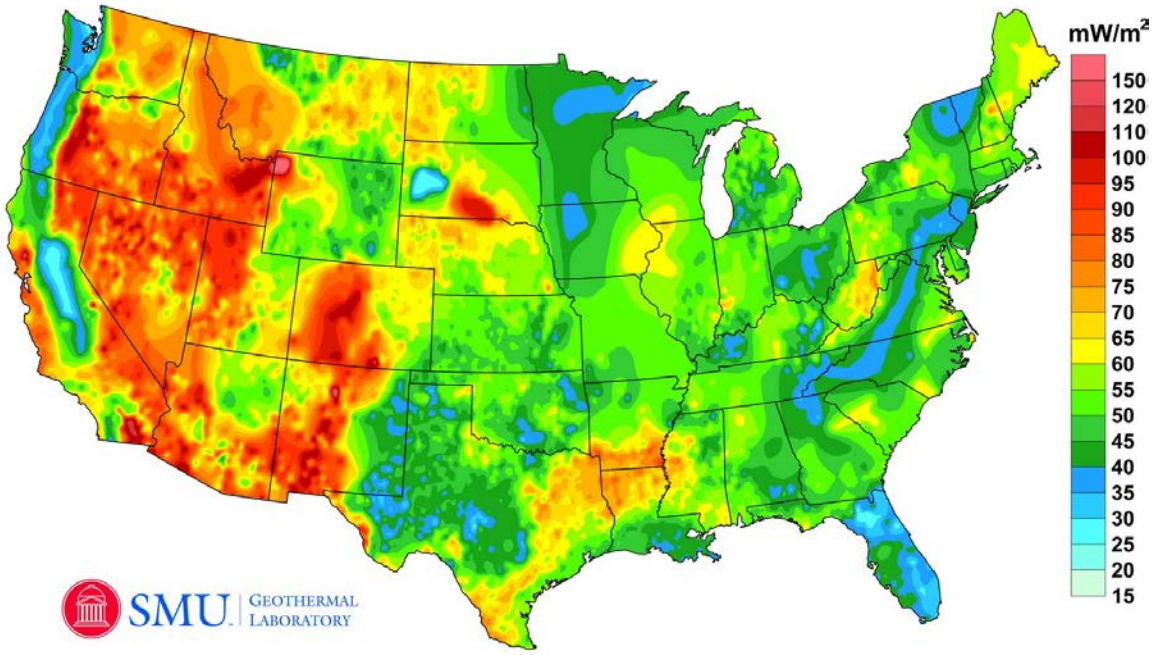

Figure 4-1. Heat flow map of the United States (Blackwell, 2012)

exploration hole drilled in 1975 about 35 km (22 mi) east of MH-2. The borehole was drilled through alternating beds of sediment and basalt and into felsic rhyolites from ~2,200 m (~7,100 ft) to TD. The drill hole is located near the basin-bounding normal fault and likely has experienced significant faulting. Arney et al. (1982, 1984) mention faulting in the context of providing accommodation space for erupting volcanics but do not provide details on fault surfaces due to their work with cuttings instead of whole core. The varying thickness in basalt units indicates normal faulting that provides the accommodation space. They describe a considerable amount of highly hydrothermally altered volcanic rocks, both basalt and rhyolite, near the bottom of the borehole indicating a geothermal resource that is extensive if it is hydraulically connected to the reservoir in MH-2. The MH-1 borehole was a geothermal exploration well drilled on the

MHAFB in 1985 to a depth of 1,342 m (4,403 ft). Details from MH-1 are scarce but the borehole penetrated about 580 m (1,900 ft) of interbedded basalt and Lake Idaho lakebed sediments until drilling through basalt from 580 m (1,900 ft) to TD (Lewis and Stone, 1988). The borehole was cored but the report does not mention fractures or fault surfaces. The other nearby drill hole is the Anschutz Federal No. 1 well located about 40 KM (25 mi) to the west-southwest of MH-2 near to the southwestern basin-bounding normal fault along the Owyhee Plateau. The borehole was logged from cuttings so fault and fracture data were not available. The lithology reveals a similar thick sedimentary lacustrine unit overlying volcanic rocks. This borehole revealed mostly rhyolite with limited basalt layers. Hydrothermal alteration concentrated in places indicates that the rocks are highly faulted and fractured in the borehole. The borehole is documented as penetrating basement granite near TD. This may be a result of the borehole crossing a dipping normal fault and penetrating the basement in the footwall of the fault.

The drill site for MH-2 was partially chosen based on the presence of an elliptical gravity high with a long axis that is sub-parallel to the axis of the plain (Figure 2-3) based on an interpretation of the Bouger gravity anomaly map from Idaho gravity data (Kucks, 1999). In an attempt to access the fracture zones around the boundary of the caldera that were expected to be zones of high fluid conductivity and convective heat flow. The gravity anomaly could be a result of underplating of the crust from the intrusion of dense mantle material (Glen and Ponce, 2002; Shervais et al., 2010). Speculation as to the presence of the structures in the graben is that a number of high-angle normal faults exist to produce the accommodation space for a larger volume of early to middle Pliocene basalts in the central part of the western SRP (Arney et al., 1982, 1984; McIntyre, 1979;

Shervais et al., 2002). The evidence of structures in the subsurface raises the prospect for geothermal development. Faulds et al. (2010) have described a suite of structural environments that best produce commercially viable geothermal resources based on projects developed between sites in the western Great Basin and in Turkey (Faulds, personal communication). Of the five scenarios they presented, three may fit the structural controls around MH-2: 1) intersections between normal faults and transversely oriented oblique-slip faults, 2) terminations of major normal faults, and 3) transtensional pull-apart zones. They describe real world examples of these structural controls being a factor in the development potential of geothermal resources. We will show that the environment around MH-2 may include one or all of the three listed here.

Methods

Whole rock core was recovered over the 540 m (1,775 ft) zone of interest (ZOI) to total depth (TD) of 1,821 m (5,976 ft) in MH-2 and wireline borehole geophysical logs measured properties of the rocks from the top of the ZOI to a depth of 1,662 m (5,456 ft). We measured shear and compressional sonic velocities in the laboratory on samples collected below 1,662 m (5,456 ft) to TD to supplement the wireline sonic log data (Chapter 2). The data were used to analyze mechanical, elastic, and other rock properties; measure fracture density, orientation, and morphology; and assess stress magnitudes and orientations. Core samples were used for unconfined uniaxial compressive strength (UCS) experiments, fracture characterization, lithological descriptions, and mineralogical analyses. Wireline logs were used to describe rock properties, calculate dynamic elastic properties and rock strength, map fracture density and orientation with ultrasonic acoustic

borehole televiewer (BHTV) data, and provide insight into stress directions and magnitudes. We summarize the results of UCS experiments and wireline log analyses and modeling. In this study, we analyze the stress data and utilize Coulomb frictional faulting theory to develop two end-member structural models that can explain our observations. The two-dimensional data allow us to constrain the range of possible explanations for our observations.

Core Data: Lithology, Fractures, and Geochemistry

The MH-2 borehole was cored with whole rock recovery > 90%. A detailed core characterization was completed over the zone of interest in MH-2 from 1,280 m (4,200 ft) to TD 1,821 m (5,976 ft) including lithology, fracture characteristics, shear failure indicators, and mechanical properties. As reported in Kessler et al. (Chapter 2), 110 samples from 55 depth locations were collected for UCS tests. The same samples were used for ultrasonic acoustic pulse velocities measured in the Experimental Geophysics Group (EGG) at the University of Alberta in Edmonton, Canada. Those velocities are used to supplement wireline acoustic velocities as described in Chapter 3. The samples were chosen independently of lithological stratigraphy to avoid a bias based on lithology. Mechanical stratigraphy can be independent of lithology (Laubach et al., 2009) so the samples were selected independently of lithological boundaries. The strategy was to collect enough samples to effectively describe the mechanical stratigraphy at a scale appropriate for the size of the potential geothermal reservoir discovered in the MH-2 borehole while ensuring that all the samples could be tested in the time available. Each sample location had two adjacent samples for UCS tests in an attempt to analyze the

ability to duplicate results from very similar rocks. Portions of the samples were powdered for XRD analysis at Vassar College in Pougkeepsie, NY.

Lithology is described here over the ZOI by mapping the major lithologic boundaries and describing the rocks based on type (crystalline basalt, altered basalt, reworked basaltic sediments, basalt breccia, or hyaloclastite). Basic lithological descriptions included textures, groundmass, phenocrysts and, when applicable, vesicles and/or amygdules were described by distribution, size, and fill type. Alteration of basalt minerals to clay is described by the full width at half maximum (FWHM), a measure of the diffracting domain size of the clays. The method is an attempt to identify the controlling factors for alteration of volcanic glass, pyroxene, or plagioclase to clay under which altering environment: weathering or hydrothermal alteration (Walker, personal communication). Fractures were characterized by type (natural or induced), morphology (planar, curved, sealed, broken, or open), and type of mineral fill (calcite, quartz, zeolites, sulphides, or clay), if present. Dip was measured with a digital protractor perpendicular to the strike line. On open fractures, the fracture faces were examined for evidence of shear slip in the form of slickenlines and the relative rake of slickenlines was measured as the orientation of slip relative to the maximum dip direction of the fracture face.

Wireline Borehole Geophysical Data

A full suite of wireline borehole geophysical logs are available from MH-2. A detailed report (Chapter 3) is available on the dynamic elastic properties calculated from sonic log data and bulk density measured from the UCS samples. We show (Chapter 3) that the dynamic data effectively replicate the static elastic properties and rock strengths

measured during the UCS experiments, and that a similar interpretation could be made from the method to calculate dynamic elastic properties and rock strength in lieu of the resource-intensive UCS experiments. We presented an analysis of wireline logs from the MH-2 borehole to interpret fracture porosity in the basaltic rocks and determined that interpretations of rock properties from wireline logs do help constrain the mechanical stratigraphic model.

In this study, we further test the mechanical model of the presence of eight or nine mechano-stratigraphic units (depending on the method of interpretation) with interpretation of fracture and stress data collected from ultrasonic acoustic borehole televiewer data (BHTV). The BHTV wireline tool measured the change in amplitude and return time in ultrasonic pulse and echoes sourced from the tool to the borehole wall. The velocity, or return time, and amplitude data can be manipulated to produce an acoustically dereived image of the borehole wall from which fracture and stress information is interpreted (Schmitt et al., 2012). The BHTV images reveal the presence and character of natural fractures, voids, breakouts, and induced tensile fractures. The images are oriented to magnetic north so visible fractures can be measured with a true orientation in addition to dip and aperture. Voids are used to identify possible permeable zones and can be used to explain core loss and discrepancies in depths between the driller's depths and the geophysicist's depths, if necessary. Breakouts and induced tensile fractures are indicators of the maximum and minimum horizontal stress directions. When a vertical borehole is drilled, the three orthogonal principal stresses that represent the far-field stresses acting on the borehole are perturbed by the newly created free surface represented by the borehole wall. The free surface requires a normal stress acting upon it

and the effective stresses σ_v, σ_H, and σ_h, acting on an infinitesimal cube in a rock mass are converted to σ_v acting vertically along the borehole wall, σ_{rr}, the radial stress acting perpendicular to the borehole wall, and $\sigma_{\theta\theta}$, that is a circumferential stress acting parallel to the borehole wall. The cylindrical void causes $\sigma_{\theta\theta}$ (hoop stress) to concentrate around the borehole wall relative to the maximum horizontal stress (S_H) direction (Schmitt et al., 2012; Zoback et al., 2003). The hoop stresses concentrate perpendicular to the maximum principal horizontal stress (Figure 4-2) and are typically three to four times the magnitude of the in situ far field maximum horizontal stress.

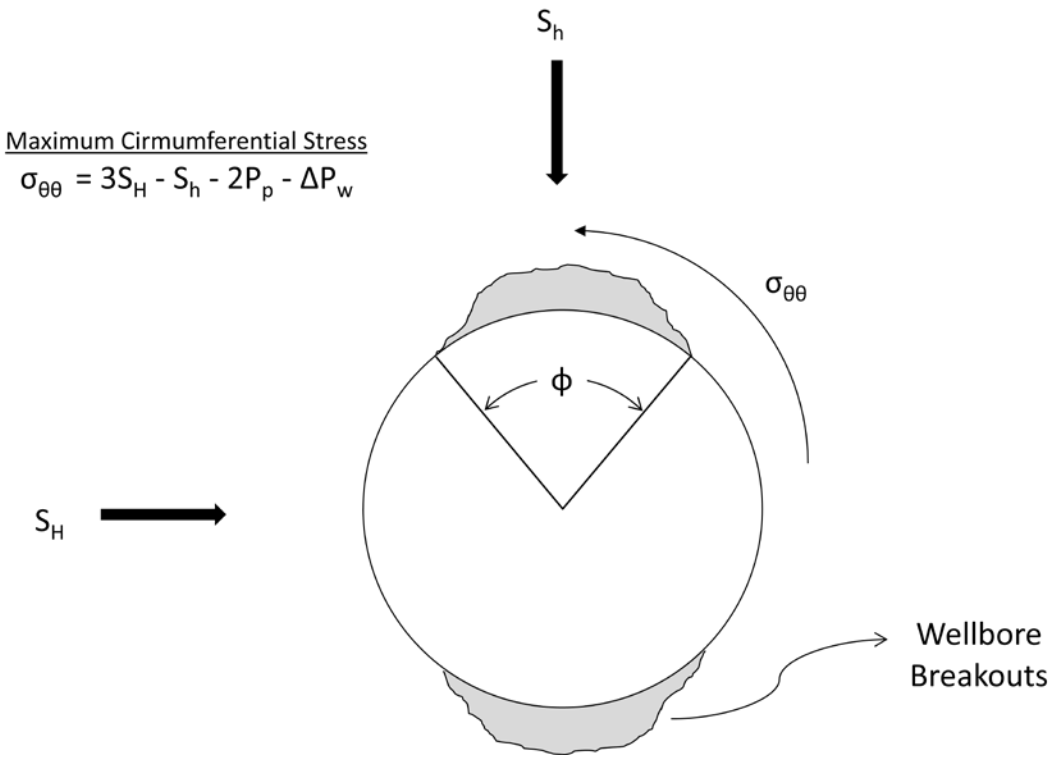

Figure 4-2. Circumferential (hoop) stress concentrations around a borehole wall and the breakouts formed from shear failure.

The concentration causes relative tension and subvertical shear failure in the borehole wall that we identify as breakouts on the BHTV log (Zoback et al., 2003). We

identify the orientation of S_H by measuring the orientation of breakouts in the oriented BHTV log and identify the orientation of the minimum horizontal stress (S_h) from interpreting the orientation of induced tensile fractures that can be identified on BHTV logs by the presence of linear subvertical cracks oriented approximately 90º to the observed breakouts at similar depths (Figure 4-3). The orientation of S_H is 90° to S_h so that we can estimate the orientation of S_h by breakout data in the absence of induced tensile fractures and vice versa.

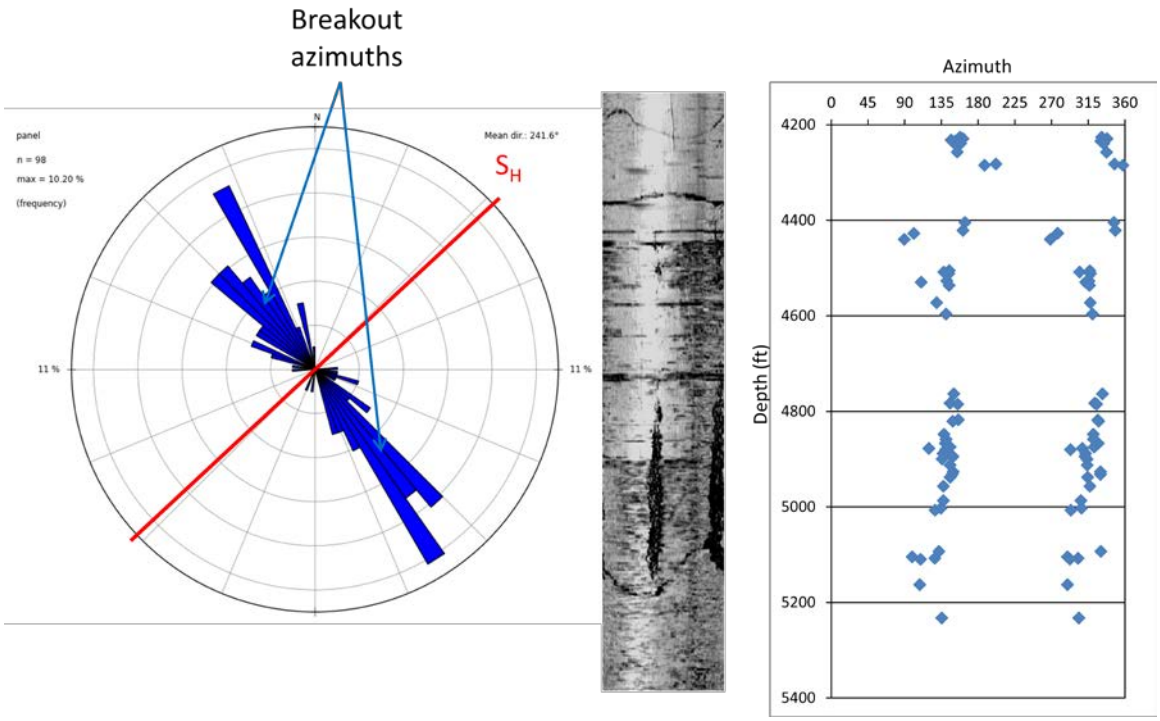

Figure 4-3. Example of breakouts in BHTV data and the orientation of S_H from breakout data

Stress Magnitudes and Mechanism of Shear Failure

The western SRP is an oblique normal fault-bounded basin which may result in complex faulting in the hanging wall of the graben (Avigad et al., 1998; Boulton and

Robertson, 2008; Rouby et al., 1996; Trench, 2008; Westaway, 1990; Zhang et al., 1991). The MH-2 borehole is located near the axis of the western SRP with a high-angle basin-bounding normal fault that defines the north-northeastern boundary of the western SRP and separates the Miocene to Pleistocene rocks in the basin from the Idaho batholith in central Idaho. Shervais et al. (2002) and Wood (1994) suggest the presence of intrabasinal normal faults (Figure 4-4) based on the stratigraphy logged in the MH-1 borehole, the Bostic 1A borehole, gravity anomaly data, and seismic reflection data, but the detailed structural geology in the basin around the MH-2 borehole is poorly understood. The borehole was drilled near the edge of a gravity high (Shervais et al., 2011) and may have been drilled near buried faults (Figure 4-4). No published stress magnitude or orientation data exist for the area. Using the stress orientation data and estimated stress magnitudes in the context of these inferences on the structural geology, we use frictional faulting theory and Andersonian mechanics to suggest the possible styles of failure that can explain the observations from the MH-2 borehole.

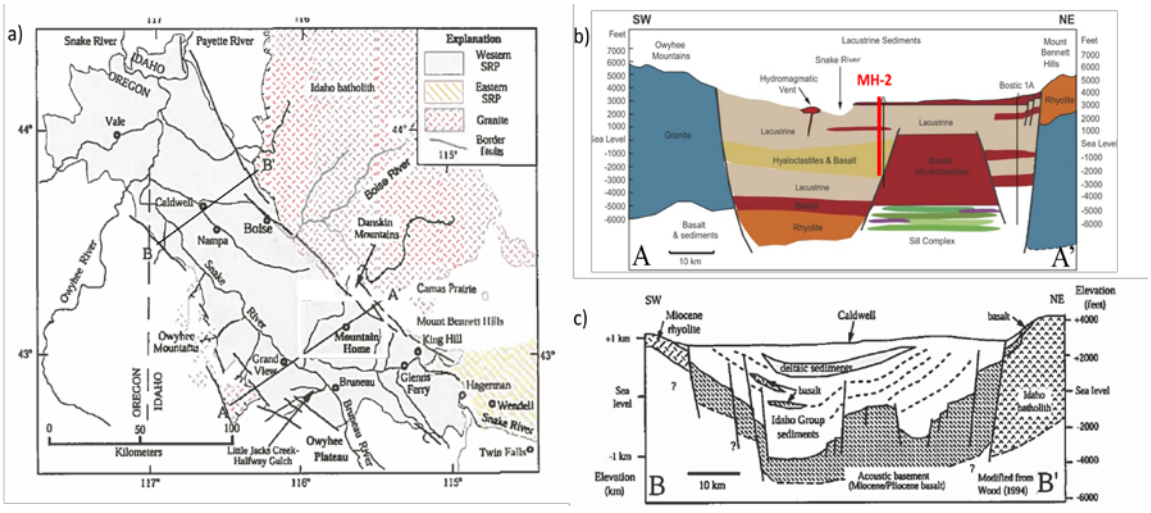

Figure 4-4. Proposed intrabasinal normal faults: a) regional map showing cross section lines and bounding faults, b) interpreted cross-section modified from Shervais (personal communication), c) interpreted cross section modified from Shervais et al. (2002).

We developed a simple geomechanical model to estimate the orientations and magnitudes of the three principal stresses. We calculated the overburden stress (S_v) using the mean bulk density of 2.64 g/cc that were measured from the UCS samples (Chapter 2):

$$S_v = \rho g h \quad (1)$$

Where ρ is the mean bulk density, g is the acceleration due to gravity, and h is the depth of investigation. Lacking empirical measurements of pore pressure in MH-2 we use the hydrostat as an estimate of pore pressure. The hydrostatic gradient is estimated to be 9.8 MPa/km. We calculate the minimum horizontal stress by assuming the coefficient of friction (μ) = 0.6 (Byerlee, 1978), hydrostatic pore pressure, and Biot's coefficient is close to zero so that equation 2 simplifies to equation 3:

$$S_h = \mu(S_v - \alpha P_p) \quad (2)$$

$$S_h = 0.6 S_v \quad (3)$$

We estimate the magnitude of S_H from breakout widths using the method described by Zoback et al. (2003). The extent to which a borehole wall deforms and experiences shear failure is a function of the maximum compressive stress and the strength of the rocks near the borehole wall. When the concentration of circumferential hoop stresses perpendicular to S_H exceed the rock strength, then shear failure occurs when the borehole deforms under in situ stresses. The time strain portion of the deformation takes place as a deepening of the breakout and the width of the breakout

remains a function of S_H. Since the angle of the breakout, ϕ, is a direct function of S_H (Figure 4-2) we use it in the calculation of S_H:

$$S_H = [(C_0 + 2P_p)/(1 - 2\cos 2\theta)] - S_h [(1+2\cos 2\theta)/(1-2\cos 2\theta)] \quad (4)$$

where,

$$\theta = \pi - \phi_{rad} \quad (5)$$

ϕ_{rad} is the angle of wellbore breakout, in radians, C_0 is the cohesive strength of the rock, and P_p is pore pressure that we estimated from the hydraulic gradient. Rock strength is used in the calculation of S_H and is represented by the cohesion coefficient (C_0):

$$C_0 = UCS/2(\mu^2+1)^{1/2} + \mu \quad (6)$$

With the stress magnitudes plotted with respect to depth, we have four stress gradients that give an indication of the faulting mechanism in the ZOI. Along with the principal stress directions and shear slip indicators mentioned above, we provide some insight into the mode of failure at depth in the vicinity of the MH-2 borehole.

We identify fault zones by grouping clusters of shear failure indicators in core. We used oriented fracture data from BHTV image logs and slip vector data from slickenlines to suggest a model for failure in MH-2. While the core is not oriented, the relationship between the relative rake and the dip of the fault can tell us about the relative motion along the fault plane. We assume that the relative rake of slickenlines suggests a mode of failure based on the angle of dip of the fault. High-angle faults with low-rake slickenlines indicate a dominant strike-slip motion on the fault and high-angle faults with

high-angle slickenlines indicate dominant dip-slip motion. We relate the fracture and slickenline orientations to the possible range of stress orientations and magnitudes to suggest the mode of failure in the fault zones in MH-2. Using the fault model and stress orientations and relative magnitudes, we suggest possible orientations for critically stressed faults near the artesian zone that are most likely to act as conduits for fluid flow. The shear stress (τ) and normal stress (σ_n) acting on a fault or fracture plane is defined as critically stressed when:

$$\tau/\sigma_n > 0.6 \quad (7)$$

Faults and fractures that meet that condition occur in predictable orientations relative to the in situ stress field. The orientation of principal stresses and relative magnitudes dictate the orientation of critically stressed faults and fractures according to Anderson's classification scheme (Figure 4-5).

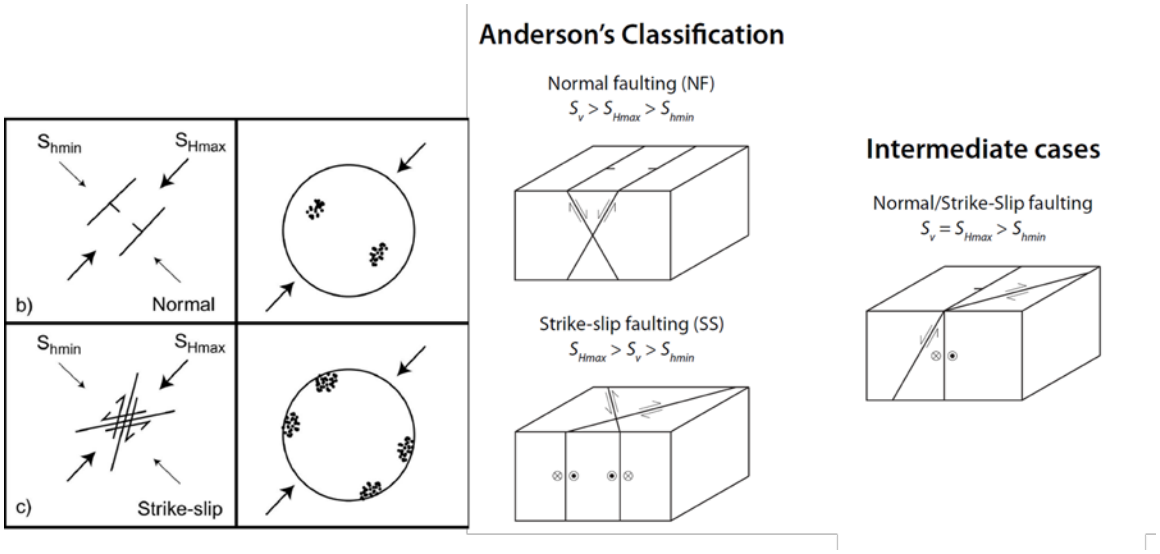

Figure 4-5. Faulting mechanisms defined by Anderson (1951) that could be applicable in the western SRP (modified from: Zoback, 2010).

In a normal faulting environment, critically stressed faults and fractures are most likely to strike parallel to S_H and dip around 60°. In a strike-slip environment, critically stressed faults and fractures are most likely to be close to vertical striking 30° away from S_H. We relate the failure models to the regional geological context and known major structures and suggest possible scenarios for probable permeable faults and fractures that can be tested by data and observations in future exploration wells.

Results

We present detailed descriptions of lithology, fracture stratigraphy, mechanical stratigraphy, shear slip indicators that represent fault zones, and an interpretation of the local stress field to describe a faulting mechanism for shear failure in the MH-2 borehole. We also introduce preliminary results from a related study on the alteration clays in the basalts that are indicative of in situ temperatures in the reservoir. The variety of data sets available provides the opportunity to test our conceptual model of the geological history and understand the current conditions by a variety of methods. The results presented here show that the various data sets indicate a consistent story of deposition, motion, and diagenesis to produce a potentially viable geothermal resource. We present the results of our analyses and interpretation and then suggest a path forward for geomechanical modeling and stress analysis to predict critically stressed fractures that could enhance permeability and might be targets for future geothermal exploration.

MH-2 Borehole Lithology

The lithology over the ZOI in the MH-2 borehole (Figure 4-6) consists of at least 29 discrete crystalline basalt flows varying in thickness from 1.5 m (5 ft) to 119 m (390 ft) that are separated by four discrete zones of interbedded hydrothermally altered basalt, reworked basaltic sediments, and basalt breccia.

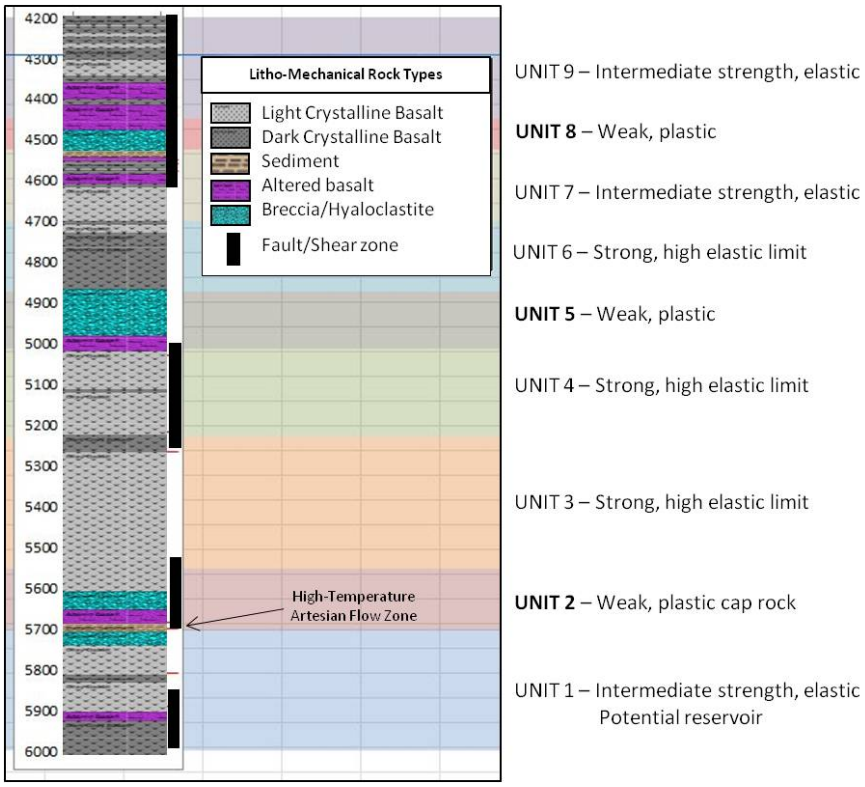

Figure 4-6. Lithological log over the zone of interest in MH-2

The crystalline basalts are generally either a light gray aphanitic basalt or a dark gray to black aphanitic basalt. Each basalt flow exhibits varying degress of vesiculation, phenocryt size, veining, and types of vein and vesicle fill. The degree of vesiculation varies from none to moderate and vesicles can be open or filled with clay, calcite, quartz, or zeolite. Where present, vesicles are evenly distributed and are planar in places.

Phenocrysts are plagioclase lathes and vary in size from microscopic to 10 mm in length. Veins are variable in complexity and location but are usually filled with a silicate or calcium carbonate. The zones of ductile, altered basalt are characterized by four main types: 1) hydrothermally altered basalt, 2) hyaloclastite, 3) hydrothermal breccias, and 4) reworked basaltic sediments. The presence of these altered and reworked rocks suggests a complex interaction of eruptions and the presence of cold surface water during the Late Miocene. The hydrothermal breccias could be the result of eruption into the lake and the resulting formation of hyaloclastite. The lake would provide a mechanism for reworking and redeposition of basaltic sediments to form the basaltic sand units. The hydrothermally altered basalts are evidence of past hydrothermal fluid flow through the basalt.

The lithology from TD of the borehole (Figure 4-6) up to the artesian flow zone at 1,745 m (5,726 ft) bgs consists of two basalt flows interbedded with one basalt breccia from 1,804 m – 1,798 m (5,920 ft – 5,900 ft) and a faulted altered basalt zone from 1,774 m – 1,769 m (5,822 ft – 5,805 ft). The lowermost basalt flow is a black aphanitic crystalline basalt with visible plagioclase lathes up to 4 mm in length with minor calcite-filled veins. Overlying the lowermost basalt flow is a ~20 ft thick hydrothermally altered basaltic breccia with a high clay content, sheared surfaces, pyrite crystals, and several rubble zones. Between the lowermost breccia and the artesian zone is a 165 ft light gray aphanitic, amygdaloidal basalt with small plagioclase phenocrysts up to 2 mm in length and minor vesiculation. Amygdules are filled with a white, powdery, non-calcareous mineral, possibly laumontite. This unit has several zones of minor alteration but a significant zone is present from 1,774 m – 1,769 m (5,822 ft – 5,805 ft). This is a light

gray fine-grained altered basalt with minor calcite filled veins and evidence of faulting along rubble zones and shear slip surfaces. The artesian flow zone at 1,745 m (5,726 ft) is at the top of the light gray basalt at the contact of the base of a ~37 m (~120 ft) thick section (Unit 2) of interbedded basaltic breccia, altered basalt, basaltic sediment, and hyaloclastite. The section is highly faulted and contains multiple shear slip surfaces. Unit 1 represents the potential geothermal reservoir and Unit 2 is the caprock that is apparently sealing the reservoir and preventing thermal and fluid loss. The combination of Unit 1 and Unit 2 comprise the target for future exploration.

The overlying section is a series of basalt flows that are the thickest units in the ZOI from 1,706 m – 1,529 m (5,600 ft to 5,017 ft). The lowermost is a massive, dark gray aphanitic basalt with small phenocrysts < 2 mm in length. This unit meets a transitional contact around 1,664 m (5,460 ft) and transitions into a light gray, aphanitic basalt with no visible phenocrysts and minor veining with non-calcareous fill (laumontite?). The thick, light gray unit is overlain by a 14-m (45-ft) thick dark gray, aphanitic basalt with 2 mm plagioclase lathes at a faulted contact at 1,603 m (5,262 ft) bgs. The upper contact of this dark basalt is also a faulted contact and juxtaposes it against a 45 m (150 ft) section of light gray aphanitic basalt with no visible crystals at the top of the unit. Chlorite-filled vesicles and plagioclase lathes up to 10 mm in length are common at the base. The texture changes and vesicles and phenocrysts decrease up section. The upper contact of these units at 1,530 m (5,020 ft) is with a 47 m (155 ft) section up to 1,483 m (4,865 ft) of light gray, highly altered and reworked basalt. The unit lacks breccias and hyaloclastite and has minimal fractures or veins from the base to 1,518 m (4,979 ft) and then grades up

section into altered basalt with regular zones of brecciated basalt with calcite cement and calcite-filled fractures. Hyaloclastite is present in some places.

Between the middle altered zone and the uppermost altered zone is a 75 m (245 ft) section of five units of alternating dark gray to black and light gray basalts. The lowermost is a 41 m (135 ft) section of dark gray, aphanitic basalt with no visible phenocrysts or vesicles. It has a greenish hue, indicating a high olivine content. Overlying this unit is another dark gray aphanitic basalt with 1 mm plagioclase lathes and intermittent zones of amygdules that are up to 0.6 m (2 ft) thick within the basalt unit. The upper portion of this section consists of light gray aphanitic basalt with chlorite-filled amygdules interbedded with two dark gray aphanitic basalt layers, each 3 m (10 ft) thick, devoid of amygdules and possessing small plagioclase lathes around 1 mm in length. The uppermost dark gray unit is in contact with the uppermost altered section in the ZOI. The uppermost altered section from 1,405 m (4,610 ft) to 1,330 m (4,365 ft) is a series of alternating thin beds < 1 m (3 ft) of light gray aphanitic, amygdaloidal basalt with plagioclase lathes ~ 1mm in length. The fracture faces in the crystalline basalt show pyrite and chalcopyrite mineralization. The crystalline basalt units are in faulted contact with hydrothermally altered basalt layers and one 15 m (50 ft) section of basaltic breccias with calcite filled fractures from 1,381 m (4,530 ft) to 1,365 m (4,480 ft) and another brecciated unit from 1,341 m (4,400 ft) to 1,330 m (4,365 ft). The extent of the uppermost altered section is 1,330 m (4,365 ft) bgs. The upper ~50 m (160 ft) consists of alternating thin beds 3 – 20 m (10-60 ft) thick of light and dark gray to black crystalline basalt with moderately dense vesicles filled with clay and calcite.

Fracture and Mechanical Stratigraphy

We interpreted the mechanical stratigraphy from a combination of static elastic properties and rock strength calculated from strain measurements during unconfined uniaxial compressive stress tests that were confirmed and verified through the calculation of dynamic elastic properties and rock strength (Chapter 2 and 3). We interpret the presence of eight to nine mechanical stratigraphic units over the ZOI. Three weak, plastic units are associated with fault zones identified by logging of shear slip surface indicators (Figures 4-7 and 4-8). The indicators are slickenlines on fracture faces. The combination of a weak, plastic unit and strong, elastic, and fractured potential geothermal reservoir were identified near TD in the MH-2 borehole (Figure 4-6). The weak unit 2 and strong unit 1 are identifiable using dynamic elastic properties and would be the target in future geothermal exploration wells. Unit 2 was likely juxtaposed with Unit 1 through oblique-normal faulting as indicated by the range of slip vectors on fault surfaces. Unit 2 may be a combination of fault breccia and gouge that has been hydrothermally altered as the fault became a conduit for fluid flow under past stress states. Under the current stress state, the fault is in frictional equilibrium and acts as a barrier to fluid flow and a hydrothermal seal to the underlying reservoir. Fracture density increases in the brittle units, particularly at the base of the strong units just above the top of a weak unit, fault, and altered zone. Fracture density decreases significantly in the weak units and goes to zero in places. Fracture stratigraphy and mechanical stratigraphy seem to be a function of rock type in this case and mimic the lithology over the ZOI. The rocks have experienced a complex structural and diagenetic history and the mechanical stratigraphy and fracture stratigraphy are a function of that history. Oriented fracture data are not available at depths around the

Unit 2 and Unit 1 boundary so, in some cases, we use the Unit 5 and Unit 4 boundary as an analog since the stratigraphic and structural relationships are similar.

Shear Slip Indicators

Orientations of 108 slip surfaces, with orientations of planes and vectors relative to the core axis, were measured on fault surfaces in the zone of interest while logging of the MH-2 core. We define the relative rake as the angle downdip along the fault plane from the strike of the fault surface. We observe both structural slickenlines and mineral slickenlines (Figure 4-7). Structural slickenlines are those with asperities on the fault surface that carved grooves in the fault faces while mineral slickenlines are those that are a result of smearing of mineral grains during slip events (Twiss and Moores, 2003). When the slickenline data are plotted with respect to depth and dip angle of the fault they occupy (Figure 4-8), the data cluster into four groups indicating four fault zones (A-D) in the ZOI. There does not appear to be a strong relationship between the dip of the fault and the slip vector of the slickenlines. However, there seems to be a slight trend in Fault Zone D with lower angle slip vectors and Fault Zones B and C appear to have slightly more high angle slip vectors. While not a statistically strong relationship, it is an indication that multiple phases of faulting took place in the past depending on the amount of normal vs. translational slip that occurred on the fault. Fault Zone D may have experienced more strike-slip motion while Fault Zones B and C may have experienced slightly more normal motion indicating a change in the stress state or a shift in the orientation of the fault planes to optimal orientation in a perturbed local stress field. The fault zones appear to be associated with the four zones of altered basalt, reworked

Figure 4-7. Examples of structural and mineral slickenlines in the MH-2 core

basaltic sediments, basaltic breccias, and hyaloclastites indicating the altered and reworked rocks are a result of hydrothermal fluid flux along a permeable critically stressed fault plane under a past stress state. The faults are clustered around the ductile units but faults are also present in the brittle units directly above and beneath the ductile units and suggest a structural component to the ductile caprock and brittle reservoir unit combination.

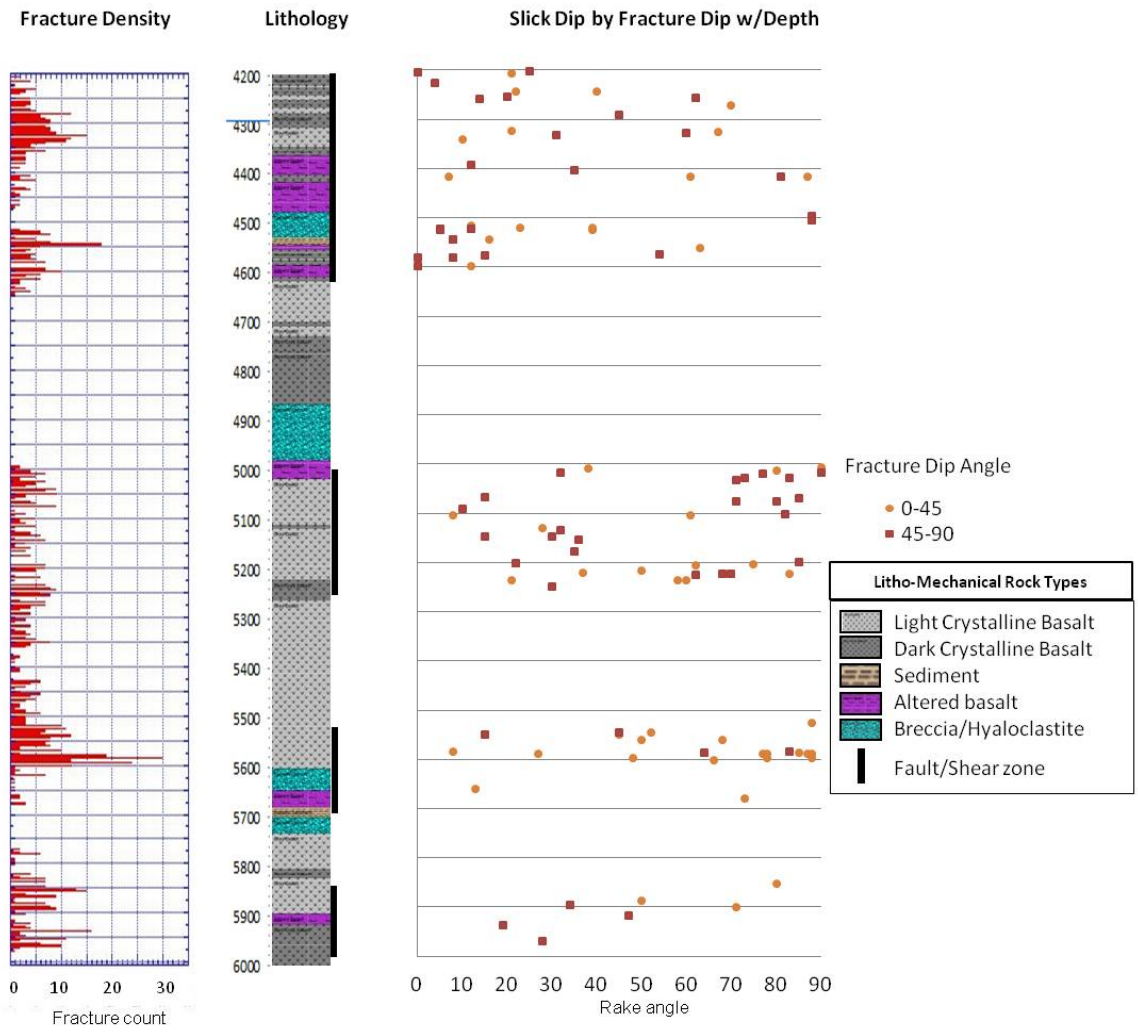

Figure 4-8. Slickenline dip relative to fracture dip

Fault Zones and Secondary Clay

The altered units are apparently associated with fault zones in the ZOI. Hydrothermally altered basalts and fault breccia in and around the fault zones is an indication that the faults were conduits for hydrothermal fluid flow at some time. The presence of reworked basaltic sediments and hyaloclastite indicates that these units are depositional and have experienced relatively little diagenesis. The ductile units are a combination of structurally emplaced depositional units interbedded with diagenetically and physically altered rock directly associated with the faults. The fault zone at the Unit1/Unit2 boundary apparently acts as a barrier to fluid flow and fracture propagation. The boundary also marks the presence of corrensite, a chlorite-smectite interlayered mineral, as a secondary clay in the altered matrix (Walker et al., 2014). Smectite is present throughout the ZOI as basalt minerals alter to clay. The addition of corrensite near the top of the reservoir is an indication that in situ temperatures in the reservoir are likely in the 200° C to 225° C range (Walker, personal communication), which is greater than the equilibrated downhole measured temperature of ~140° C.

State of Stress

Ultrasonic acoustic borehole televiewer data (Figure 4-3) were used to determine principal horizontal stress directions and magnitudes. The orientations of the borehole breakout data are consistent over the interval of the ZOI and indicate a consistent maximum principal horizontal stress (S_H) direction of 047° (Figure 4-3). The horizontal stress orientations represent the present-day state of stress and do not necessarily represent the state of stress that caused the failure that has taken place on the major basin

bounding faults in the western SRP. These stress data are the first reported for southwestern Idaho and the western SRP. The stress orientations are consistent with stress orientations from northern and central Nevada and are nearly perpendicular to S_H orientations to the northeast in the Idaho batholith (Figure 4-9). The north-northwest trending basin and the S_H orientations in northern and central Nevada may reflect the influence of shear in the west in reaction to the impact of the passing dextral motion of the Pacific plate against the North American plate. The oblique, transtensional deformation is accommodated by oblique shearing in the in the Walker Lane Shear Zone to the west (Zoback, 1989). Similar oblique-normal faulting mechanisms along the SRP basin-bounding faults to the northeast of the study area do not explain the orientation of S_H in MH-2. The present-day local state of stress in MH-2 is inconsistent with Anderson's classification of faulting mechanisms (Figure 4-5) and would have to be oriented NW, parallel to the basin axis, in order to produce normal and strike-slip failure on fault planes that strike to the NW and dip to the SW at high angles. In that scenario, S_v would be the maximum principal stress (S_1) and S_H would be the intermediate principal stress (S_2).

The differential stress magnitudes between S_v and S_H would have to be small if the faults experienced both normal and strike-slip failure. Stress magnitudes (Figure 4-10) were calculated using equations 1-4. The S_H magnitudes indicate that the stress state dictates a normal faulting environment:

$$S_v > S_H > S_h \quad (6)$$

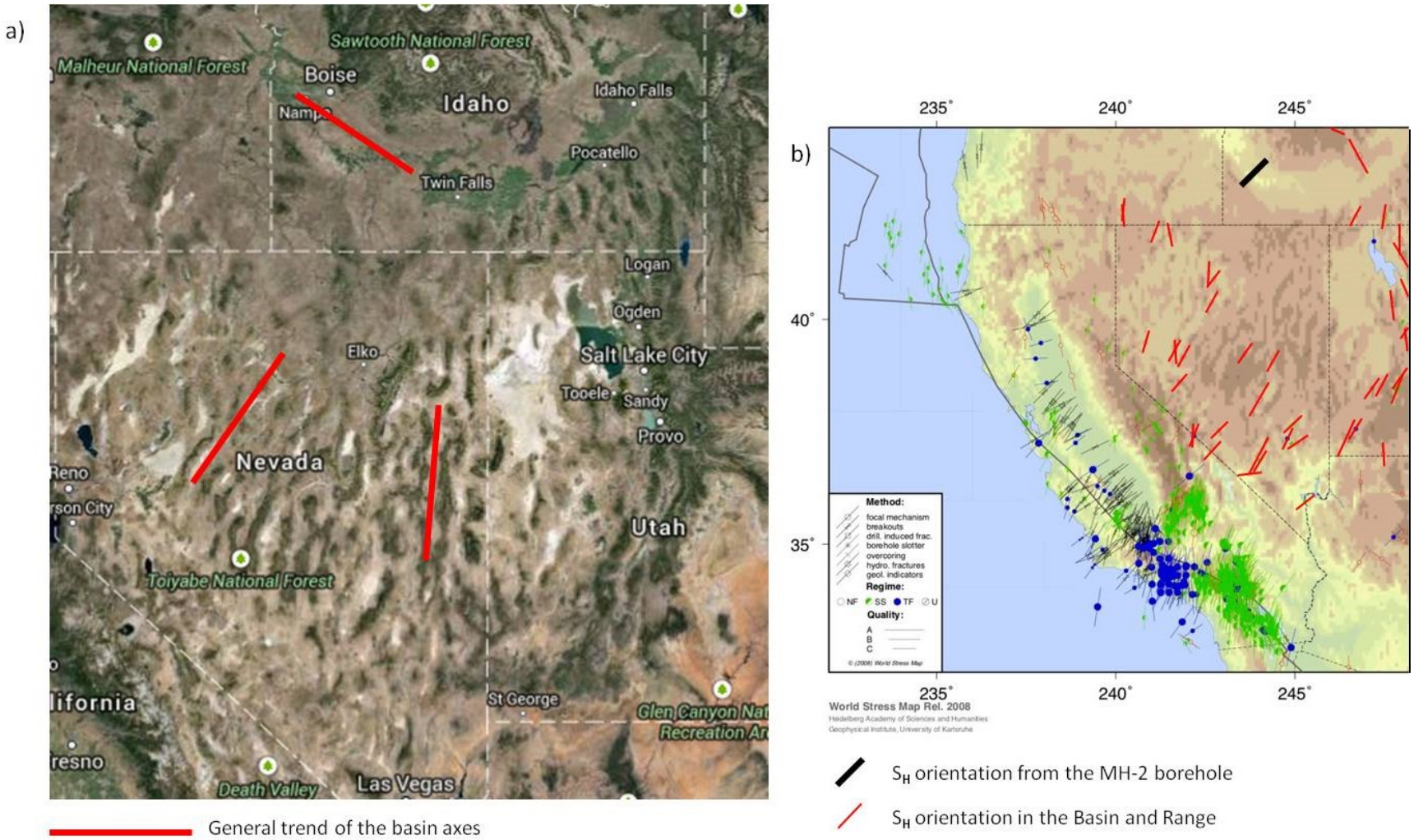

Figure 4-9. Regional map comparing a) the orientation of the western SRP to the B&R grabens and b) the World Stress Map S_H orientations, Basin and Range stresses highlighted in red and MH-2 in black.

Variability and uncertainty is high in the S_H magnitude calculations but we see that they generally plot below the magnitude of S_v and greater than the S_h lithostat (Figure 4-10). The magnitudes that plot below S_h are calculated from sites near the very weak, plastic units and are likely so weak that the brittle failure they exhibit in the borehole does not relate to the in situ maximum stress. Most of the stress load is accommodated in these samples through viscoplastic deformation so that brittle failure occurs at a stress load that is not proportional to the far-field maximum horizontal stress. The other samples are in some cases very close to S_v so we consider the possibility of multi-mode failure mechanisms in the area and a structural model that could accommodate oblique normal/strike-slip failure on faults around MH-2 that are optimally oriented for failure.

Discussion

GPS motion vectors indicate current extension to the west-northwest in the Basin and Range and western SRP (Payne et al., 2012). The northeast orientation of S_H in the MH-2 borehole and the north-northeast orientation of stress state indicators in the Basin and Range is consistent with this present-day extension direction. Measured strain rates in the Basin and Range are ~$12.2 \pm 4.7 \times 10^{-9}$ yr^{-1} based on GPS velocity measurements, the strain rate in the western SRP is negligible and is indistinguishable from zero (Payne et al., 2012). The lack of active deformation in the western SRP indicates the faults are in a state of frictional equilibrium and the minimal deformation that takes place occurs as aseismic creep along the faults (Zoback, 2010).

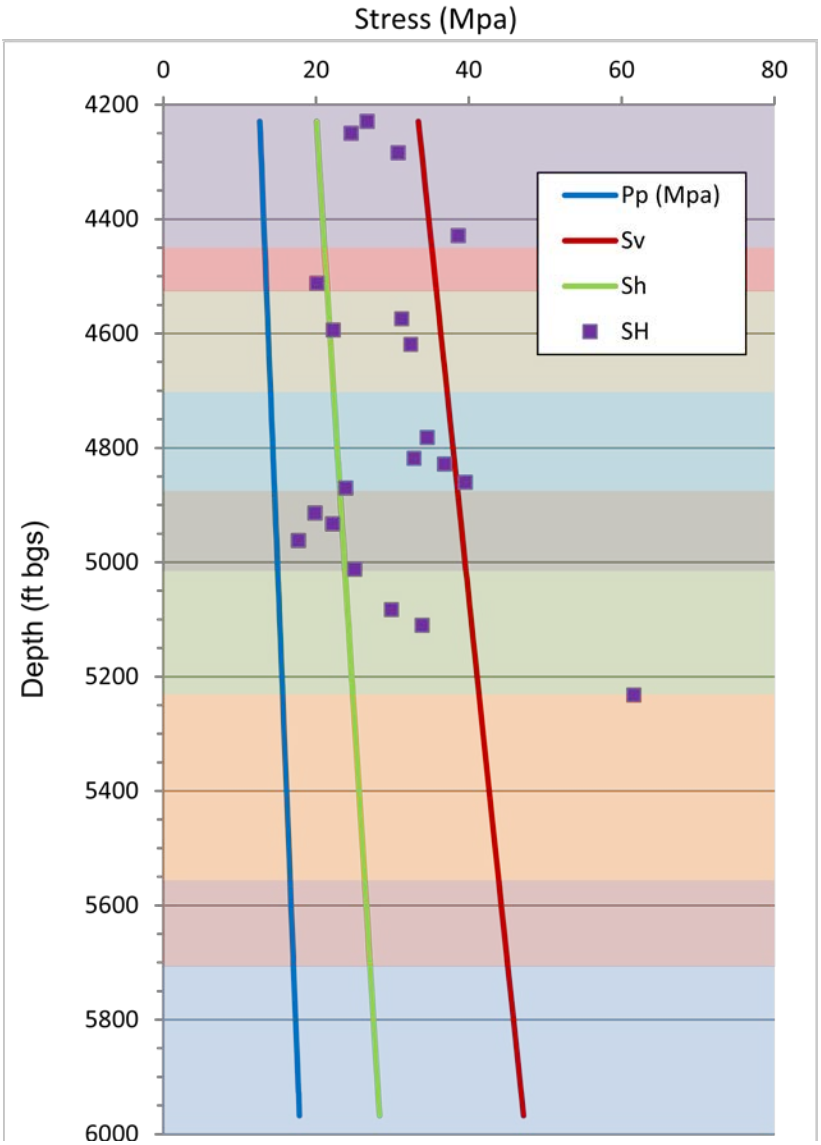

Figure 4-10. Hydrostatic (P_p), lithostatic (S_v), and S_h gradients with calculated S_H magnitudes from borehole breakout widths

Fractures and Lithology

Interpretation of the lithological relationships, fracture stratigraphy, shear slip indicators, and the in situ stress field indicates a complex structural scenario in the MH-2 borehole. We suggest the lithology is the primary factor controlling the distribution,

density, and intensity of fractures and the state of stress allows us to predict both the potential structural context and which fractures have the potential to connect into networks of permeable fluid pathways (Chapters 2 and 3). Elastic rock properties are the primary controlling factor for the presence of fractures but the orientation and magnitude of the stress tensors relative to the orientation of the fractures controls which fractures in a given population will be critically stressed and most likely to be permeable enough to conduct fluids effectively (Franquet et al., 2008; Hennings et al., 2012; Rogers, 2003). When the ratio of normal stress to shear stress on the fracture plane exceeds 0.6, then the fracture has a higher probability of being conductive. Knowing the absolute orientation of fractures in space relative the orientation of the stress field is critical to identifying the proportion of potentially permeable fracture in a system.

A model of the regional structure is important to estimate possible fracture populations in both density and orientation. Considering the state of stress and a simple geomechanical model, we suggest a structural model that explains our observations in MH-2, adheres to frictional faulting theory and Anderson's fault classifications, and provides a context to predict the orientation and density of critically stressed faults and fractures. A one-dimensional source of data limits the certainty of a structural interpretation but still provides insight into the kinds of structures that could produce the lithological, structural, and geomechanical conditions we observe in the MH-2 borehole.

The lithological relationships we observe in MH-2 indicate a complex history of terrestrial volcanism, lacustrine volcanism, hydrothermal alteration, and deposition of basaltic sediments. Crystalline basalts are often in sharp contact with hyaloclastite, hydrothermally altered basalt, and/or reworked basaltic sediments. The sharp contacts are

often along shear zones represented by clusters of shear slip surfaces on fracture faces (Figure 4-10). The upper ~150 m (500 ft) of the ZOI consists of thin beds of alternating crystalline basalt with altered or reworked units. The beds are bounded by many shear surfaces, indicating thicknesses are structurally altered. The lower part of the ZOI, from 1,430 m (4,700 ft) to TD, consists of thicker packages of crystalline beds interbedded with discrete packages of altered and reworked units. The lowermost package of altered rocks is the weak unit that accommodates stress through viscoplastic deformation and we interpret it as a cap rock seal to the potential underlying reservoir. The distinct character of each rock type indicates a spatial and temporal variance in how the rocks were deposited. The alternating nature of the terrestrially deposited basalts and lacustrine basalts is an indication of the cyclicity in the presence of lakes in the paleo-western SRP. The distribution of fractures in the MH-2 borehole closely mimics the lithological boundaries where brittle crystalline basalt rocks are juxtaposed against ductile hyaloclastite or altered/reworked basalt units. The rock properties are distinct and the fractures correspond to the rock properties (Chapter 2 and 3). We cannot determine the amount of offset along the faults in a single borehole but the distinct change in lithology from weak, plastic units to strong, elastic units that we interpret as a potential cap rock/reservoir structural and stratigraphic relationship and the clustering of shear slip surfaces near those contacts suggests a large enough amount of offset in the fault zones to juxtapose the lithologic units and create a structural trap for hydrothermal fluids. The lithological relationships, between surface mapping and logging of units in the Bostic-1A well, indicate up to 2,700 m (9,000 ft) of offset along the basin- bounding faults so that we would expect some of that offset to be accommodated on the faults in MH-2. The

wide distribution of slip angles (Figure 4-10) on the shear surfaces indicates oblique failure in the fault zones and suggests that a complex fault zone could be producing the permeability and storage for the potential geothermal reservoir. Critically stressed faults have a tendency to increase fault permeability when the rocks are strong enough to prevent fault gouge from decreasing permeability in the fault zone (Morris et al., 2012; Reeves et al., 2012). Both the weak units and strong units are experiencing the same stress gradient (Figure 4-10). It is more likely the weak rocks produce fault gouge when stresses exceed the plastic/ductile limit and the rocks begin to exhibit brittle deformation (Rogers, 2003). The strong rocks are likely strong enough to exhibit minimal fault gouge. The artesian zone encountered at 1,745 m (5,726 ft) depth is an indication that fault gouge is not significantly limiting fluid flow along the faulted surfaces in the strong zone. It also is an indication that alteration, fault breccia, and fault gouge is limiting fluid flow in the weak unit overlying the reservoir.

State of Stress and Structure

The orientation of the in situ stress field is inconsistent with what we would expect from the basin-bounding normal faults at the surface that are exposed to the NE and SW. Based on the oblique extension of the western SRP graben, we would expect a NW oriented S_H and NE orientation of S_h. However, we see the principal stresses oriented at ~90° to this direction so that S_H is oriented NE and S_h oriented parallel to the basin axis (Figures 9 and 10). The nearest stress orientation indicators based on breakout data and earthquake focal mechanisms are from the Basin and Range in Nevada and S_H orientations from the Columbia River Basalts in Oregon (Heidbach et al., 2008). In

Oregon, S_H orientations are predominantly oriented NNE. The S_H orientations in the Basin and Range in northern Nevada are similar to the S_H orientation in MH-2. Most are oriented northeast-southwest. The obvious limitation of a Basin and Range-type model to explain the stress orientations is the orientation of the western SRP bounding normal faults relative to the majority of basins in the Basin and Range. The western SRP is almost orthogonal to the majority of grabens in the Basin and Range, especially when compared to those closest to southern Idaho and the western SRP (Figure 4-11).

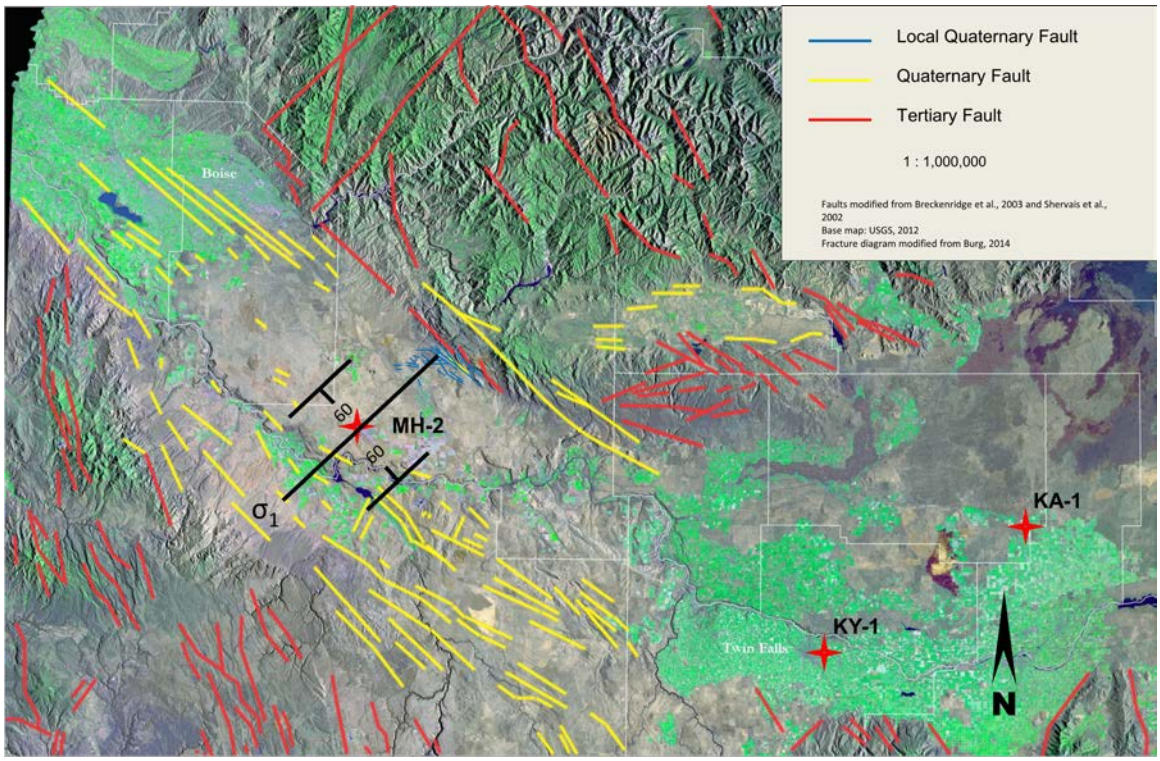

Figure 4-11. Potential orientations of normal faults as predicted from Andersonian failure mechanisms

The stress state, however, provides some insight into the faulting mechanism. The S_H magnitudes calculated from wellbore breakouts (Figure 4-10) suggest that S_H is less than S_v indicating a primarily normal faulting environment. A normal fault next to MH-2

would be predicted to strike NE and dip around 60° to the NW or the SE (Figure 4-11) as dictated by the orientation of the stress field and the relative stress magnitudes. The mechanism we propose to produce a fault oriented this way in the oblique-extensional environment of the western SRP is a nearby fault oriented to the northeast. This kind of fault could be produced as an accommodating antithetical fault in a stepover ramp between two larger en echelon normal faults that strike to the northwest (Figure 4-12).

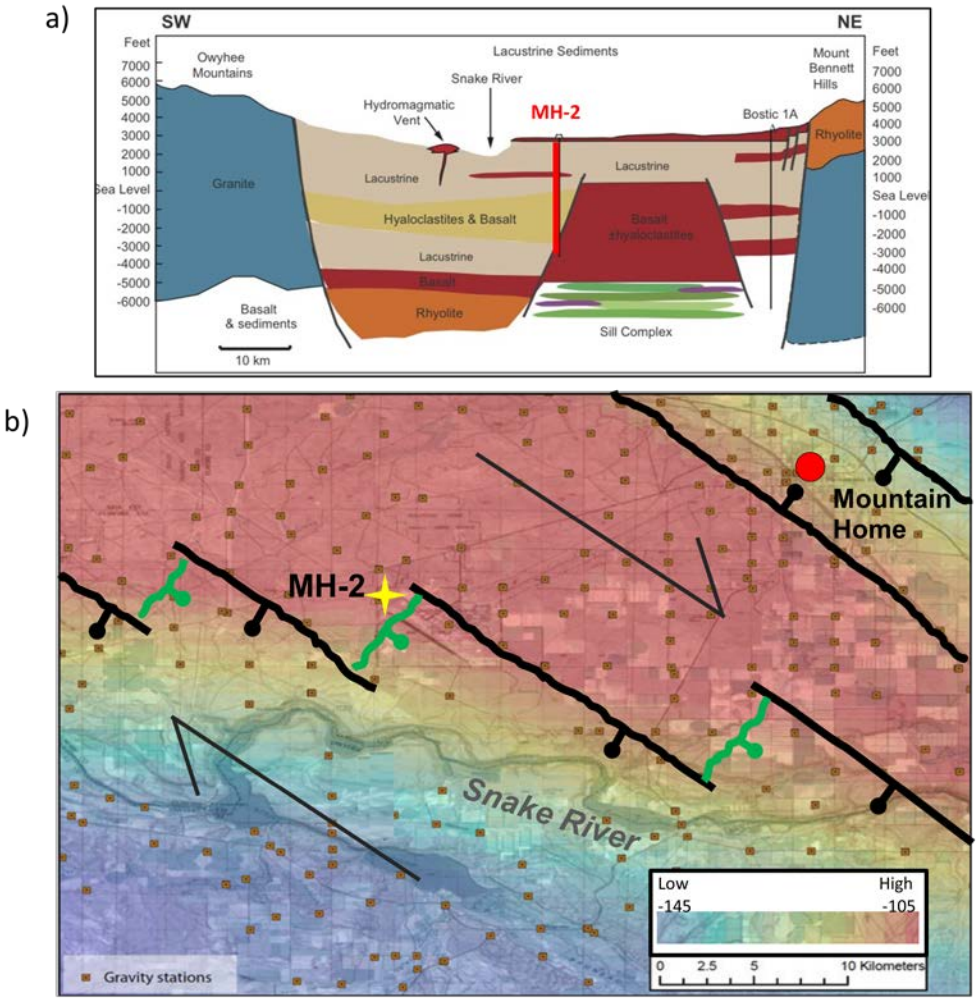

Cross-section modified from Shervais et al., 2013; Gravity map courtesy of Shervais et al., 2011.

Figure 4-12. Cross section (a) and conceptual model (b) of step-over faults (green lines) connecting en echelon normal faults (black lines) around the gravity high.

The MH-2 borehole was drilled on the boundary of a gravity high and the cross-section interpretation indicates that it was drilled nearby a buried intrabasinal normal fault at the boundary of a rhyolitic block creating the gravity high. En echelon faults often produce antithetical oblique-normal faults in the accommodation space between the stepover on the ramp between the fault tips and are often where successful geothermal fields are located due to the enhanced permeability in the complexly faulted zone (Faulds et al., 2011).

We assume a normal hydrostatic gradient for our stress analysis and recognize uncertainty in the calculated S_H magnitudes is high. The high geothermal gradient and high bottom-hole temperatures can cause elevated pore pressure (Barker, 1972; Luo and Vasseur, 1992; Swarbrick, 2012; Zoback, 2010). As pore pressure rises above the hydrostat with depth and temperature it can both reduce the differential stress, stress anisotropy, and also the total stress on the rocks. We consider a scenario where S_H is close to or larger than S_v so that strike-slip faulting mechanisms dominate. In this scenario, Unit 5 acts as a hydrothermal barrier and prevents fluid escape from the underlying units and pore pressure increases above the hydrostat (Figure 4-13). We see that an increase in pore pressure below Unit 5 causes an increase in the magnitude of S_H so that S_H is larger than S_v and the differential stress is decreased. Strike-slip faulting mechanisms would have to dominate in this scenario. Considering the oblique-extensional environment, we can envision that slip occurs in a combination of normal and right-lateral strike-slip motion on an antithetical fault on the ramp between the fault tips of two larger dextral oblique-slip faults.

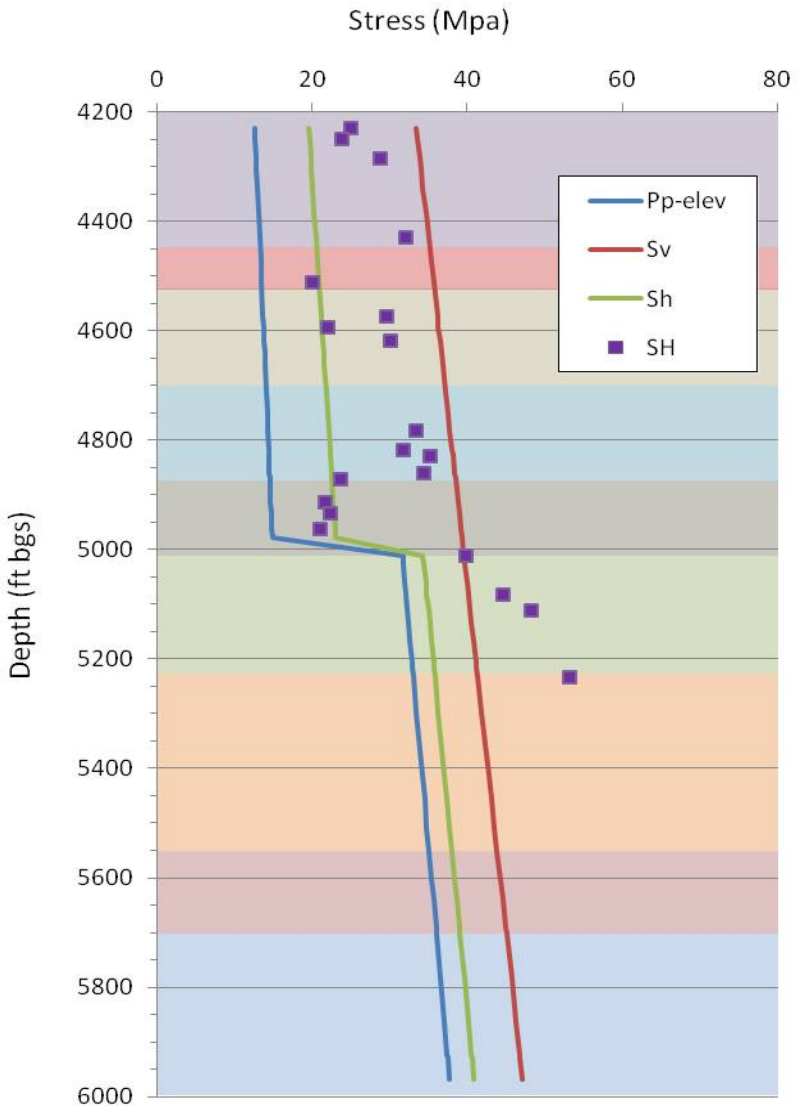

Figure 4-13. Stress gradients under a hypothetical overpressured zone below the unfractured Unit 5. Stress differential is low and S_H magnitudes suggest the possibility of strike-slip faulting at depth.

This is a special case and is speculative due to a lack of in situ pore pressure measurements but many geothermal reservoirs are known to be overpressured so it is worthwhile to consider the consequences of the scenario. The presence of borehole breakouts indicates that stress anisotropy is high enough to preferentially strain the borehole to a depth of 1,594 m (~5,232 ft). Below that, BHTV data are not available to

determine the extent of wellbore breakouts but breakouts are less prevalent near the bottom of the BHTV log that indicates a decrease in the differential stress with depth. Elevated temperatures could have raised pore pressure and may be playing a role in limiting the active deformation and reducing the strain rate in the western SRP around the MH-2 borehole. Elevated pore pressure would also increase the probability of the faulting mechanisms to exhibit both strike-slip and normal motion. An intermediate faulting mechanism could increase the range of orientations for critically stressed faults and fractures that could increase the total fracture permeability in the reservoir. This phenomenon has been observed in other fractured geothermal reservoirs: Dixie Valley and Desert Peak in Nevada (Faulds et al., 2011) and other reservoir types: Yucca Mountain, the North Sea Chalk, the Timor Sea, and the Visund oil and gas field in the North Sea (Hennings et al., 2012; Zoback, 2010).

Our analysis suggests that MH-2 was drilled near a stepover fault that connects the fault tips of two large en echelon faults along the southeastern edge of the gravity high (Figure 4-12). We consider a structural scenario of en echelon large normal faults with small antithetical step-over faults connecting the fault tips on the ramps. The stepover faults would be oriented NE-SW with normal faulting motion down to the SE (Figure 4-12) with a component of dextral strike-slip oblique motion. Faults oriented in this direction with normal motion down to the SE would explain the stress orientations and magnitudes in our geomechanical model. The structural model also provides a mechanism to accommodate a component of strike-slip motion considering the uncertainty the S_H magnitudes. The step-over ramp fault model also satisfies the requirements of Andersonian fault mechanics and explains our observations of the stress

state but also allows for a component of dextral-oblique motion from the Basin and Range.

Conclusions

We examined the lithological, fracture, and stress data from the MH-2 borehole and provided geomechanical and geological models that explain our observations. We interpret the data from MH-2 to provide the framework for a context under which further geothermal exploration can take place. We show that the potential geothermal reservoir is capped by a weak, viscoplastic unit that could be arresting fracture propagation. The weak unit is associated with a fault zone and we have interpreted the fault as a conduit for hydrothermal fluid flow along the fault at some point in the past. The fault motion created fault breccia and the hydrothermal fluid altered the basalt to clays, specifically, Corrensite, at the Unit 1/Unit 2 boundary that indicates high in situ reservoir temperatures around 225° C. The artesian flow zone is located at the base of the weak unit and suggests the fault zone no longer acts as a conduit for fluid but rather a barrier to fluid flow and a thermal barrier. The cap rock is juxtaposed against the strong, elastic formation that we consider a potential fractured reservoir. The resulting spatial relationship is an apparent structural trap for geothermal fluids. The regional structures that control the emplacement of weak cap rock material on top of a strong fractured reservoir are complex. The stress data and the amount of apparent offset in the borehole are strong indications the MH-2 borehole penetrated a complex structural environment. The implications for the complexity are that future exploration wells will likely encounter structures and lithology that could be difficult to correlate to the MH-2 borehole.

We suggest focusing on the weak/strong units as a target in future exploration wells.Our observations show that the weak units are associated with fault zones that are acting as a reservoir seal and flow barrier making the weak units good targets to identify potential reservoir intervals in future exploration wells because they can be identified during drilling or after wireline logging. Artesian flow from the high-temperature flow zone encountered in MH-2 is strong evidence of a potential reservoir large enough to support commercial development of geothermal energy in the region. The evidence presented here indicates a strong potential for commercial development. Part of the recommended effort to delineate and assess the potential for the reservoir to produce commercial geothermal energy is to assess the extent of the possible fracture networks through discrete fracture network modeling and 3D stress analysis. The data presented here will be part of a foundation to build models that will assess the extent of fracture permeability and storage. More data are needed but the MH-2 borehole data and analysis is the foundation upon which future work will build.

References

Anderson, E.M., 1951. Dynamics of Faulting and Dyke Formation with Application to Britain. Hafner Publishing Company, New York, pp. 206.

Arney, B.H., Gardner, J.N., Bellnomi, S.G., 1984. Petrographic analysis and correlation of volcanic rocks in Bostic 1-A well near Mountain Home, Idaho. Los Alamos National Laboratory Report LA-9966-HDR, 29.

Arney, B.H., Goff, F., Harding Lawson Associates, 1982. Evaluation of the hot dry rock geothermal potential of an area near Mountain Home Idaho. Los Alamos National Laboratory Report LA-9365-HDR, 65.

Avigad, D., Baer, G., Heimann, A., 1998. Block rotation and continental extension in the central Aegean Sea: palaeomagnetic and structural evidence from Tinos and Mykonos (Cyclades). Earth & Planetary Sci. Letters 137, 23-40.

Barker, C., 1972. Aquathermal pressure – role of temperature in development of abnormal pressure zones. Am. Assoc. Petrol. Geol. Bull. 56, 2068 – 2071.

Benford, B., Crowley, J., Schmitz, M., Northrup, C.J., Tickoff, B., 2010. Mesozoic magmatism and deformation on the northern Owyhee Mountains Idaho: Implications for along-zone variations for the western Idaho shear zone. Lithosphere, 2, 93-118.

Blackwell, D.D., 2012. Geothermal heat flow map of the U.S. (http://www.smu.edu/~/media/Site/Dedman/Academics/Programs/Geothermal%20Lab/Graphics/SMU2011USHeatFlowMap.ashx?la=en).

Bonnichsen, B., Leeman, W.P., Honjo, N., McIntosh, W.C., Godchaux, M.M., 2008. Miocene Silicic Volcanism in Southwestern Idaho: Geochronology, Geochemistry, and Evolution of the Central Snake River Plain. Bull. of Volc. 70, 315 – 342.

Bonnichsen, B., Godchaux, M.M., 2002. Late Miocene, Pliocene, and Pleistocene geology of southwestern Idaho with emphasis on basalts in the Bruneau-Jarbidge, Twin Falls, and western Snake River Plain regions. In: Bonnichsen, B., White, C.M., McCurry, M., (Eds.), Tectonic and Magmatic Evolution of the Snake River Plain Volcanic Province. Idaho Geol. Surv. Bull. 30, 233–312.

Boulton, S.J., Robertson, A.H., 2008. The Neogene-Recent Hatay Graben, South Central Turkey: graben formation in a setting of oblique extension (transtension) related to post-collision tectonic escape. Geol. Mag. 145, 800-821.

Breckenridge, R.M., Lewis, R.S., Adema, G.W., Weisz, D.W., 2003. Miocene and younger faults in Idaho. Idaho Geological Survey, Moscow, Idaho.

Byerlee, J., 1978. Friction of Rocks. Pure and Applied Geophysics, 116, (4-5), 615-626.

Faulds, J.E., Hinz, N.E., Coolbaugh, M.F., Cashman, P.H., Kratt, C., Dering, G., Edwards, J., Mayhew, B., McLachlan, H., 2011. Assessment of Favorable Structural Settings of Geothermal Systems in the Great Basin, Western USA. In: Trans. Geothermal Resources Council Annual Meeting, October 2011, San Diego, CA. 777–783.

Faulds, J.E., Coolbaugh, M.F., Benoit, D., Oppliger, G., Perkins, M., Moeck, I., Drakos, P., 2010. Structural controls of geothermal activity in the northern Hot Springs Mountains, western Nevada: the tale of three geothermal systems (Brady's, Desert Peak, and Desert Queen). Trans. Geothermal Resources Council, 34, 622-630.

Franquet, J.A., Krisadasima, S., Bal, A., Pantic, D.M., 2008. Critically-stressed fracture analysis contributes to determining the optimal drilling trajectory in naturally fractured reservoirs. Int. Petrol. Tech. Conf. 3-5 December, Kuala Lumpur, Malaysia.

Glen, J.M.G., Ponce, D.A., 2002. Large-scale fractures related to inception of the Yellowstone hotspot. Geology, 30, 647–650.

Heidbach, O., Tingay, M., Barth, A., Reinecker, J., Kurfeß, D., Müller, B., 2008. The World Stress Map database release 2008. doi:10.1594/GFZ.WSM.Rel2008.

Hennings, P., Allwardt, P., Paul, P., Zahm, C., Reid, R., Alley, H., Kirschner, R., Lee, B., Hough, B., 2012. Relationship between fractures, fault zones, stress, and reservoir productivity in the Suban gas field, Sumatra, Indonesia. Am. Assoc. Petrol. Geol. Bull. 96, (4), 753-772. doi:10.1306/08161109084.

Kucks, R.P., 1999. Bouguer gravity anomaly data grid for the conterminous US: In, U.S. Geological Survey, National geophysical data grids; gamma-ray, gravity, magnetic and topographic data for the conterminous United States. U.S. Geological Survey Digital Data Series DDS-9.

Laubach, S.E., Olson, J.E., Gross, M.R., 2009. Mechanical and Fracture Stratigraphy. Am. Assoc. of Petrol. Geol. Bull. 93, (11), 1413-1426.

Lewis, R.E., Stone, M.A.J., 1988. Geohydrologic data from a 4,403-foot geothermal test hole, Mountain Home Air Force Base, Elmore County, Idaho. U.S. Geol. Surv. Open-File Rep. 88-166.

Luo, X., Vasseur, G., 1992. Contributions of compaction and aquathermal pressure to geopressure and the influence of environmental conditions. Am. Assoc. of Petrol. Geol. Bull. 76, 1550-1559.

Malde, H.E., 1991. Quaternary geologic and structural history of the Snake River Plain, Idaho and Oregon. In: Morrison, R.B., (Ed.), Quaternary Non-Glacial Geology: Conterminous United States: Geological Society of America, Boulder, Colorado, The Decade of North American Geology, K2, pp. 251-281.

McCurry, M., Watkins, A.M., Parker, J.L., Wright, K., Hughes, S.S., 1996. Preliminary volcanological constraints for sources of high-grade rheomorphic ignimbrites of the Cassia Mountains, Idaho: Implications for the evolution of the Twins Falls volcanic center. Northwest Geology, 26, 81–91.

McIntyre, D. H., 1979, Preliminary description of Anschutz Federal No. 1 drill hole, Owyhee County, Idaho. U. S. Geol. Surv. Open-File Rep. 79-651.

Morin, R.H., Carleton, G.B., Poirier, S., 1997. Fractured-aquifer hydrogeology from geophysical logs; the Passaic Formation, New Jersey. Groundwater, 35, (2), 328-338.

Morris, A.P., Smart, K., Ferrill, D.A., Reish, N., Cowell, P.F., 2012. Fault compartmentalization in a mature clastic reservoir: an example from Elk Hills Field, California. Search and Discovery Article #40907.

Payne, S.J., McCaffrey, R., King, R.W., Kattenhorn, S.A., 2012. A new interpretation of deformation rates in the Snake River Plain and adjacent basin and range regions based on GPS measurements. Geophys. J. Int. 189, 101 -122.

Pierce, K.L., Morgan, L.A., 1992. The track of the Yellowstone hotspot: Volcanism, faulting, and uplift. In: P.K. Link, M.A. Kuntz, L.B. Platt, (eds.), Regional Geology of Eastern Idaho and Western Wyoming. Geological Society of America Memoir 179, 1-53.

Reeves, D.M., Pholl, G., Lyles, B., Faulds, J., Louie, J., Ehni, B., Kratt, C., Cooper, C., Parahsar, R., Pullammanappallil, S., Noel, D., 2012. Geothermal resource characterization and evaluation at Astor Pass, Nevada. Geothermal Resources Council Annual Meeting 2012, Reno, NV, USA, 30 September.

Rogers, S.F., 2003. Critical stress-related permeability in fractured rocks. Geol. Soc. London, Special Publications, 209, 7-16.

Rouby, D., Fossen, H., Cobbold, P.R., 1996. Extension, displacement, and block rotation in the larger Gullfaks area, northern North Sea: determined from map view restoration. Am. Assoc. of Petrol. Geol. Bull. 80, (6), 875-890.

Ruez Jr., D.R., 2009. Framework for stratigraphic analysis of Pliocene fossiliferous deposits at Hagerman Fossil Beds National Monument, Idaho. Rocky Mtn. Geol. 44 (1), 33-70.

Sant, C.J., 2012. Geothermal Alteration of Basaltic Core from the Snake River Plain, Idaho. Master's Thesis, Utah State University, Logan, Utah.

Schmitt, D.R., Currie, C.A., Zhang, L., 2012. Crustal stress determination from boreholes and rock cores: fundamental principles. Tectonophysics, 580, 1-26.

Shervais, J.W., Schmitt, D.R., Nielson, D., Evans, J.P., Christiansen, E.H., Morgan, L, Shanks, W.C.P., Prokopenko, A.A., Lachmar, T., Liberty, L.M., Blackwell, D.D., Glen, J.M., Champion. D., Potter, K.E., Kessler, J.A., 2013. First results from HOTSPOT: The Snake River Plain Scientific Drilling Project, Idaho. U.S.A. Sci. Drill. 15, 36 – 45.

Shervais, J.W., Evans, J.P., Christiansen, E.J., Schmitt, D.R., Liberty, L.M., Blackwell, D.D., Glen, J.M., Kessler, J.A,, Potter, K.E., Jean, M.M., Sant, C. J., Freeman, T.G., 2011. Hotspot: The Snake River Geothermal Drilling Project – An Overview. Geothermal Res. Counc. Trans. 35, 995 – 1003.

Shervais, J.W., 2010, Phase 1 Report: The Snake River Geothermal Drilling Project – Innovative Approaches to Geothermal Exploration. Report to the Dept of Energy DE-EE0002848.

Shervais J.W., Shroff, G., Vetter, S.K., Matthews, S., Hanan, B.B., McGee, J.J., 2002. Origin and evolution of the western Snake River Plain: Implications from stratigraphy, faulting, and the geochemistry of basalts near Mountain Home, Idaho. In: Bonnichsen, B., White, C.M., McCurry, M., (Eds.), Tectonic and Magmatic Evolution of the Snake River Plain Volcanic Province. Idaho Geol. Surv. Bull. 30, 343-361.

Swarbrick, R., 2012. Review of pore-pressure prediction challenges in high-temperature areas. The Leading Edge, 1,288- 1,294.

Trench, D., 2008. The termination of the Basin and Range province into a clockwise rotating region of transtension and volcanism, central Oregon. Masters Thesis, Oregon State University, Corvalis, Oregon.

Twiss, R.J., Moores, E.M., 2003. Structural Geology. W.H. Freeman, New York.

Walker, J., Wheeler, J., Boersma, A., Ewen, K., 2014. The smectite to corrensite transition: preliminary results from the MH-2(B) borehole, western Snake River Plain, Idaho. poster: Clay Minerals Society Annual Meeting, May, 2014, College Station, Texas.

Westaway, R., 1990. Block rotation in western Turkey: 1. Observational evidence. J. Geophys. Res. 95, (B12), 19,857-19,884.

Wohletz, K.H., Heiken, G., 1992. *Volcanology and Geothermal Energy*. University of California Press, Berkeley, CA, pp. 432.

Wood, S., 1994. Seismic expression and geologic significance of a lacustrine delta in Neogene deposits of the western Snake River Plain, Idaho. Am. Assoc. of Petrol. Geol. Bull. 78, (1), 102-121.

Wood, S.H., Clemens, D.M., 2002. Geologic and tectonic history of the western Snake River Plain, Idaho and Oregon. In: Bonnichsen, B., White, C.M., McCurry, M., (Eds.), Tectonic and Magmatic Evolution of the Snake River Plain Volcanic Province. Idaho Geol. Surv. Bull. 30, Ê69-103.

Zhang, P., Slemmons, D.B., Mao, F., 1991. Geometric pattern, rupture termination and fault segmentation of the Dixie Valley – Pleasant Valley active normal fault system, Nevada, USA. J. Struct. Geol. 13, (2), 165-176.

Zoback, M.D., 2010. Reservoir Geomechanics, Cambridge University Press, New York, pp. 461.

Zoback, M.D., Barton, C.A., Castillo, D.A., Finkbeiner, T., Grollimund, B.R., Moos, D.B., Ward, C.D., Wiprut, D.J., 2003. Determination of stress orientation and magnitude in deep wells. Int. J. Rock Mech. Mining Sci. 40, 1049 – 1076.

Zoback, M.L., 1989. State of stress and modern deformation of the northern Basin and Range province. J. Geophys. Res. 94, (B6), 7,105-7,128.

CHAPTER 5

CONCLUSIONS AND IMPLICATIONS

The primary task of this project was to characterize the fractures, interpret the distribution of rock properties, and describe the present-day stress state in the MH-2 borehole. We approached building a foundation of geological information from MH-2 with a geomechanical perspective knowing that many successful geothermal systems in the Basin and Range and western U.S. are associated with complex fracture systems located around major geological structures. While our descriptions and interpretations are from a single two-dimensional data source, they do provide the basis for which further geological descriptions, interpretations, and geothermal exploration can take place.

We completed a basic lithologic description of the stratigraphy in the MH-2 borehole and documented the presence of four basic rock types: crystalline basalt with varying degrees of crystallization, alteration, vesiculation, and amygdules; interbedded sedimentary lacustrine thin bed and reworked basaltic sedimentary rocks; highly altered basaltic units with high clay content; and hyaloclastite and basaltic breccias. The lithologic units typically exhibit sharp contacts that are associated with fractures that exhibit strong shearing. The spatial relationship of the contacts and shear slip indicators suggests the sharp contacts are related to faulting in the borehole. Highly altered basaltic rocks are are in sharp contact with virgin crystalling basalt. Had the basalt been hydrothermally altered in place, we might expect to see a gradual change in lithology.

We document the fracture stratigraphy over a zone of interest above and including the upper portion of a potential geothermal reservoir and made an interpretation of

mechanical stratigraphy from static elastic properties and rock strength. We verified that interpretation by making an independent interpretation from dynamic calculations of elastic properties and rock strength. That verification provided a number of important insights to both the geological structure and future exploration of the potential geothermal system: 1) dynamic data can be effectively used to make a comparable interpretation of mechanical stratigraphy as would have been made from static data, 2) an empirical model to calculate dynamic rock strength from dynamic elastic properties was developed, allowing for a reasonable estimate of rock strength from wireline log data, 3) while we showed the dynamic data duplicated the static data well quantitatively, an empirical model was developed to calibrate dynamic elastic properties to static data if the dynamic data in future exploration wells require it and, 4) the effectiveness of using wireline log data saves the time and expense of conducting UCS experiments and expedites the interpretation in future geothermal exploration wells.

We demonstrate that the mechanical stratigraphy controls the distribution of fractures in the MH-2 borehole. While the brittle mechanical units host the majority of the fractures, the ductile units are mostly devoid of them. The ductile unit 2 overlies the potential geothermal reservoir so this characteristic may have important implications as a caprock and seal the potential reservoir. Emplacement of Unit 2 over the potential reservoir may also have important implications for our interpretation. If Unit 2 was emplaced by faulting over Unit 1 that hosts the potential reservoir, then future study is required to determine if Unit 2 was altered from its original basalt into the ductile rock it is today and then emplaced over Unit 1 at the fault contact between the units or if Unit 2 was altered as a result of faulting and the fault acting as a conduit for hydrothermal fluids

to be transported along the fault zone and altering Unit 2 in place. Our interpretation is that it is likely a combination but the sharp contact indicates that some faulting took place post alteration of Unit 2 and it is likely that Unit 2 was at least partially exposed to hydrothermal fluids during faulting.

Beyond providing the data needed to make calculations for dynamic elastic properties and rock strength, we show that the log data can be used to support the identification of fracture zones, high porosity zones, and major brittle/ductile boundaries. One of the most useful wireline logs is the ultrasonic acoustic televiewer (BHTV) log. The BHTV log is a powerful data set that we used to interpret oriented natural fractures, induced tensile fractures and borehole breakouts, and borehole conditions such as washouts, cave-ins, etc. that helped us interpret the other wireline data and identify the cause of anomalies. The BHTV data allowed us to corroborate the fracture data we observed in core with the fractures we could see in the borehole in the BHTV log. The data also allowed us to identify the orientation of the maximum and minimum principal horizontal stresses that contribute greatly to the structural interpretation.

Shear indicators and stress state allow us to put bounds on structural style and explain observations using Andersonian mechanics and Mohr-Coulomb failure criteria. A structural interpretation of the stress state and location of shear slip indicators suggests the borehole drilled through fractures and faults that are subjected to localized perturbed stresses associated with the large basin-bounding normal faults of the western SRP. Specific faulting mechanisms could not be ascertained but end-member scenarios were described.

This project provides a fundamental geological and geomechanical assessment of

the geology in the subsurface below the Mountain Home, Idaho area and in a zone of interest associated with a geothermal reservoir with commercial potential. We have collected and interpreted data to demonstrate the basic lithological, mechanical, and structural scenarios that might be encountered in future exploration wells. We have demonstrated a complex relationship between the rocks, the hydrothermal fluids, and the regional structures that will affect the extent and viability of the geothermal resource.

Further study is recommended to better constrain the stratigraphic and structural relationships in the area and define the extent and potential of the geothermal reservoir. Additional expoloration boreholes will be required to complete the assessment but more work can be done from the MH-2 core and borehole data. Detailed petrophysical modeling of porosity and permeability and laboratory work on core to determine pore throat sizes will be needed to assess the potential of matrix contribution to fluid storage and flow. The matrix-fracture interaction will be important to the viability of production from the reservoir. This study provides the foundation for which those data can be analyzed. This project has demonstrated that the lithological, fracture, and geomechanical data all indicate there is potential for commercial geothermal energy development at Mountain Home, Idaho.

APPENDICES

Appendix A: Core data

(electronically submitted)

Appendix B: Geomechanical data

(electronically submitted)

Appendix C: Permission Letters

Date: 11/28/14

Kelly Bradbury
Geology Department
Utah State University
4500 Old Main Hill
Logan, Utah USA 84322

Dear Kelly:

I am in the process of preparing my dissertation in the geology department at Utah State University. I hope to complete my degree program in geology.

I am requesting your permission to include the attached material as shown. I will include acknowledgments and/or appropriate citations to your work as shown and copyright and reprint rights information in a special appendix. The bibliographic citation will appear at the end of the manuscript as shown. Please advise me of any changes you require.

Please indicate your approval of this request by signing in the space provided, attaching any other form or instruction necessary to confirm permission. If you charge a reprint fee for use of your material, please indicate that as well. If you have any questions, please call me at the number below.

I hope you will be able to reply immediately. If you are not the copyright holder, please forward my request to the appropriate person or institution.

Thank you for your cooperation,

James A. Kessler

1-919-475-4160

I hereby give permission to James A. Kessler to reprint the following material in his dissertation.

Signed: Kelly K Bradbury

Date: 11/28/14

Xiwei Chen
Department of Physics
4-181 CCIS
University of Alberta
Edmonton AB T6G 2E1
CANADA

Dear Xiwei:

I am in the process of preparing my dissertation in the geology department at Utah State University. I hope to complete my degree program in geology.

I am requesting your permission to include the attached material as shown. I will include acknowledgments and/or appropriate citations to your work as shown and copyright and reprint rights information in a special appendix. The bibliographic citation will appear at the end of the manuscript as shown. Please advise me of any changes you require.

Please indicate your approval of this request by signing in the space provided, attaching any other form or instruction necessary to confirm permission. If you charge a reprint fee for use of your material, please indicate that as well. If you have any questions, please call me at the number below.

I hope you will be able to reply immediately. If you are not the copyright holder, please forward my request to the appropriate person or institution.

Thank you for your cooperation,

James A. Kessler

1-919-475-4160

I hereby give permission to James A. Kessler to reprint the following material in his dissertation.

Signed: 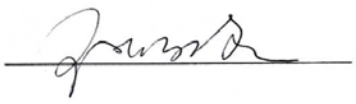

Date: 11/28/14

Michael Strange
Geoscience Department
University of Nevada, Las Vegas
4505 S. Maryland Pkway
Las Vegas, Nevada, USA 89154

Dear Mike:

I am in the process of preparing my dissertation in the geology department at Utah State University. I hope to complete my degree program in geology.

I am requesting your permission to include the attached material as shown. I will include acknowledgments and/or appropriate citations to your work as shown and copyright and reprint rights information in a special appendix. The bibliographic citation will appear at the end of the manuscript as shown. Please advise me of any changes you require.

Please indicate your approval of this request by signing in the space provided, attaching any other form or instruction necessary to confirm permission. If you charge a reprint fee for use of your material, please indicate that as well. If you have any questions, please call me at the number below.

I hope you will be able to reply immediately. If you are not the copyright holder, please forward my request to the appropriate person or institution.

Thank you for your cooperation,

James A. Kessler

1-919-475-4160

I hereby give permission to James A. Kessler to reprint the following material in his dissertation.

Signed: Michael Strange

CURRICULUM VITAE

James A Kessler

Contact Information

Mail: 4100 Greenbriar Dr. #409
Houston, TX 77098

Phone: (919) 475-4160 (cell)

E-mail: jkessler191@hotmail.com

Education

Ph.D. Utah State University – Geology, 2014, Advisor: Dr. James P. Evans

- Dissertation Title: *In situ Stress and Geology from the MH-2 Borehole, Mountain Home, Idaho: Implications for Geothermal Exploration from Fractures, Rock Properties, and Geomechanics*

M.S. Northern Arizona University – Geology, 2002, Advisor: Dr. Abe E. Springer

- Thesis Title: *Grand Canyon Springs and the Redwall-Muav Aquifer: Comparison of Geologic Framework and Numerical Groundwater Flow Models*

B.S. University of Oregon – Geological Sciences, 1998

- Senior Project: Compilation of survey maps of Crack-in-the-Ground, OR
- National Association of Geoscience Teachers (NAGT) Field Camp Award (1997)

Summary of Work Experience

Occidental Oil and Gas Corporation (2/14 to present)
Geologist – fracture and geomechanics specialist
Houston, Texas

Encana Oil & Gas Inc. (5/13 – 8/13)
Geologist Intern, Plano, Texas

Occidental of Elk Hills, Inc. (10/12 – 12/12)
Geoscience Intern, Bakersfield, California

Golder Associates Inc. (7/12 – 9/12; 3/13 – 5/13)
Geologist Intern, FracMan Technology Group, Redmond, Washington

Utah State University (7/10 – 12/13)
Graduate Research Assistant, Department of Geology, Logan, Utah

RTI International (10/03 - 6/10)
Hydrogeologist/Geologist II, Environmental Sciences Group
Research Triangle Park, North Carolina

Los Alamos National Laboratory (5/01 – 9/03)
Graduate Research Assistant, Earth and Environmental Science Division
Los Alamos, New Mexico

Northern Arizona University (8/99 – 5/01)
Graduate Research Assistant, Department of Geology, Flagstaff, Arizona

Restaurant and Landscaping Work (12/98 – 7/99)
Park City, Utah

U.S. Geological Survey (6/98 – 11/98)
National Association of Geoscience Teachers (NAGT) Intern, Earthquake Hazards Program
Menlo Park, California

Professional Training

- *Geomechanics for Unconventionals*, Oil Field Geomechanics, LLC, Houston, TX, 2014
- *Applied Concepts in Naturally Fractured Reservoirs*, AAPG Short Course, Houston, TX, 2014
- *Seismic Geomorphology and Seismic Stratigraphy: Extracting Geologic Insights from 3-D Seismic Data*, AAPG Short Course, Long Beach, CA, 2012
- *Deltas: Processes, Stratigraphy, and Reservoirs*, AAPG Short Course, Long Beach, CA, 2012
- *Fundamentals of Seismic Structural Analysis and Hydrocarbon Entrapment Analysis*, GSA Short Course, Minneapolis, Minnesota, 2011
- *Basic Well Log Analysis*, AAPG Short Course, Denver, Colorado, 2011

Areas of Technical Experience

- Fracture characterization and core rock mechanical analysis
- Geomechanical and stress state modeling
- Familiarity with geologic, geomechanical, fracture, and reservoir modeling software: Kingdom, WellCAD, FracMan, Phase 2
- Geographic Information Systems (ArcGIS, Surfer)

- 3-D numerical groundwater flow modeling (Groundwater Vistas)
- Watershed delineation and runoff modeling (TOPMODEL, SPUR)

Awards and Grants

- ExxonMobil Geoscience Research Grant, 2013
- Society of Petrophysicists and Well Log Analysts (SPWLA) Foundation Grant, 2011
- Geological Society of America (GSA) Graduate Student Research Grant, 2011
- Grand Canyon Monitoring and Research Center (GCMRC) Research Grant, 2000
- National Association of Geoscience Teachers (NAGT) Field Camp Award, 1997

Recent Publications and Presentations

Shervais, J W., Schmitt, D. R., Nielson, D., Evans, J. P., Christiansen, E. H., Morgan, L., Shanks, W. C. P., Prokopenko, A. A., Lachmar, T., Liberty, L. M., Blackwell, D. D., Glen, J. M., Champion, D., Potter, K. P., and Kessler, J. A., 2013, First Results from HOTSPOT: the Snake River Plain Scientific Drilling Project, Idaho, U.S.A., Scientific Drilling, no. 15, doi: 10.2204/iodp.sd.15.06.2013.

Kessler, J. A., Evans, J.P., Shervais, J.W., and Schmitt, D., 2011, Preliminary Fracture Description from Core, Lithological Logs, and Borehole Geophysical Data in Slimhole Wells Drilled for Project Hotspot: The Snake River Geothermal Drilling Project, Abstract H21E-1181, AGU 2011 Fall Meeting, San Francisco, CA, December 5-9.

Kessler, J.A. and Evans, J.P., 2011, Fracture Distribution in Slimholes Drilled for Project Hotspot: The Snake River Geothermal Drilling Project and the Implications for Fluid Flow: GRC's 35th Annual Meeting and GEA Trade Show, San Diego, CA, October 23 – 26.

Kessler, J.A., Evans, J.P., Schmitt, D.R., 2011, Rock Property Descriptions Interpreted from Borehole Geophysical Data Collected in Slimholes Drilled for Project Hotspot: The Snake River Geothermal Drilling Project: GSA Rocky Mountain/Cordilleran Section Meeting, Logan, Utah, Abstracts, v. 43, no. 4, p. 40.